Assessment and mapping of soil water repellency using remote sensing and prediction of its effect on surface runoff and phosphorus losses

---

A thesis

submitted in partial fulfilment

of the requirements for the Degree of

Doctor of Philosophy

at

Lincoln University

by

Mohamed Bayad

Lincoln University

2021

Abstract of a thesis submitted in partial fulfilment of the requirements for the Degree of Doctor of Philosophy.

Abstract

Assessment and mapping of soil water repellency using remote sensing and prediction of its effect on surface runoff and phosphorus losses

by

Mohamed Bayad

The soil water repellency spatial and temporal dynamics remain ambiguous. Water repellency is an inherent soil property that refers to the impedance in dry soil wetting. This phenomenon was ascribable to the hydrophobic compounds coating the soil particles and has emerged as a recalcitrant issue impacting multiple processes upon agroecosystems. The apprehensions around soil water repellency include its impact on surface runoff, plant growth, and nutrients losses (e.g. phosphorus). The soil hydrophobic compounds, which are intrinsic constituents of the soil carbon pool, have different sources including plant leaves and roots, soil microbial communities and fungi. Previous methods for water repellency measurements are laborious, time-consuming and costly. The raison d'être of this thesis was to i) explore and test novel approaches for estimation of soil water repellency in pastoral ecosystems, and ii) study the factors controlling soil water repellency and assess its impact on surface runoff volumes and phosphorus losses in surface runoff. In the present work, multiple remote sensing approaches were tested to assess and map soil water repellency at multiple scales. The liaison between water repellency and soil surface reflectance was exploited to access the water repellency using the satellite multispectral reflectance and hyperspectral satellite data. A novel approach implicating the use of time series of surface reflectance and water deficit data was used to study the impact of both surface biomass and soil moisture temporal dynamics on the occurrence of water repellency and carbon content in pastoral systems. Multispectral broadband data from both Landsat-7 and Sentinel-2 satellites showed big potential for assessing soil water repellency and carbon content in permanent pastures. Partial least square regression models were calibrated and cross-validated using topsoil measurement of water repellency and soil carbon from 41 and 35 pastoral sites that were matched with reflectance spectra from Landsat-7 and Sentinel-2, respectively. Soil carbon showed higher predictability compared to water repellency with R^2_v=0.50, $RMSE_v$=2.58 when using Landsat-7 spectra. The higher predictability performance for water repellency persistence was reached using Sentinel-2 spectral (R^2_v=0.45; $RMSE_v$=0.98). However, using hyperspectral narrowband data from the Hyperion satellite showed a

higher prediction accuracy (R^2_v=0.78; $RMSE_v$=0.58). Prediction performance was generally higher when using the calibration sets, indicating the possibility of improving these prediction models when using larger datasets. A novel approach was tested using multiple predictors for soil water repellency occurrence. The predictors included time series of surface biomass assessed through normalised difference vegetation index (NDVI) and soil moisture data estimated through water deficit and synthetic aperture radar satellite data. The results showed an attractive opportunity for water repellency and soil carbon mapping. Three machine learning algorithms including artificial neural networks, random forest, and support vector machine were trained and cross-validated using multiple configurations of satellite time-series data and topsoil measurement from 58 pastoral sites. Random forest and support vector machine ($RMSE_v$=0.82 and 0.87, respectively) outperformed artificial neural networks ($RMSE_v$=1.23). With increasingly available remote sensing data, the use of satellite time-series data will open unprecedented opportunities for soil carbon, water repellency mapping, and potentially other functional chemical and physical soil attributes.

To understand water repellency dynamics and evaluate their impact on surface runoff and phosphorus losses in pastoral soils, two experiments were conducted. The first experiment aimed to understand the relationship between the actual water repellency persistence and water content in drying hydrophobic soils. The second experiment had the objective to evaluate the impact of soil water repellency on the surface runoff and phosphorus losses in runoff. Results from the first experiment showed that the actual water repellency increased dramatically when water content decreased, especially when moisture dropped below a critical value. Using lab measurements, the actual water repellency was modelled using a simple sigmoidal model, as a function of water content, the potential water repellency, and two characteristic parameters related to the response curve shape. Results from the runoff trial showed that the surface runoff was influenced by soil water repellency to some extent (R^2=0.46). Although more than 90 % of phosphorus losses happened in incidental losses following fertiliser application, the data point to non-incidental phosphorus loads being related to soil water repellency (R^2=0.56). These results bespoke the effect of soil water repellency on background phosphorus losses through surface runoff during post-summer runoff events in pastoral ecosystems.

Keywords: Soil water repellency, soil hydrophobicity, soil carbon, pastures, remote sensing, multispectral topsoil reflectance, hyperspectral topsoil reflectance, Sentinel-2, Landsat-7, Hyperion Sensor, remote sensing time series, water deficit time series, normalised difference vegetation index.

Acknowledgements

I would like to express my acknowledgements and gratitude to the people who helped me accomplish this work. First, many thanks to my supervisors for their guidance and support. Special thanks to Dr Henry Chau, Assoc. Pr. Jim Moir, Pr. Leo Condron, and Dr Stephen Trolove for dedicating their time and efforts to planning, implementing experiments and reviewing results. My sincere thanks and considerations to Neil Smith, Nigel Beale for the scientific and technical support and for inspiring me through the valuable discussions. I would like to thank Siyu Wang for helping me with soil samples processing and water repellency measurement in the lab.

I acknowledge and thank the Mohammed VI Polytechnic University (UM6P) and OCP Morocco for funding this research. The consistent support and guidance from the AgrobioSciences Program team and ESAFE professors helped me to accomplish the research in the best conditions possible. I would like also to thank Blinc Innovation Team for supporting and facilitating my stay in New Zealand. Special thanks to Toni Laming for her kindness and support.

I express my sincere gratitude to Mike Manning, Thomas Taylor, and the Innovation & Strategy Team at RavensDown for their hospitality and for helping with finding and proving access to soil sampling sites in the North Island of New Zealand. Thanks to RavensDown board members, I learned a lot about New Zealand's farming systems, culture, and great human values.

Many thanks to Dr Karin Muller from Plant and Food Research Ltd for sharing her knowledge and expertise and supporting this research by providing advice and valuable data. An important part of this work was achieved thanks to her collaboration and help. I would like to thank Mike Slay for the interest he showed in this research and for helping to locate water repellent soils in Hasting farms and identifying plant species.

Collaboration with North-West Agriculture and Forestry University (NWAFU) in China has provided a valuable platform of discussions, advice, and funding for this research. Special thanks to Pr. Li Yi and students from NWAFU for their great hospitality and collaboration.

Many thanks to John and Paulette Parker and Matt Cook for giving me access to their farm and facilitating the soil sampling and runoff trail in Hastings, Hawkes Bay. I express my sincere gratitude for their matchless kindness and hospitality.

I dedicate this thesis to my family and friends I could not have achieved it without their unconditional love and support. Many thanks go to my dear Olivia for her continuous support. Many thanks to Alvand, Tommy, Josh, and Fraser for their hospitality and kindness.

To my father, in loving memory.

Table of Contents

List of Tables

List of Figures

Chapter 1

Introduction

Soil water repellency (SWR) is a widespread phenomenon that refers to the delay of water absorption in hydrophobic dry soils. This issue has been identified in different soils and climate combinations (Dekker et al., 2005). Theoretically, the origins of water repellency are the hydrophobic compounds coating the hydrophilic soil minerals. This causes water droplets to ball up on the dry soil surface and prevent it from infiltration (Doerr et al., 2000). The decrease in water infiltration has major repercussions for water runoff, plants growth and nutrient loss (Leitch et., 1983). In New Zealand, SWR has negative environmental and economic consequences on the pastoral systems. In a study of 15 pastoral sites, Müller et al., (2010) reported that SWR caused pastures growth to decrease between 5 and 20% and increased the risk of herbicides loss through the water surface runoff. The authors stated that SWR constitutes a risk for New Zealand's pasture production, particularly with eventual climate changes leading to periodic summer droughts. In another study, Müller et al., (2014) demonstrated that a large part of the variability in pasture production was affected by the degree and the persistence of SWR. In Australia, this issue affects more than 10 Mha of arable soils (Roper et al., 2015). In pastures, losses related to water repellency are significant and have been reported to be around 30% annually for dry-sown lupin (Blackwell et al., 1994). The decrease in water filtration is presumed to be an important cause of increases in runoff, erosion and nutrient loss (Leitch et al., 1983). To properly understand this problem, an effective characterisation of water repellency and its dynamics is needed. Knowing the severity, nature and occurrence probability of SWR in different points of an agricultural field may help reduce nutrient loss through site-specific management (e.g. fertiliser application). There are numerous methods to measure SWR in the laboratory and the field, however, these conventional methods are time-consuming and point scale measurements. Thus, the possibility of constructing reliable spatial and temporal data using these methods is limited. There were a few attempts at characterising SWR spatial and temporal dynamics using novel approaches. Infrared thermography (Abrantes et al., 2017) and laboratory visible and near-infrared spectroscopy (Kim et al., 2014) were tested as an alternative method for the assessment of SWR. These studies showed promising results, indicating the potential of the remote sensing approach for water repellency assessment. However, there was no research work on the possibilities of using remote sensing to assess SWR in the field, at farm or regional scale. The spatial characterisation of SWR in pastures could provide valuable data, which will help in the decision making related to fertilizers application, water repellency remediation

approaches, and grazing and thus reduce surface water runoff and phosphorus loss in surface runoff. This general introduction discusses research history, current methodologies and understanding of soil water repellency. The knowledge gaps related to the impact on surface runoff, soil nutrient movement and the possibilities of using remote sensing as novel approach for water repellency will be highlighted.

1.1 Chronological and global highlights

Soil water repellency historical background was reviewed by DeBano (2000). They highlighted that Schreiner and Shorey (1910) were the first to report a soil that could not be wetted either by irrigation, rain, or water movement from the subsoil. The period between the 1920s and the 1940s saw the earliest development of the understanding of SWR occurrence. Albert and Köhn (1926) work on water repellent sands and report on the creation of artificial catchments by Kenyon (1929) were the only publications implicating SWR in this period. Several studies started emerging in several journals in the 1940s. Jamison (1947) demonstrated that the low soil wettability reduced the citrus orchards' productivity in Florida, USA. Low wetting soils were also reported in the Netherlands by (Domingo 1950). In the late 1950s, Woudt (1959) reported that organic coatings of soil particles altered the soils' wettability in New Zealand. The 1960s and 1970s decades witnessed important milestones in SWR research. Many intelligible studies from the USA and Australia targeted a broad range of aspects of water repellency. Over 80 publication was published on different aspects of water repellency in this period (Fig. 1). A major milestone was the development of a physical method to characterise SWR using the contact angle method by Letey et al., (1962). The number of publications on SWR has increased exponentially after the 1980s in different parts of the world.

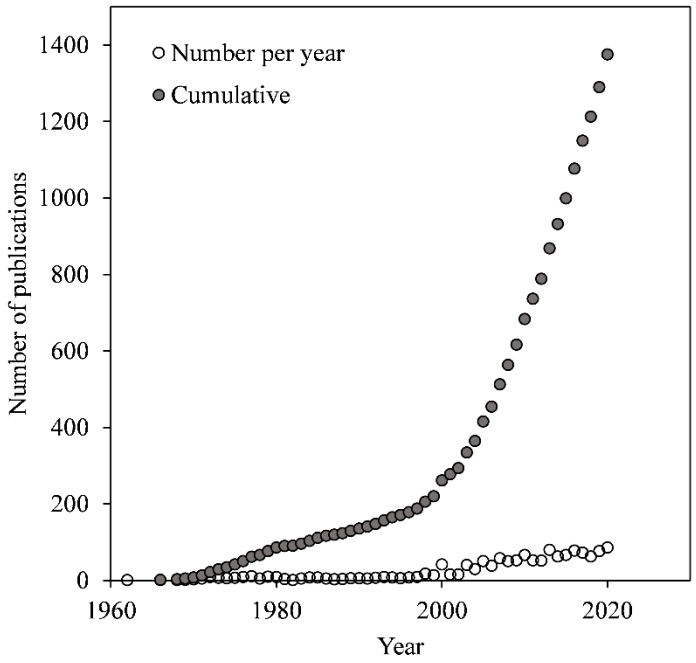

Figure 1-1 Number of publications and the cumulative number of publications on soil water repellency. Data acquired from Scopus database. The search was conducted within the article title, abstract, and Keywords using "soil water repellency" keywords.

The scientific production in different regions of the world translates the wide range of climates, soils, and ecosystems where water repellency issues might arise (Fig. 2). Water repellency has been the object of systematic studies since the 1960s and gained remarkable effervescence after the year 2000. The number of documents by country published between the 1960s and 2020 shows that the USA, Australia, Netherlands, New Zealand had the higher number of publications on soil water repellency (Fig. 2).

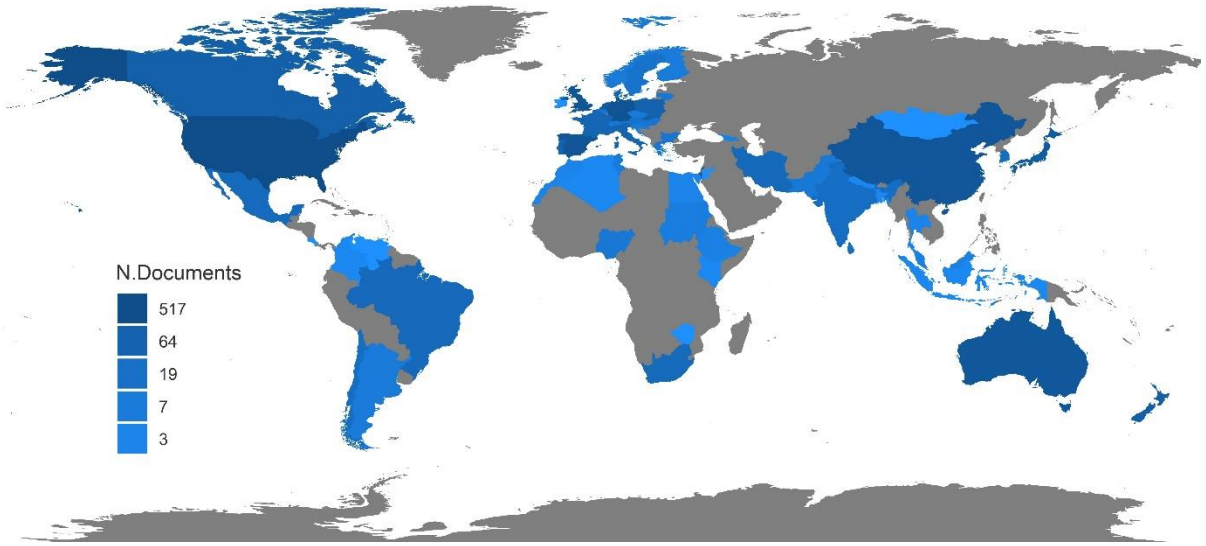

Figure 1-2 Number of publications per country between 1960 and 2020. Data was acquired from the Scopus database. The search was conducted within article title, abstract, and Keywords using "soil water repellency" keywords and over 1400 publications were found.

1.2 Characterisation of soil water repellency

Soil water repellency has been reported to decrease water infiltration, inducing runoff and soil erosion. A better understanding of the SWR required an advanced characterisation of the components causing hydrophobicity in soils. Characterisation of SWR was reviewed by Doerr et al., (2000). Several investigations have been done to chemically characterise the hydrophobic materials causing SWR. Horne and McIntosh, (2003), extracted organic compounds from sandy soils of the southwest coast of New Zealand's North Island and classified the extractions into lipid and water-soluble fractions. Identification of the extractions showed that lipid fraction contains neutral, acidic, and polar lipids. The water-soluble fraction was reported to show amphipathic characteristics. This study showed that water repellency was ruled by the nature of the organic compounds rather than the total carbon content. Another investigation by Franco et al., (2003) on the physicochemical characteristics of hydrophobic Australian sands was carried out through the extraction and the analysis of natural waxes coating the sands. The analysis of the extracted waxes showed that they comprised mainly branched and unbranched C_{16} to C_{36} fatty acids and their esters, phytanols, alkanes, phytanes and sterols. McKissock et al., (2003) had established a link between SWR and aliphatic C and kaolin measured using diffuse reflectance infrared Fourier transform. This method was suggested earlier by Capriel et al., (1995) to estimate SWR in the lab, based on the principle that

the hydrophobicity of organic matter is caused by methine, methyl, and methylene groups present in aromatic and aliphatic compounds.

The potential SWR, which is the higher level of water repellency can attend, is related to the chemistry, amount, and arrangement of the hydrophobic compounds at soil particles at the nanoscale. However, the actual soil water repellency is highly affected by soil water content. Previous research showed that generally SWR is negatively correlated with soil moisture in field conditions (Dekker et al., 2001; Müller et al., 2014). In a study of the relationship between the severity, the persistence of SWR and the critical water content (CWC) in soils from 13 sites including natural, reclaimed and agricultural soils, Chau et al., (2014) found that high severity does not necessarily mean a long persistence or high CWC. The authors reported that the measured values of severity and persistence are associated with differences and variations in surface energy between water and the soil surface, respectively. This examination of repellency variations as a function of CWC for the studied soils revealed different patterns. Some soils showed a rapid decrease of contact angle when water content increased; this indicated less severity, regardless of the initial repellency. Other soils showed a slow decrease in contact angle at low water contents, which indicated high severity and a need for more water or surfactant for remediation (Chau et al., 2014). Most of the previous work on the SWR-soil moisture relationship was carried out by changing soil moisture by adding water and measuring the repellency level after equilibrium for specific water content. However, studying water repellency as a function of moisture for drying soil could have different dynamics. The only study that investigated the water repellency characteristic curves in drying soils was carried out by Li et al., (2016) using artificially hydrophobised soils. However, understanding the characteristic curves of naturally hydrophobic drying soils is needed. This could allow the modelling and mapping of the actual water repellency levels, using soil moisture data and the potential SWR level which per se could be estimated using a remote sensing approach.

1.3 Soil water repellency measurements

To make comparisons amongst the overwhelming number of works on SWR in different areas around the world it was necessary to work with standardised methods. Traditionally, different methods have been proposed for SWR measurement. The following section provides an overview of the different methods used in SWR characterisation as reviewed by Letey et al., (2003).

1.3.1 Contact angle

The wettability of a solid is tied to the value of the solid-liquid contact angle. When a droplet of water is placed on a hydrophobic surface, it balls up, and thus forms a large contact angle with

this surface. However, water droplet placed on a hydrophilic surface tends to spread and have a narrow contact angle (Fig. 3).

Figure 1-3 Representation of the variation of the contact angle as a function of water repellency (from Deurer & Müller, 2010)

To measure the contact angle, Letey et al., (1962) assumed the soil to be presented by cylindrical capillaries. The pressure (P) applied to the liquid rising on these capillaries was expressed by capillary and gravitational forces. The capillary pressure is:

$$P_c = \frac{2\gamma \cos\theta}{r} \quad (1\text{-}1)$$

where θ is the solid-liquid contact angle, r in the capillary radius, and γ is the liquid-air surface tension. The gravitational pressure is:

$$P_g = \rho g h \quad (1\text{-}2)$$

where ρ the liquid density, g the gravitational constant, and h the height of the rise.

Since $P_c = P_g$ at the equilibrium, the height of the capillary rise is:

$$h = \frac{2\gamma \cos\theta}{\rho g r} \quad (1\text{-}3)$$

Letey et al., (1962) found that ethanol wet all the soil materials with a contact angle of zero. This helps in deducing the capillary radius, which in turn could be used to determine the contact angle for water or other solution used in infiltration. Thus, the contact angle could be calculated using the following equation:

$$\cos\theta = \frac{h_w \gamma_e \rho_w}{h_e \gamma_w \rho_e} \quad (1\text{-}4)$$

where $h_w \gamma_w \rho_w$ and $h_e \gamma_e \rho_e$ are the height of the rise, liquid-air, and surface tension of water and ethanol, respectively.

1.3.2 Water drop penetration time

The water drop penetration time (WDPT) approach involves placing water drop on the soil surface and recording the time it takes to penetrate (Letey et al., 2003). As the water penetrates the soil when the contact angle θ is less than 90º, WDPT measures the time taken by θ to change from values >90º to 90º. Doerr et al., (1998) standardised the WDPT method by placing 5 or 15 droplets of distilled water on the soil surface. The penetration time was recorded for each drop and the median was considered to represent the WDPT. For soil water repellency classification, this standardization used 11 penetration time categories instead of only five (Bisdom et al., 1993) to ensure high resolution of WDPT.

1.3.3 Ninety-degree surface tension

Based on the assumption that liquids can penetrate the soil only if θ is less than 90º, (Watson and Letey, 1970) proposed the liquid surface tension that enters the soil at 90º to be an index of SWR. To identify this surface tension, a series of dilutions of ethanol in water are prepared and the respective drops are placed on the soil surface. The increasing gradient of ethanol concentrations engenders decreasing surface tensions. Drops with a surface tension higher than that of the soil surface will persist on the surface, while the drops with inferior surface tension will enter immediately. The 90° surface tension was assumed to be the transition from penetration to persistence on the soil surface with five seconds as an arbitrary time of drop infiltration (Letey et al., 2003).

1.3.4 Molarity of Ethanol Droplet test

The molarity of ethanol drop (MED) test is derived from the 90º surface method as they share the same principle and logic, except that it considers the ethanol molarity of the droplet as an index of water repellency (instead of the surface tension). King, (1981) used ethanol solution of concentrations intervals of 0.2 M with a range of 0-5 M. Water repellency was represented by the ethanol molarity of the droplet that entered the soil surface in 10s. Only four classes of water repellency were adopted based on MED values (7 classes were used by Doerr, (1998)).

1.3.5 Solid-air surface tension

A key physical characteristic of a solid is the solid-air surface tension γ_s. The measurement of this property that affects the wetting behaviour provides valuable information. Carrillo et al., (1999) and Letey et al., (2003) combined previously published developments to measure the solid-air

surface tension. In this development, the solid-vacuum surface tension was assumed to be equal to solid-air surface tension (γ_s) and the liquid-vacuum surface tension to be equal to liquid-air surface tension(γ_l). Carrillo et al., (1999) used the equation:

$$\gamma_{sl} = \gamma_s + \gamma_l - 2\phi(\gamma_s\gamma_l)^{1/2} \quad (1\text{-}5)$$

where the constant ϕ is a function of molecular properties of the solid and the liquid with empirical values ranging from 0.5 to 1.15 and approximately unity for a water-hydrocarbon system (Adamson 1982). Assuming the liquid is in contact with soil for a certain time and become stationary. This leads to a speeding equilibrium pressure equal to zero ($\gamma_s = \gamma_l$). Young (1805) suggested that the contact angle θ at three phases contact is determined by balance of surface tensions (Fig. 1-4). This assumption could formally be translated to the following equation (Makkonen 2016).

$$\gamma_s = \gamma_{sl} + \gamma_l \cos\theta$$
$$\gamma_l \cos\theta = (\gamma_s - \gamma_{sl}) \quad (1\text{-}6)$$

Image removed for Copyright compliance

Figure 1-4 Young's representation for the contact angle between a solid and liquid drop and its vapour (from Makkonen, 2016)

Combining Eq. 1-5 and 1-6, we get

$$\cos\theta = 2(\gamma_s/\gamma_l)^{1/2} - 1 \quad (1\text{-}7)$$

For the ninety-degree surface tension $\gamma_l = \gamma_{ND}$ (θ=90°; $\cos\theta = 0$) Eq. 1-7 becomes

$$\gamma_s = \gamma_{ND}/4 \quad (1\text{-}8)$$

1.3.6 Breakthrough pressure head

Soil water repellency is a transient property. Thus, contact with water causes soil wettability changes over time. Carrillo et al., (1999) proposed a technique to measure the initial soil-water contact angle. For contact angle θ>90°, a positive pressure should be applied to force water infiltration into the capillary tube. This pressure was named the breakthrough pressure head (h_p) and was calculated using the following equations:

$$h_p = {}^{2[(\gamma_w\gamma_{ND})]^{1/2} - \gamma_w}/_{r\rho g} \quad (1\text{-}9)$$

The contact angle, θ, was related to γ_{ND}through the submission of Eq. (1-6) into Eq. (1-5)

$$\cos\theta = [(\gamma_{ND}/\gamma_w)^{\frac{1}{2}} - 1] \quad (1\text{-}10)$$

These equations were validated using experimental apparatus that records the breakthrough pressure head when water penetrates sand packed in a plastic column (Carrillo et al., 1999). The soil pore radius, r, can be computed using the values of h_p and γ_{ND}.

This overview of the main methods used for SWR characterisation shows that their major limitation is that they are dedicated to point-scale measurements. However, previous research has established that SWR has a very high spatiotemporal variability. In a study investigating the temporal variation of the field actual SWR on sandy forest soil, Buczko et al., (2005) found a notable seasonal variability from being extreme in summer to low in autumn. In the same vein, Dekker et al., (2001) found a pronounced spatial variability of SWR in soil depth varying from 0 to 19 cm. Horizontal and vertical SWR variation in afforested mine soils was noticed at the decimetre scale (Gerke et al., 2001), and has even a considerable variability at the millimetre scale in grassland soils (Hallett et al., 2004). This evidence regarding the temporal and spatial variability of SWR highlight the difficulties in (1) precisely assessing its level in different points of the field using the conventional methods; (2) predicting its occurrence over a small lapse of time. Therefore, new tools and methods are needed to track SWR temporal and spatial dynamics. Another major limitation of these methods is they are time-consuming. This makes it very difficult to construct spatiotemporal data, describing SWR variations in the field using these methods. Settling for data generated by these point measurements obfuscate our understanding of this phenomenon and its repercussion on pastoral ecosystems. Remote sensing could provide a promising solution to map SWR dynamics instead of using interpolations of point scale data. However, there has been a diminutive effort in using remote sensing for SWR assessment in the past. Testing the possibilities of using topsoil reflectance through both multispectral and hyperspectral satellite data for SWR estimation is needed.

1.4 Hyperspectral remote sensing

Methods of SWR measurement are laborious, costly, and involve point scale measurements, which means mapping SWR at the farm or regional scale is constrained. Remote sensing could provide an efficient technique for mapping SWR at multiple scales. Visible, near-infrared (Vis-NIR), and shortwave-infrared (SWIR) hyperspectral remote sensing have opened new possibilities for assessing topsoil attributes and creating digital soil maps. Numerous studies proved that hyperspectral remote sensing can be useful for estimating multiple soil properties. Well-known examples include soil C (Castaldi et al., 2016; Cécile Gomez et al., 2008; Leone & Escadafal, 2001) soil

texture (Casa et al., 2013; Galvão et al., 2008), pH and EC (Ben-Dor et al., 2002). Empirical models were developed to estimate soil properties that are associated with chemical chromophores altering surface reflectance at specific bands (e.g. OH groups in clays) (Ben-Dor et al., 1999) or properties that are reliably correlated with them (e.g. soil C with nitrogen). Hence, correlations of SWR with soil C (Hermansen et al., 2019a) and specific organic materials (Bisdom et al., 1993) could be utilised to predict SWR from surface reflectance signatures. However, no study has investigated the capability of remote sensing surface reflectance data for SWR assessment. Earlier attempts used laboratory VNIR/SWIR spectroscopy for estimating the potential SWR (Kim, I. et al., 2014) and predicting the relationship between SWR and soil moisture (Hermansen et al., 2019b; Knadel et al., 2016). Nevertheless, characterising SWR using satellite data presents a matchless advantage to map soil properties at larger scales, i.e., from farm to regional scale. Evaluating soil surface reflectance satellite data for predicting SWR and soil C has not been attempted in permanent pasture systems. Working with hyperspectral satellite data presents three major challenges. First, because of its high dimensionality, hyperspectral data storage and processing represent an issue to be reckoned with; especially when dealing with data at regional scales. Second, often adjacent bands provide similar information, thus for many applications, bands redundancy will be present. Third, to maintain the classification accuracy, the number of observations required to train a classifier increases exponentially when the number of bands in the image increases. In the past twenty years, multiple hyperspectral sensors have been used for soil C monitoring at different scales, in different studies. These studies used ground, airborne and spaceborne sensors. However, there were very few applications of spaceborne hyperspectral sensors compared to airborne hyperspectral sensors. The revisit feature and the global coverage provided by satellite data poses key advantages over ground and airborne hyperspectral data. These unique features raised special attention to the satellite hyperspectral sensors for soil C assessment and mapping. Although the prevalent number of studies implicating airborne data, the number of studies using satellite hyperspectral data is still very limited (Table 1-1). In this thesis, the use of hyperspectral satellite data from Hyperion was tested for modelling and estimating SWR and soil C levels in permanent pastures.

Table 1-1 Case studies on the use of hyperspectral remote sensing to estimate soil organic carbon.

Sensor	Method	n	R^2	RMSE	RPD	Research
AHS	PLSR	306	0.54	6.08	1.50	(Stevens et al., 2010)

	PLSR	81	0.75	2.2	1.9	(Steinberg et al., 2016)
	PLSR	89	0.78	7.01	2.13	(Peón et al., 2017)
APEX	PLSR	88	-	3.6	2.1	(Castaldi et al., 2018)
AISA	PLSR	40	0.89	0.27	3.03	(Kanning et al., 2016)
AVNIR	MLR	321	0.48	0.08	-	(DeTar et al., 2008)
CASI	SMLR	50	0.74	0.49	-	(Uno et al., 2005)
	ANN	50	0.59	0.59	-	(Uno et al., 2005)
	PLSR	234	0.85	5.1	1.86	(Stevens et al., 2006)
	SVM	45	-	0.12	2.05	(Gholizadeh et al., 2018)
HyMAP	PLSR	72	0.90	0.29	-	(Selige et al., 2006)
	MLR	72	0.86	0.22	-	(Selige et al., 2006)
	PLSR	95	0.02	2.6	0.99	(Gomez et al., 2012)
	PLSR	142	0.98	0.67	7.48	(Patzold et al., 2008)
		61	0.87	0.08	2.90	(Schwanghart et al., 2011)
		204	0.83	1.05	2.45	(Hbirkou et al., 2012)
		38	0.71	1.64	1.80	(Gerighausen et al., 2012)
		42	0.73	0.25	1.94	(Vohland et al., 2017)
Hyperion	PLSR	303	0.52	4.88	-	(Jaber et al., 2011)
	SPR	303	0.39	5.76	-	(Jaber et al., 2011)
	PLSR	65	0.51	0.73	1.43	(Gomez et al., 2008)
	PLSR	49	0.63	1.60	1.65	(Lu et al., 2013)
	PLSR	33	0.71	0.26	1.88	(Zhang et al., 2013)
		713	0.27	0.46	1.23	(Castaldi et al., 2016)
		111	0.61	0.76	-	(Minu et al., 2017)
	PLSR	72	-	0.38	-	(Castaldi et al., 2014)
	SMLR	39	0.62	9.05	1.62	(Peón, Recondo, et al., 2017)
	PLSR	31	0.66	0.18		(Nowkandeh et al., 2018)
HyperSpecTIR	PLSR	269	0.65	0.19	-	(Hively et al., 2011)
ProspecTIR	PLSR	60	0.75	2.22	1.98	(Franceschini et al., 2015)
RDACS/H-3	PLSR	645	0.56	-	-	(Bajwa and Tian 2005)
TASI	PLSR	52	0.80	0.11	-	(Eisele et al., 2012)
	PLSR	58	0.95	0.08	4.51	(Pascucci et al., 2014)

1.5 Multispectral remote sensing

Even though satellite hyperspectral remote sensing offers a useful tool to estimate soil properties, the limited availability of hyperspectral data has impeded its use. Till 2018, Hyperion aboard Earth Observing 1 (EO-1) was the only functional hyperspectral sensor (Folkman et al., 2001). The newly deployed hyperspectral sensor PRISMA (Loizzo et al., 2018) offers a spectral resolution of 10 nm, a spatial resolution of 30 m for VNIR/SWIR bands, 10 m for panchromatic bands, a swath width of 30 km and a revisit time of 7 days. In comparison with hyperspectral sensors, multispectral sensors like Landsat-7 have a lower spectral resolution. Still, Landsat-7 provides the most valuable multispectral global archive (Kovalskyy & Roy, 2013). The recently implemented Sentinel-2 satellites by the European Space Agency (ESA) offer multispectral images with high revisit times (2-3 days) that include 13 bands (VNIR/SWIR) and have a spatial resolution between 10 and 60 m (depending on the bands). Yet a small number of studies accomplished good accuracy in predicting topsoil physical and chemical properties using multispectral satellite images. Using Sentinel-2 multispectral data, Vaudour et al., (2019) obtained a useful model with an intermediate prediction accuracy for soil C (R^2=0.56; RMSE=1.23), pH (R^2=0.51; RMSE=0.51), and CEC (R^2=0.75; RMSE=1.23) in a temperate and in a Mediterranean region. In terms of comparison between hyperspectral and multispectral remote sensing, Castaldi et al., (2019) reported that there was no considerable difference between the spatial variability of soil C maps obtained from Sentinel-2 data and the ones derived by hyperspectral airborne data for a study area dominated by cropping. Likewise, Gomez et al., (2018) reported that there was no substantial difference between Sentinel-2 and hyperspectral (airborne and satellite) data in estimating clay content in a semiarid Mediterranean region.

Prediction accuracies of remote sensing methodologies rely on the quality of the remote sensing data, modelling approach, and the ground-truthing conducted. Remote sensing using satellite data poses many challenges including the atmospheric interaction with reflected electromagnetic radiation, surface roughness and the nature of the land cover. Ben-Dor, (2002) reviewed in detail the challenges and the difficulties influencing quantitative remote sensing of soil properties. Estimating the topsoil properties of permanent pastures is even more challenging because of the additional complexity through the temporal dynamics of the surface biomass and water content. Surface biomass in permanent pastures impedes bare soil surface reflectance acquisition. Hence, finding a reliable procedure to deal with this issue is required. In permanent pastures, topsoil spectra could be obtained by selecting dates with the least surface biomass using an NDVI threshold. Grass surface biomass and per cent ground cover are positively correlated with NDVI values (Prabhakara et al., 2015). Regarding the topsoil moisture effect on surface reflectance,

the increase in water content decreases surface reflectance over the whole VIS-NIR and SWIR spectrum and especially in 1200, 1400, and 1800 nm wavelengths (Lesaignoux et al., 2013; Lobell & Asner, 2002). Hence, the moisture effect could be reduced by considering spectra with the highest reflectance from time-series data as dry topsoil spectra. This approach will be tested on Landsat-7 and Sentinel-2 time series to determine its efficacy in acquiring topsoil spectra to be used for modelling soil C and SWR.

1.6 Predicting the occurrence of soil water repellency using remote sensing time series data

Previous attempts tested lab visible and near-infrared spectroscopy for SWR assessment (Kim et al., 2014; Hermansen et al., 2019b). Although these studies proved promising results, acquiring topsoil surface reflectance can be challenging using satellite data. Issues like cloud cover and permanent vegetation cover make it difficult to acquire soil reflectance values. Numerous studies used different approaches such as normalised difference vegetation index (NDVI) (Burnham and Sletten 2010; Zhang et al., 2019), or NDVI and multiple environmental predictors to assess and map soil carbon at regional scales (Wang et al., 2017). The later approach relies on the surface biomass dynamics and important variables influencing soil C cycling, such as precipitation, temperature, and land use. This approach could help predict the occurrence of SWR based on temporal dynamics of key factors controlling hydrophobic compounds cycling in the soil C pool.

Water deficit and pasture management are crucial factors controlling surface biomass temporal dynamics. Remote sensed surface biomass and water deficit temporal dynamics could offer a useful tool to predict SWR occurrence in permanent pastures. However, testing this novel approach with real data from pastoral systems is needed to draw any conclusions on its efficacy. Assessment of surface moisture using the Synthetic Aperture Radar (SAR) and surface biomass using satellite multispectral data could provide a large advantage in terms of spatial and temporal assessment of biomass dynamics. Satellite multispectral reflectance gives valuable information of the aboveground biomass state, which is directly involved in the cycling of hydrophobic compounds. The normalised difference vegetation index is highly correlated with surface biomass and surface cover percentage (Prabhakara et al., 2015). Synthetic Aperture Radar backscatter showed a high relationship with the soil surface moisture (Zhang et al., 1998). Exploiting the available NDVI, water deficit and SAR time series (TS) data could allow the evaluation of surface biomass dynamics and therefore, reflect the impact on SWR occurrence. These interactions between topsoil moisture, biomass temporal dynamics, and the appearance of water repellency are still scantily understood.

Jaramillo et al., (2000) theorised that dry conditions would result in low biomass production rates and, thus, a lesser likelihood for the development of SWR. While humid conditions are beneficial for biomass production and, therefore, to produce hydrophobic compounds from decomposed biomass. According to this theory, carbon and hydrophobic materials share the same cycling mechanisms, assuming that hydrophobic compounds are a natural component of the soil C pool in pastoral ecosystems. In the present thesis the use of water deficit, NDVI and SAR time series data will be tested to predict the occurrence of SWR in pastures.

1.7 Effect on hydrological processes

1.7.1 Effect on water dynamics and evaporation

Much of the literature on SWR pays attention to its effect on water movement. Numerous authors have considered the effect of water repellency on surface runoff, water infiltration, and evaporation. Ritsema and Dekker, (1994) showed that water paths were affected by the degree of water repellency and that the repellent volumes between these paths temporary prevented water and solute transport. In the same vein, Burch et al., (1989) noted that soil surface water repellency reduces water infiltration and caused runoff in a forested catchment to increase significantly. Similarly, in Japanese cypress forests, surface runoff was increased by SWR which, in its turn, was influenced by the length of the drying period between rainfall events and thus by soil water content (Miyata et al., 2007). Clay soils with grass cover showed the presence of preferential water flow paths due to water repellency (Dekker and Ritsema, 1996). These preferential flow paths have also been found in sandy soils, where water and solute flows are influenced by extreme water repellency (Ritsema and Dekker, 1995; Ritsema et al., 1993). Doerr et al., (2003) identified water repellency as a major cause of the reduction of soil wettability and its associated flow response at a laboratory scale. In an investigation into raindrop impact on soil particles mobilization, Ahn et al., (2013) found that SWR affected splash erosion, causing the water droplet to induce higher and longer trajectories for hydrophobic soil particles than hydrophilic ones. Regarding water evaporation, SWR was reported to reduce water evaporation from the soil. Rye and Smettem, (2017) showed that the increase in water repellency led to a significant decrease in water evaporation. In this study, the soils covered with a decreasing repellent layer over 10 to 30 cm depth exhibited evaporative losses over 70% lower than the wettable soils.

1.7.2 Soil water repellency and water content relationship

The actual SWR level is strongly related to soil water content. Water repellency as a function of water content, which is commonly referred to as the SWR characteristic curve has been examined in numerous studies (Chau et al., 2014a; Hermansen et al., 2019a; Wijewardana et al., 2016). Nevertheless, most of the prior studies were dedicated to the water repellency severity and soil moisture relationship, and less work has been made on SWR persistence dynamics. The characteristic curves of SWR severity as a function of soil water content have been examined in reclaimed soils (Chau et al., 2014a), pastoral (Hermansen et al., 2019a), and a forest ecosystem (Karunarathna et al., 2010). Different studies showed that the SWR severity characteristic curves are usually a unimodal curve where the contact angle increases with decreasing water content, achieves a peak, and then declines again (Kawamoto et al., 2007). Other studies showed bimodal response curves, sigmoidal curves or irregular patterns (Chau et al., 2014a; Hermansen et al., 2019a). The issue with the patterns observed in these lab studies is that water repellency dynamics are different from the observed field patterns. Most of the field work showed that the actual water repellency increased dramatically with soil water content decrease. Results from Dekker et al., (2001) who studied soil water repellency persistence in dune sands showed a significant increase of water repellency persistence when water content drops below a *critical* value. The difference between these patterns observed in the field and the laboratory simulation could be due to the differences in drying and wetting regimes. To simulate the SWR persistence dynamics in drying periods, soil drying conditions need to be similar to field drying. In the present thesis, we investigated the effect of soil drying on water repellency persistence dynamics of hydrophobic pastoral soils. This will help comprehend and quantify the impact of dying on soil water repellency occurrence in pastoral soil.

1.8 Effect of runoff nutrient losses in pastoral systems

Fertilisers are critical inputs in the New Zealand agricultural systems. The use of fertilisers has increased over the last 50 years, with phosphorus (P) as the main fertiliser nutrient applied in the sheep-beef farms. However, P application to these pastoral systems and its release from catchments to streams was associated with water quality issues. In fact, in addition to nitrogen, P is a key element that sustains aquatic biomass growth. Therefore, these two elements are a potential source of drinking water pollution but also limiting factors of eutrophication inducing alga blooms and dead zones in aquatic ecosystems (Conley et al., 2009; McDowell et al., 2020). Phosphorus control alone has been proven to abate eutrophication in many studies reviewed by Schindler and Vallentyne, (2008).

Phosphorus loss can have both anthropogenic and (or) natural causes. Transport processes are the link between agroecosystems and catchments estuaries. The combination of the dominant transport processes with land management results in *critical source-areas* in catchments (Gburek et al., 2005). These particular and identifiable areas are the most susceptible to P loss (Gburek et al., 2005). Identification of P losses applies an understanding of the mechanisms of P mobilization and an accurate examination of soil physicochemical characteristics, agricultural practices and climatic factors. Haygarth and Jarvis, (1999) described two basic mechanisms generally known to be involved in P mobilization. (1) Solubilization, which is a chemical process, was defined as all P from analysis after a <0.45 µm filtration. This process involves the transfer of P from a solid phase to a soluble phase (soil solution) due to chemical non-equilibrium between the two phases. And (2) the physical detachment of soil colloids and particles associated with P by the kinetic energy of water. When it comes to the soil, the type and acidity are the main criteria determining how P reacts with soil minerals. Condron et al., (2005) and Shen et al., (2011) reviewed the physicochemical factors influencing P retention and availability. In acidic soils, P retention is dominated by Al and Fe oxides and hydroxides; for instance, hematite, gibbsite and goethite (Parfitt 1989). In neutral and calcareous soils, P mainly occurs as Ca- and Mg-phosphates precipitates or sorbed to Ca- and Mg-carbonates (Lindsay and Moreno, 1960). Although the soil chemical properties determine P availability, the hydrological processes are still decisive in P transport and fate (McDowell 2012). Rainfall intensity and frequency influence the amount and concentration of P lost through the runoff or drainage. Rainfall events with high intensity resulted in P losses through the surface runoff and the losses were accentuated when the soils became water repellent after a dry period (McDowell 2012).

Multiple trials on P losses in pastoral soils indicated that P losses via surface runoff decreased exponentially after P-fertiliser application, with the higher losses recorded in the first overland flow event following P fertiliser application (McDowell et al., 2003; McDowell et al., 2003; Nash et al., 2005). These trials show in the early runoff events subsequent to fertiliser application are mainly influenced by fertilisers' solubility and application rate. However, P losses concentration in surface runoff is independent of the fertilisers' solubility or application rate after this period (after three important runoff events) (McDowell et al., 2003). Nash et al., (2019) theorised that P exports from the topsoil are controlled by transfers of P precipitates from fertiliser granules after fertilisers application. This form of P mobilisation, which is a direct export of the P source itself, has been considered *incidental* (Gburek et al., 2005; Preedy et al., 2001). Therefore, the application rate and fertiliser solubility are the most important factors during this period. The subsequent period P losses are related to soil P status (McDowell and Catto 2005). These *background* losses were considered

non-incidental. McDowell and Condron (2004) reported that P losses in simulated runoff are highly correlated with soil P extractability by water and suggested the use of H_2O extractable P to assess non-incidental P concentrations in runoff. However, estimation and modelling of P loads in surface runoff require an understanding of the relationship between P concentrations and runoff volumes. Nash et al., (2019) reported that TP concentrations in individual runoff events were unrelated to runoff volumes in field conditions. Lucidly, it is difficult to comprehend the relationship between runoff magnitude and P concentrations in surface runoff without dealing with incidental and non-incidental P separately. The effect of severe hydrophobicity on non-incidental P losses in surface runoff is unknown in post-summer runoff events, in field conditions. In the present thesis, surface water runoff and P concentration in runoff were quantified in a field trial including wettable and hydrophobic soils in post-summer runoff events. This trial had the objective to understand the implication of SWR in P losses in both incidental and non-incidental P losses in pastoral soils.

1.9 Remediation of SWR

A range of remediation strategies has been used to reclaim repellent soils. Müller and Deurer, (2011) review 12 key direct and indirect remediation strategies. Direct strategies including clay spreading, surfactants, cultivation and aeration aim to eliminate SWR causes. While indirect strategies that include liming, fungicides and slow-release fertilisers aim to alleviate the symptoms and the environmental impact of water repellency. The authors highlighted that it is not easy to remedy SWR using easily measurable and site-specific soil and vegetation properties and attributed this to the poor understanding of SWR evolution in the field. Amongst the different remediation methods, clay spreading has been largely used against SWR. This strategy has significantly enhanced the wettability of repellent sandy soils in Australia (Cann 2003). However, clay spreading may be very costly if clay is not available close to the application site. Organic amendments can increase significantly the repellency of agricultural soils. Provided that the organic compost will potentially become the main inputs of future farming systems, innovative and cost-effective methods are needed to decrease their effect on soils wettability. In an attempt to reduce the hydrophobicity of an organic amendment, thermal treatment was adopted by Comino et al., (2017) who effectively treated olive mill pomace waste by heating it to 275 °C. Heat has been also used to reduce SWR and increase water infiltration rate in soil aquifer treatment (Nadav et al., 2013). This method seems to be practical as it does not need a chemical surfactant or any other agent to control the water repellency of the organic amendment.

Surfactant application is a common practice in agriculture and golf courses since the 1960s. When dissolved in water, surfactants decrease surface tension. The decrease in surface tension of water results in lowering its contact angle with soil and thus enhancing soil wettability. Surfactants are well known for the remediation of water repellency in turfgrass sandy soils (Kostka, 2000; Oostindie et al., 2008). Different field trials showed that surfactants application considerably decreased the critical moisture content and water repellency in the surface layer (Dekker et al., 2003), restored turfgrass quality in severely water repellent golf greens (Aamlid et al., 2009), and improved the homogeneity on the wetting and enhancing grass performance (Cisar et al., 2000). Dekker et al., 2019 theorised that the increase in turfgrass quality is related not only to the improvement in wetting distribution but also to the effect on nitrogen availability. However, the study they conducted to test this hypothesis showed no significant differences in NO_3, NH_4, and total soluble nitrogen, between control and surfactant treatments. Testing the efficacy of these products is limited due to the unpredictability of SWR occurrence. Leinauer et al., (2007) tested 10 different commercial wetting agents and reported that SWR was significantly decreased by these products, particularly at the surface (2.5cm depth). In a study on the use of surfactants to improve irrigation efficiency in golf putting greens in the southeast US, (Karnok and Tucker, 2008) reported that wetting agents enhanced the uniformity of water infiltration and thus decreasing the need for irrigation. Implementing a suitable remediation strategy at larger scales requires the assessment and mapping of water repellency for site-specific remediation. The remote sensing methodologies explored in this thesis would provide a unique advantage in mapping and remediating soil water repellency at larger scales.

1.10 Hypothesis and objectives

Hypothesis: Soil properties that are highly correlated with soil hydrophobicity and have high effect on soil surface reflectance can be used assess soil water repellency in permanent pastors.

General objective: Investigate the factors controlling the soil water repellency in pastoral systems and assess its levels using multispectral, hyperspectral, surface biomass, and water deficit temporal dynamics in permanent pastors.

Specific objective 1: To assess the factors controlling the actual and the potential soil water repellency and evaluate the effect of SWR on surface runoff and phosphorus losses.

Specific objective 2: To assess the capabilities of multispectral, hyperspectral, and surface biomass and moisture temporal dynamics for soil water repellency and soil carbon assessment in permanent pastures.

Chapter 2: The relationship between SWR persistence and soil moisture in hydrophobic soils.

Chapter 3: Surface runoff and losses of phosphorus from hydrophobic pastoral soils.

Chapter 4: Time series of remote sensing and water deficit to predict the occurrence of SWR.

Chapter 5: The potential of multispectral satellite data to predict SWR and soil C in pastures.

Chapter 6: hyperspectral satellite data to assess SWR and soil C in pastures.

Chapter 7: Summary**.**

Figure 1-5 Hypothesis, general and specific objectives and the organisation of the thesis chapters.

Chapter 2

The relationship between soil moisture and soil water repellency persistence in hydrophobic soils

This chapter has been published in a special issue: Soil water repellency, Water Journal.

Water **2020**, *12*(9), 2322; **https://doi.org/10.3390/w12092322**

2.1 Abstract

In this work, we modelled the response of soil water repellency (SWR) persistence to the decrease in moisture in drying soils, and we explored the implication of soil particle size distribution and specific surface area on the SWR severity and persistence. A new equation for the relationship between SWR persistence and soil moisture (θ) is described in this chapter. The persistence of SWR was measured on ten different hydrophobic soils using water drop penetration time (WDPT) at decreasing levels of gravimetric water content. The actual repellency persistence showed a sigmoidal response to soil moisture decrease, where $\mathrm{R_a}(\theta) = \mathrm{R_p}/1 + \mathrm{e}^{\delta(\theta-\theta_c)}$. The suggested equation enables one to model the actual SWR persistence $(\mathrm{R_a})$ using θ, the potential repellency $(\mathrm{R_p})$ and two characteristic parameters related to the shape of the response curve. The two parameters are the critical soil moisture θ_c, where the $\mathrm{R_a}$ increase rate reaches its maximum, and the parameter δ affecting the steepness of the curve at the inflexion point of the sigmoidal curve. Data shows that both soil carbon and texture are controlling the potential SWR in New Zealand pastures.

2.2 Introduction

Soil water repellency refers to the inability of soils to absorb water. This phenomenon has been identified in different soils and climate combinations (Dekker et al., 2005). Theoretically, the origin of water repellency is due to hydrophobic materials coating the soil particles (Bisdom et al., 1993). Doerr and Thomas (2000) theorised that after the amphiphilic molecules have been separated from the mineral particles during the wetting of the soil (making the soil particles wettable), these molecules remain intact. When the soil moisture becomes low enough during the drying process, their polar groups re-associate and interact through the hydrogen bonds, forcing the molecules back into position with the polar heads attached to the mineral surface and the non-polar tails orientated

outwards resulting in the reestablishment of hydrophobicity (Dekker and Ritsema 1994; Doerr et al., 2000; Doerr and Thomas 2000; Kaiser et al., 2015; Kawamoto et al., 2007; Tschapek 1984). Therefore, soils express water repellency when moisture drops below a critical water content. This issue has serious implications in decreasing water infiltration (Leighton-Boyce et al., 2007), inducing surface runoff, nutrient losses through runoff (Jeyakumar et al., 2014) and causing preferential flow (Jonge et al., 2009).

Soil water repellency can be characterised by two different criteria. Its severity or degree, which is an estimate of the soil surface tension, indicates the initial strength of the repellency between water and soil surface. The persistence is a measure of how long it takes to break down the repellent property after prolonged contact with water to make the soil wettable again. The severity of SWR can be estimated using the molarity of ethanol drop (MED) (Letey et al., 1962), contact angle (CA) (Carrillo et al., 1999) or, sessile drop methods (Bachmann, Ellies, and Hartge 2003; Chau et al., 2010). The persistence of soil water repellency (SWR) can be estimated using water drop penetration time (WDPT). The water drop penetration time approach involves placing a water drop on the soil surface and recording the time it takes to penetrate (Letey et al., 2003). As water infiltrates the soil surface when the contact angle is less than 90°, WDPT measures the time taken by the contact angle to change from values > 90° to 90° (Letey et al., 2003) or 0° if a complete drop penetration is considered (Letey et al., 1962).

The actual SWR level is tightly related to soil moisture. Soil water repellency as a function of θ, which is usually referred to as the SWR characteristic curve and has been investigated in different studies (Chau et al., 2014; Hermansen et al., 2019b; Wijewardana et al., 2016). However, most of the previous work has focused on SWR severity and moisture relationship (Chau et al., 2014; Hermansen et al., 2019b; Karunarathna et al., 2010), and less effort has been made on SWR persistence dynamics. The characteristic curves of SWR (MED or CA) as a function of soil moisture (θ) have been studied in reclaimed and agricultural soil (Chau et al., 2014), pastures (Hermansen et al., 2019b) and, forest ecosystems (Karunarathna et al., 2010). In a study of the relationship between the SWR severity and water content in natural, reclaimed and agricultural soils, Chau et al., (2014) revealed that SWR severity showed different patterns in drying soils. Some soils showed a rapid decrease in the contact angle when θ increased; this indicated less severity, regardless of the initial repellency. Other soils showed a slow decrease in contact angle at higher water contents, which indicated high severity and the need for more water or surfactants for remediation (Chau et al., 2014). The SWR severity characteristic curves are typically a unimodal curve where the contact angle increases with decreasing θ, reaches a peak and then decreases again (Kawamoto et al., 2007). Other studies

showed bimodal response curves, sigmoidal or irregular patterns (Chau et al., 2014; Hermansen et al., 2019b).

The SWR severity is a measure of the initial strength of the soil hydrophobicity and does not describe how soil behaves in prolonged contact with water. Thus, SWR measured with MED or CA, for example, does not permit the perception of how SWR influences natural hydrological processes. The parameters controlling the SWR persistence response to drying are to date, still poorly understood. The only study implicating modelling the persistence of SWR in drying soils was conducted on artificially hydrophobised soils (Li et al., 2016). Data from this study showed a typical sigmoidal curve of WDPT (θ) for sand and unimodal curves for finer textures. Artificially induced hydrophobicity has been used in many studies to understand the impact of water repellency on hydrological processes at the theoretical level. However, the stable characteristics of the artificial hydrophobic chemicals used for this purpose make it difficult to compare results with naturally hydrophobic soils. Natural SWR represents unique features because it results from a combination of natural hydrophobic materials of different sources (Franco et al., 2003). Modelling the SWR persistence characteristic curves is urgently needed for naturally hydrophobic soils. This will help to understand and quantify the impact of SWR on runoff and nutrients losses to waterways in agroecosystems.

Characterisation of actual SWR and water content relationship was assessed in field conditions (Müller et al., 2014; Ritsema and Dekker 1994), by adding water or drying soils in laboratory conditions (Hermansen et al., 2019b; Kawamoto et al., 2007; King 1981). Using air or oven-dry (65 °C) soils gives an estimate of the potential SWR, which is the highest level that SWR can reach when the soil dries out completely (Deurer et al., 2011; Ritsema and Dekker 1994). Estimation of the potential SWR provides insight into the potential consequences of soil hydrophobicity in an eventual drought situation. However, only in-situ measurement at field moist conditions gives the actual SWR level (Müller et al., 2014). Adding water would simulate the soil wetting phase but does not give information about SWR dynamics during the drying phase (Li et al., 2016). On a drying soil surface, the hydraulic potential is constantly changing, and hydrophobic compounds would not have the same behaviour toward soil minerals, as if they remained at constant water content for 48 h. Thus, understanding the SWR–moisture natural dynamics needs the closest possible scenario to field dry conditions. Moreover, the drying temperature has a significant effect on the reestablishment of SWR in sands (Dekker et al., 1998). The micromorphological investigation by Dekker et al., (1998) showed that high drying temperatures caused an increase in the formation of organic materials coatings responsible for SWR. Hence, soil drying at 105 °C used in some studies can give an incorrect estimate of SWR. Air drying was suggested as a laboratory approach to study the SWR–moisture

relationship in different studies (Doerr and Thomas 2000). Still, the effect of drying temperature on SWR reestablishment for different soil textures, is not fully understood.

Throughout the literature, there have been substantial advances in understanding the soil properties affecting the potential SWR. There is a strong indication of organic compounds' implication on controlling the potential SWR (Regalado and Ritter 2006; Wijewardana et al., 2016). However, a large body of research shows the implication of soil texture as another important factor controlling SWR levels. Although SWR can occur in a wide range of soil textures (Deurer et al., 2011; Mcghie and Posner 1980; Wallis et al., 1991), sandy soils are more susceptible to coating by hydrophobic materials because of their low surface area (SA) (Wallis and Horne 1992). In a study of fire-induced SWR, DeBano et al., (1970) reported that the thickness of the hydrophobic layer increased with the decrease in clay content resulting in significantly higher water repellency in sands compared to heavy textured soils. Soil specific surface area (SA) would be a key factor controlling SWR occurrence in the pastoral systems in New Zealand. Yet, a complete assessment of the SA influence on water repellency needs data that include a wide range of SWR, soil C and SA. Hermansen et al.'s (2019) survey on the South Island of New Zealand included a wide range of soil C. Still when it comes to texture, this survey included mainly silt, silt loam and sandy loam (no clay and only one sandy textured soil) (Hermansen et al., 2019b). Thus, it is difficult to draw a solid conclusion on the impact of soil texture and SA on the potential SWR. This chapter aims to:

i) Model actual SWR persistence as a function of θ and the potential SWR in drying hydrophobic soils;
ii) Examine the implication of soil particle size distribution and SA in controlling the potential SWR through a combination of published datasets from New Zealand case studies.

2.3 Theory

Different models were suggested by Li et al., (2016) for SWR characteristic curves for artificially hydrophobised soil (e.g., Gaussian and Lorentzian models). However, measurements of SWR persistence showed a consistent sigmoidal response to the decreasing θ in naturally hydrophobic soil. A suitable form of equations that perfectly simulate the response of SWR persistence R_a to soil moisture θ (g g^{-1}) is the following reversed sigmoidal equation:

$$R_a(\theta) = \frac{R_p}{1 + e^{\delta(\theta - \theta_c)}} \quad (2\text{-}1)$$

where R_p is the potential persistence of SWR (R_p = Log WDPT(s) of dry soils) and the parameters θ_c and δ are curve characteristics that need to be determined for each soil type through fitting

experimental data to the model. Factors controlling R_p, including soil C, texture and pH, will be discussed in section 4.2. The first and second derivatives of Equation (2-1) are

$$R_a'(\theta) = \frac{-\delta R_p e^{\delta(\theta-\theta_c)}}{[1+e^{\delta(\theta-\theta_c)}]^2} \quad (2\text{-}2)$$

$$R_a''(\theta) = \frac{\delta^2 R_p e^{\delta(\theta-\theta_c)}\left[e^{2\delta(\theta-\theta_c)}-1\right]}{[1+e^{\delta(\theta-\theta_c)}]^4} \quad (2\text{-}3)$$

For $\theta = \theta_c$, $R_a$reaches its half potential, the first derivative R_a' is in its minimum and the second derivative R_a'' is equal to 0 (inflexion point):

$$R_a(\theta_c) = \frac{R_p}{2} \quad (2\text{-}4)$$

$$R_a'(\theta_c) = \frac{-\delta R_p}{4} \quad (2\text{-}5)$$

$$R_a''(\theta_c) = 0 \quad (2\text{-}6)$$

The higher the factor δ, the lower the curve slope value at the inflexion point. Thus, this parameter describes how SWR persistence changes with the drying rate. The higher δ, the faster the transition from the wettable to the water repellent state when drying soils. Parameter θ_c is moisture at the inflexion point that corresponds to half of the potential persistence. Dekker and Ritsema (1994) introduced the critical water content as the value above which the soil is wettable, and below is water repellent. However, the repellency at this moisture level is easily reversible and not necessarily critical. Here, we introduce a new definition of the critical water content θ_c that corresponds to the highest increase in SWR persistence in drying soils, and it is significantly difficult to rewet hydrophobic soils past this point. Determination of θ_c is essential for the prediction of soil moisture effect on the surface runoff during rain events after dry periods.

2.4 Materials and Methods

In the present study, soil properties analysis was carried out as the following: SWR persistence and severity was measured on nine soil samples from nine pastoral sites representing four soil orders: Recent (Entisols, Inceptisols), Brown (Inceptisols), Pallic (Alfisols) and Pumice (Andisols) (New Zealand Soil Classification (Hewitt 2010) and Soil Taxonomy equivalent (Schoeneberger et al., 2012). Water repellency persistence vs. water content was measured on ten hydrophobic soils representing four soil orders and a wide range of textures (Table 1). The actual persistence of SWR (R_a) was measured using the WDPT method. The soil samples were brought to saturation and gradually air-dried at room temperature (20 to 22 °C). Five replicates of WDPT measurements were carried out

using 40 µL drops of deionised water that were placed on the soil smoothed surface, and the full drop penetration time was recorded in seconds (s) (Doerr 1998). Measurement of WDPT was carried out at different levels (around 10% reduction each step) of gravimetric soil moisture (g g^{-1}). When moisture reached a stable minimum, air drying samples were dried at 105 °C for dry soil weight estimation. The estimation of the SWR degree was done by the MED method. Ethanol concentrations of 0, 3, 5, 8.5, 13, 24 and 36% by volume were prepared, and five droplets of 40 µL were placed on the smoothed soil sample surface. The molarity of the ethanol test was represented by the ethanol concentration of the droplet that entered the soil surface in 5 s.

To assess the effect soil particle size, SA and C content on the severity and the persistence R_p, we aggregated the published soil data from three recent New Zealand Studies (Hermansen et al., 2019b; Müller et al., 2014; Simpson et al., 2019). Eight soils and their respective particle size distribution data were sampled by Whitley (2018) from eight dryland pasture sites, including three from the North Island and five from the South Island of New Zealand. We measured the persistence and the degree of SWR on these soils.

Observed values of the actual SWR persistence (Log WDPT) and water content were used to find the two parameters of the curve that best fit the experimental data and have the lowest RMSE:

$$\mathrm{RMSE} = \sqrt{\frac{1}{n}\sum_{i=1}^{n}(R_{a_i} - R_{o_i})^2} \tag{2-7}$$

R_{o_i} are the observed values of SWR persistence and R_{a_i} are the fitted values using Equation (1). The specific surface area of sand and silt fractions a_s, were estimated based on particles size distribution using the following equation by Hillel (2013):

$$a_s = \frac{6}{\rho_s}\sum\left(\frac{f_i}{d_i}\right) \tag{2-8}$$

where f_i is the mass fraction of particles with a diameter d_i and ρ_s is the respective particle density (2.65 g cm^{-3} for sand and silt and 2.67 g cm^{-3} for clay were used). For clay fraction, surface area a_c was estimated using Equation (2-9) (Hillel 2013):

$$a_c = \frac{2f_c}{\rho_s l} \tag{2-9}$$

where f_c is the mass fraction of clay particles, l is the thickness of clay platelets assumed to have an average of 4.10^{-9} m. Total soil specific area SA is then estimated as the sum:

$$SA = a_s + a_c \tag{2-10}$$

2.5 Results and Discussions

2.5.1 The Actual SWR (R_a) as Function Soil Moisture

The potential WDPT of air-dry soils varied between 38 and 8460 s (R_p from 1.57 to 4.2) (Table 2-1). This means that water repellency classes varied from strong to severe according to the classification suggested by Doerr (1998). Total carbon ranged between 3.6 and 12.9 % (Table 2-1). Water repellency persistence (WDPT) increased significantly with decreasing soil moisture. All the studied samples representing different soil orders, textures and potential SWR represented a sigmoidal response to the decrease in soil moisture where WDPT attends a maximum for air-dry soils. This typical sigmoidal response of WDPT to moisture decrease was observed in dunes sand (Dekker et al., 2001), SWR in New Zealand hydrophobic soils determined by sessile drop method (Wijewardana et al., 2016), hydrophobic peat (Michel 2009), post-fire hydrophobic soils (Stoof et al., 2011) and Portuguese sandy loam and loamy sand in a forest ecosystem study (Doerr and Thomas 2000). However, the present result is different from the data reported by Li et al., (2016), who established SWR persistence curves for artificially hydrophobised soils using octadecylamine ($C_{18}H_{39}N$). Data from this study showed that the SWR persistence curve represented typical sigmoid shape for sand samples while it presented unimodal curves for loam, clay loam and silt loam samples. Results from studies using artificially hydrophobised soils cannot be generalised as a universal model for hydrophobic soil. Natural SWR is caused by a complex combination of organic materials (e.g., plants fragments, roots) (Bisdom et al., 1993) and hydrophobic compounds (Franco et al., 2003). Organic materials are a principal component in high C soils. For these reasons, natural SWR is difficult to simulate by adding one hydrophobic compound to the soil. Efforts have been made to understand the reestablishment of SWR. This theory fits well with our experimental data showing a sigmoidal increase in SWR persistence in drying soils. The present data fit well with the conceptual model of SWR development (Doerr et al., 2000). From the sigmoidal curves in the present study, three phases can be observed (Figure 2-1, a-f). (i) The wettable phase where the hydrophobic compounds are detached from the soil minerals (suspended in water). (ii) The transition phase, which corresponds to the exposure of the mineral surfaces to the attachment of the hydrophobic compounds (from the first SWR appearance to the inflexion point). In this phase, the increase in SWR persistence is exponential. (iii) The saturation phase extends from the inflexion point to a stable maximum. This final phase represents the coating of soil minerals that is limited by the saturation of the available surface area and the amount of the hydrophobic compounds.

Table 2-1 Potential soil water repellency (SWR), C content and texture of different soil samples and the fitted model parameters with their respective RMSE. Water drop penetration time (WDPT) was measured on individual samples using five water drops at five to six decrements.

Sample	NZ Classification	WDPT s	Texture	C %	R_p Log s	θ_c g g $^{-1}$	δ	RMSE Log s
1	Pallic Orthic Brown	3900	Clay loam	12.89	3.68	0.35	18.69	0.18
2	Typic Orthic Pumice	3660	Sand	4.93	3.56	0.13	49.06	0.01
3	Typic Immature Pallic	168	Loamy Silt	3.6	2.23	0.13	57.28	0.00
4	Typic Orthic Pumice	8460	Sand	4.6	4.2	0.19	14.93	0.24
5	Mottled Argillic Pallic	782	Silt loam	8.65	2.78	0.26	33.46	0.11
6	Pallic Orthic Brown	604	Silt loam	6.69	2.78	0.17	48.84	0.13
7	Mottled Argillic Pallic	286	Light silt loam	7.4	2.42	0.29	27.75	0.24
8	Pallic Orthic Brown	604	Silt loam	6.69	2.78	0.21	37.32	0.22
9	Mottled Argillic Pallic	38	Light silt loam	4.92	1.57	0.16	33.29	0.14
10	Mottled Argillic Pallic	1800	Light silt loam	5.86	3.25	0.17	34.65	0.03

After fitting the sigmoidal function (Equation (2-1)) to the experimental data and analysing the relationship between the three parameters of the equation, the following patterns have been observed. There was no evident relationship between the measured R_p and the critical water content θ_c (Table 2-2). This means that the potential hydrophobicity does not control the level of moisture below; drying soils become critically water repellent (peak in the $R_a'(\theta)$). Nevertheless, there was a strong correlation between C and θ_c with R = 0.91 (R^2 = 0.82). We theorize that θ_c is logically controlled by the amount and the type of hydrophobic materials present in the C pool, as there are different compounds involved in this process (Franco et al., 2003; Horne and McIntosh 2003). There was a relatively low determination coefficient (R^2 = 0.19) for the linear regression

between the R_p and δ coefficient that is involved in the steepness of the slope at the inflexion point. The higher R_p is, the lower the coefficient δ is and thus, the smoother the transition between the wettable and the repellent phases when drying the soils. The lower R_p is, the higher δ is, and therefore, the steeper is the increase in SWR persistence when water content drops near θ_c. When it comes to the relationship between θ_c and the coefficient δ, there was a moderate linear relationship with $R^2 = 0.45$. The lower θ_c is, the steeper the slope is near the inflexion point (lower δ) and vice versa. However, one Orthic Pumice soil diverged from this rule with a relatively low θ_c and δ (Figure 2-1, d). This suggests that SWR persistence develop smoothly when this soil dries out, without a sudden transition toward the potential value R_p. An investigation at the nanoscale is needed to understand how soil properties, such as texture and soil order, affect the hydrophobic compounds' behaviour toward soil minerals.

Table 2-2 Coefficient of determination of linear regressions between C (%) and the model parameters R_p(Log s), θ_c (g g^{-1}) and δ.

	C	R_p	θ_c	δ
C	1	0.06	0.82	0.24
R_p		1	0.04	0.19
θ_c			1	0.45
δ				1

The present soils showed significantly different critical soil moisture θ_c going from 0.13 to 0.35 g g^{-1} and different steepness curves at the inflexion point δ, going from 14.9 to 57.3 (Table 2-1). Data from (Dekker et al., 2001) showed that the water content below which sand becomes repellent changes with soil depth. This suggests different θ_c levels over the soil profile. The decrease in θ_c would result from decreasing concentrations of hydrophobic materials in the C pool with depth if we assume that they occur at the soil surface. Indeed, hydrophobic compounds can result from plant leaves and root decomposition (Bisdom et al., 1993; Franco et al., 2003; Mao et al., 2014) that are probably the main source of hydrophobicity in New Zealand pastoral systems. The potential SWR persistence is controlled by many parameters, including soil C, particle size distribution and the type and the amount of the hydrophobic materials in the C pool. In the second part of the results (Section 4.2.), a detailed analysis of the implication of C and particle size on the distribution in the potential SWR is presented.

From the fitted curves of the studied soils (Table 2-1 and Figure 2-1, a-f), we can differentiate three SWR persistence patterns, representing three soils categories. Soils with low θ_c

(0.13 to 0.17 g g^{-1}) and a steep slope at θ_c (δ from 48.8 to 57.3). These soils are less susceptible to persistent SWR in the drying phase compared to soils with higher θ_c. However, the R_a increase rate in these soils is very high when moisture drops near θ_c. This implies that a persistent water repellency can appear suddenly when water content approaches θ_c in these soils. The second category represents a low δ and high θ_c. These soils express a smooth increase in SWR persistence when going from saturated soils to the critical moisture θ_c. However, the high θ_c (0.26 to 0.35 g g^{-1}) means that these soils are more prone to SWR in the early stages during the dry periods. The third pattern was observed in the soils with the relatively higher θ_c and steepness at the inflexion point. In these soils, a persistent repellency would develop promptly in the early stages of a dry period. Remediation strategies (e.g., surfactant application) would be necessary for the second and the third categories to attenuate the agro-environmental effect of SWR (Müller and Deurer 2011a).

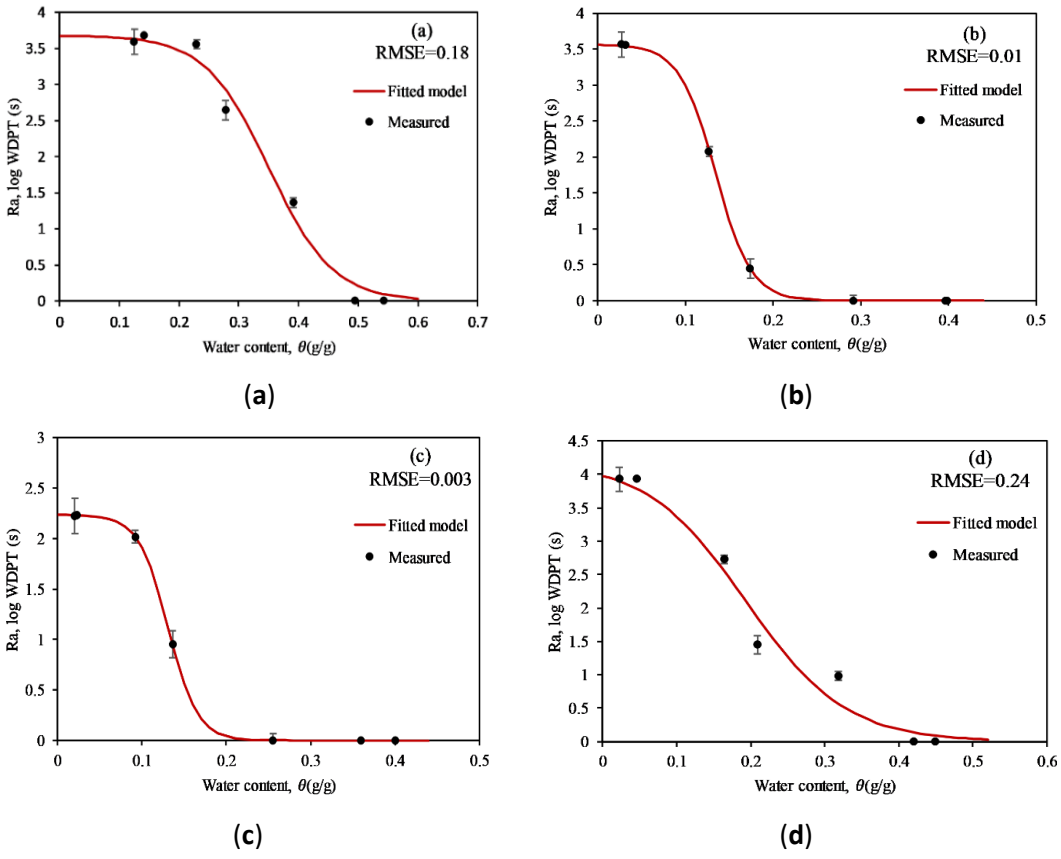

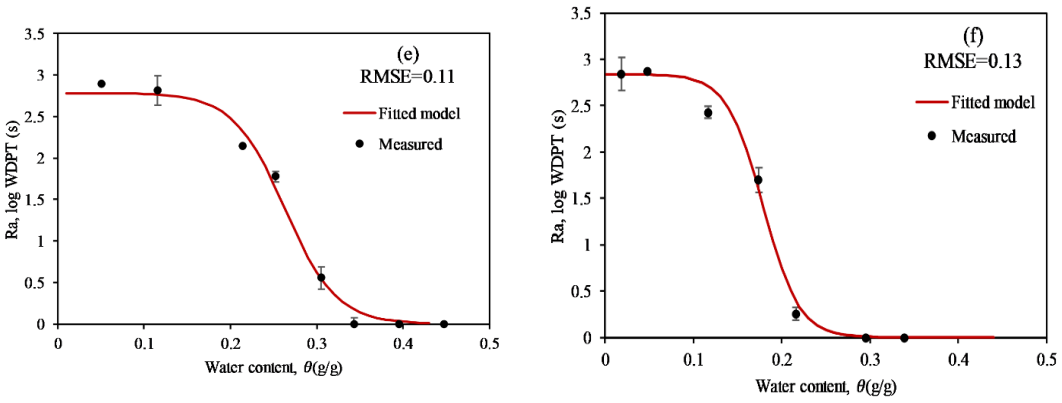

(e) (f)

Figure 2-1 Persistence of soil water repellency (SWR) (Log water drop penetration time (WDPT) (Log s)) as a function of water content θ (g g^{-1}) measured during dying soil samples and corresponding fitted curve using the Equation (2-1) for the first six soils from Table 1: (a) Pallic Orthic Brown, (b) Typic Orthic Pumice, (c) Typic Immature Pallic, (d) Typic Orthic Pumice, (e) Mottled Argillic Pallic, (f) Pallic Orthic Brown.

2.5.2 Soil Properties Controlling the Potential SWR (R_p)

Modelling the actual persistence of SWR (R_a) using the sigmoidal function (Equation (2-1)) needs a determination of the potential SWR (R_p). Data from a wide range of soil textures from fine (34% clay, 40% silt) to coarse (85% sand) (Table 2-3) showed a strong implication of soil C and soil texture in controlling R_p. In this combined dataset, carbon content ranged from 2.49 to 12.89% (Table 2-3). Soils showed different levels of SWR persistence ranging from wettable (Log WDPT = 0) to severe persistence (Log WDPT = 3.95) and a MED from 0 to 27%. Podzol and Pumice orders represented a higher severity (27 and 24%, respectively), while Ultic and Semiarid showed the lowest MED values (3 and 1.5%, respectively). There was a significant positive correlation between WDPT and MED, the reported persistence of Ultic soil from (Müller et al., 2014) was the highest (Log WDPT of 3.95), followed by the Pumice order (Log WDPT of 3.83). Many studies demonstrated that high persistence does not necessarily mean high severity of SWR (Chau et al., 2014).

Table 2-3 Soil characteristics from our study and other studies including pH, sand, silt, clay, C contents, surface area (SA), the molarity of ethanol drop (MED) and Log WDPT.

Soil Order (NZ)	*n*	pH	Silt g g^{-1}	Sand g g^{-1}	Clay g g^{-1}	SA m^{2}g^{-1}	C %	MED %	Log WDPT Log s	Study
Recent	1	5.3	0.36	0.55	0.09	1.84	2.49	0.00	0.00	This study: Sampled by Whitley et al., (2018)
Brown	1	5.2	0.39	0.34	0.28	5.31	12.89	13.00	3.73	
Pumice	1	5.2	0.14	0.86	0.01	0.16	4.93	24.00	3.77	
Pallic	1	5.6	0.32	0.62	0.06	1.17	2.74	0.00	0.00	
Brown	1	5	0.39	0.48	0.13	2.52	6.18	5.00	1.54	
Pallic	1	5.2	0.47	0.5	0.03	0.74	3.6	13.00	2.84	
Brown	1	4.7	0.32	0.51	0.17	3.27	4.91	6.75	1.87	
Pumice	1	5.1	0.14	0.85	0.01	0.18	6.7	24.00	3.89	
Brown	21	5.3	0.58	0.34	0.08	1.66	6.3	7.50	ND*	Hermansen et al., (2019)
Pallic	12	5.5	0.73	0.21	0.06	1.30	3.8	3.00	ND	
Podzol	12	5.4	0.62	0.29	0.09	1.89	9.5	27.00	ND	
Recent	18	5.2	0.67	0.25	0.08	1.66	4.2	9.00	ND	
Semiarid	9	5.6	0.48	0.40	0.13	2.52	4.1	1.50	ND	
Pallic	12	4.5	0.22	0.49	0.27	5.61	11.6	2.00	3.07	Müller et al., (2014)
Ultic	9	4.9	0.41	0.25	0.34	6.53	8.1	3.00	3.95	
Recent	6	4.5	0.64	0.32	0.04	0.96	9.06	11.50	3.65	Simpson et al., (2019)
Brown	6	4.7	0.49	0.49	0.02	0.56	8.69	10.00	3.71	

(*) not measured in the study.

The persistence of SWR estimated was significantly (R = 0.66; $p < 0.05$) correlated with soil C (Table 4). The simple linear regression between Log WDPT and C had R^2 of 0.44 and RMSE of 1.15 Log s. Using both C and SA in multiple linear regression (MLR) improved the prediction of Log WDPT (R^2 = 52, RMSE = 1.12 Log s) (Figure 2-2, d).

$$Log\ WDPT = 0.38\ C - 0.029\ SA + 0.60 \quad (2\text{-}11)$$

This level of correlation is in agreement with previous results from a New Zealand North Island survey on SWR, which showed an R of 0.61 (R^2 = 0.37) between C and Log WDPT (Deurer et

al., 2011). Hermansen et al., (2019) reported a high correlation between SWR severity (measured with MED) and organic C with an R = 0.82 (R^2 = 0.68) in the South Island of New Zealand survey. Unlike the aggregated dataset in the present work, the soil dataset from this survey contains mainly coarse- and medium-textured soils (sand, sandy loam, silt loam). Only six soil samples out of 78 soils were silty clay and silty clay loam, and only one sand textured sample. Although MED had no significant correlation with soil properties (Table 2-4), C content, sand, silt, clay and SA seem to affect the MED unobtrusively. The SA was negatively correlated with MED, and C was positively correlated with MED (Table 2-4). As clay contributed significantly to the estimated SA (R = 1 and p < 0.001), there is a strong indication that there is an opposing contribution of SA and C in the expression of the severity of SWR. An increase in the amount of the hydrophobic compounds in soil C pool enhances the coating of minerals surfaces. However, this process might be restricted by the high SA in clays.

Table 2-4 Pearson product moment correlation matrix of pH, silt (g g^{-1}), sand (g g^{-1}), clay (g g^{-1}), SA (m^2 g^{-1}), C (%), MED (%), Log WDPT (Log s).

	pH	Silt	Sand	Clay	SA	C	MED	Log WDPT
pH	1	0.2	−0.03	−0.29	−0.29	−0.54 *	−0.01	−0.49
Silt		1	−0.85 ***	−0.15	−0.13	−0.06	−0.15	0.01
Sand			1	−0.4	−0.42	−0.23	0.34	−0.09
Clay				1	1 ***	0.53 *	−0.38	0.13
SA					1	0.53 *	−0.39	0.13
C						1	0.29	0.66 *
MED							1	0.65 *
Log WDPT								1

p levels: * 0.05, ** 0.01, *** 0.001 Multiple linear regression (MLR) modelling showed that C (p = 0.024), sand, silt, clay (p = 0.022 each) similarly contribute at 70% of MED variation with an RMSE of 5.4% (Equation (2-9), Figure 2-2 a). In contrast, an MLR model based on C and SA showed that they contributed significantly (p = 0.009 and 0.005, respectively) to 48% of MED variation with an RMSE of 6.59% (Equation (2-13), Figure 2-2 b, c).

$$MED = 1.41\,C + 161.61\,sand + 161.44\,silt + 161.04\,clay - 16148.23 \quad (2\text{-}12)$$

$$MED = 1.89\,C - 0.41\,SA + 4.27 \quad (2\text{-}13)$$

Carbon was moderately correlated with clay content and SA (R = 0.53; *p* = 0.028) (Table 2-4). The estimation of SA was not 100 per cent accurate based on a coarse particle size distribution alone. In soil with high variability in particle type, using the particle size distribution can underestimate SA by one-two orders (Koptsik et al., 2003). Thus, an accurate estimation of MED was possible based on C content and improved estimation of SA.

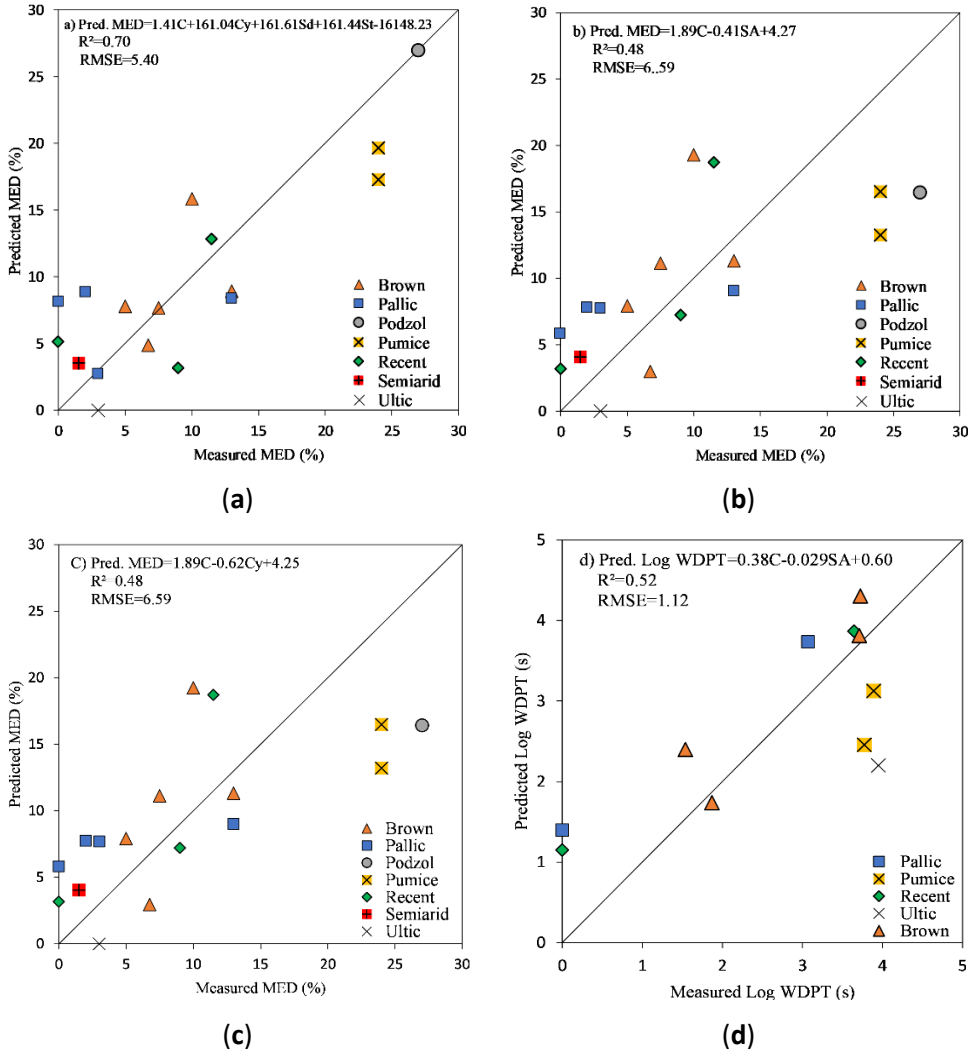

Figure 2-2 Multiple linear regressions (MLR) for the molarity of ethanol drop (MED) using (a) carbon and soil particles size distribution; (b) carbon and surface area (SA); (c) carbon and clay (Cy); and (d) the MLR for Log WDPT using C and SA.

2.6 Conclusions

The suggested equation enables modelling of the actual repellency persistence (R_a) to the moisture decrease in drying hydrophobic soils using the potential repellency (R_p) and two shape parameters θ_c and δ. The curve shape parameters give valuable information on how SWR persistence behaves in the drying period. In the studied hydrophobic soils, three main patterns were observed in the response curves $R_a(\theta)$. (i) The first pattern is associated with soils that have low θ_c and high δ (steep slope at θ_c). These soils were less prone to express persistent SWR in the early stages of the dry period. Nevertheless, SWR persistence increased suddenly when moisture drops near θ_c. (ii) The second pattern represents soils with low δ and high θ_c (0.26 to 0.35 g g^{-1}), which meant prompt development of SWR in the early stages of dry periods, although there was a smooth increase in SWR persistence. (iii) The third pattern showed a relatively higher θ_c and steepness at the inflexion point δ. This implies that a persistent repellency would appear suddenly in the early stages of the summer period. A nanoscale investigation of soil properties controlling the SWR persistence dynamics in drying soil is needed to understand better these patterns and how they would affect plant growth and hydrological processes.

When it comes to soil properties controlling the potential water repellency R_p, carbon and soil texture showed strong implications in this regard. The present data from pastoral soils showed that C has a significant influence on the potential severity of SWR and the critical soil moisture in hydrophobic soils. Both the specific surface area and soil C contribute to controlling the potential SWR degree in the studied soils. The present model and results will serve for a better understanding of SWR behaviour in drying hydrophobic soils and its hydrological implications.

Chapter 3

Surface runoff and losses of phosphorus from hydrophobic pastoral soils

3.1 Abstract

The impact of soil water repellency (SWR) on soil phosphorus (P) mobility in surface water runoff remains contentious. Although SWR may cause a significant increase in surface runoff, especially in post-summer rainfall events, whether it contributes to background phosphorus losses remains unclear. Surface runoff and phosphorus concentrations in runoff were measured on hilly Allophanic pastoral soils with different water repellency levels using seven runoff collectors. Phosphorus fertiliser was broadcasted at 18 kg P ha^{-1} in the summer over dry soils. Runoff volumes and P concentrations were measured after each rain event prompting surface runoff. The highest runoff/rainfall ratios were observed at the early rainfall events following the dry summer and then decreased significantly by the end of autumn and winter. The post-summer surface runoff correlation with SWR had an R^2 of 0.46, and hydrophobic soils had significantly higher runoff ratios than wettable soils. Measurements of the dissolved reactive phosphorus (DRP) and total phosphorus (TP) in the surface runoff showed decreasing exponential trends with the highest values recorded at the first runoff event following P fertiliser application, where over 90% of losses occurred (incidental losses). After the incidental loss phase, DRP concentrations were related to surface runoff ratio, soil P extractability by water, and SWR. Our data point to non-incidental TP loads being related to SWR (R^2=0.53). The present results will improve the understanding of the SWR effect on surface runoff and will reconcile the controversy regarding its contribution to non-incidental P losses.

3.2 Introduction

Soil water repellency (SWR) is an intrinsic physicochemical property controlling water infiltration in hydrophobic soils. This phenomenon has been reported in different soils and climate conditions (Mao et al., 2019). It is caused by the hydrophobic organic compounds that coat the soil mineral particles and reduce the soil wettability. In the agroecosystems, this issue has severe consequences for runoff (Jeyakumar et al., 2014), plant growth (Osborn et al., 1967) and nutrient losses (Müller et al., 2018). Different studies reported the significant effect of SWR on runoff in fire-induced SWR situations (Ferreira et al., 2016; Granged et al., 2011; Imeson et al., 1992; Larsen et al., 2009), forest (Miyata et al., 2007), and pastoral ecosystems (Müller et al., 2018; Wallis et al., 1991). Water repellency increased runoff three times in eucalyptus forest soil study (Burch, Moore, and Burns 1989) and 16 times in fire-induced hydrophobicity in a forest study (Leighton-Boyce et al., 2007). Lemmnitz et al., (2008) studied the temporal dynamics of surface runoff in wettable and hydrophobic sand and reported that seasonal variations in the actual water repellency caused an increase of runoff coefficient in the summer and autumn. In a pastoral case study, a run-on simulation on a water repellent Andosol, Müller et al., (2018) showed that 88 % of the run-on water was collected as surface runoff, while no runoff was observed when using an aqueous ethanol solution to separate the effect of soil hydrophobicity from other hydrological processes (e.g. slaking). However, the authors used a 1h simulated run-on equivalent to 60mm/h rainfall intensity. Such a storm event has an annual recurrence interval longer than 100 years for the soil sampling site. Studying this issue under field conditions would give better insight into the interactions between SWR and surface runoff.

Phosphorus (P) fertilisers application in pastoral systems and their release from catchments to streams has been associated with water quality issues (Condron et al., 2005; Sharpley et al., 2001). In fact, in addition to nitrogen, P is a crucial element that sustains aquatic biomass growth. Therefore, these two elements are potential sources of drinking water pollution but limiting factors of eutrophication inducing alga blooms and dead zones in marine ecosystems (Conley et al., 2009). Phosphorus control alone has been proven to decrease eutrophication in many studies reviewed by Schindler and Vallentyne (2008).

Identification of P losses applies the understanding of P mobilization mechanisms and the accurate examination of soil physicochemical characteristics, agricultural practices, and climatic factors. Haygarth and Jarvis, (1999) described two basic mechanisms generally known to be involved in P mobilization. (1) Solubilization, which is a chemical process, defined as all P in water after a

<0.45 µm filtration. This process involves the transfer of P from a solid phase to a soluble phase due to non-chemical equilibrium between the two phases. And (2) the physical detachment of soil colloids and particles associated with P by the kinetic energy of water (i.e. surface runoff). Soil type and acidity are the main criteria determining how P reacts with soil minerals. Condron et al., (2005) reviewed the physicochemical factors influencing P retention and availability. Although the soil chemical properties determine P availability, the hydrological processes are still critical in P transport and fate (McDowell 2012; Haygarth et al., 2005). Phosphorus can be transported from soils to waterways through different pathways. Infiltration-excess surface runoff, which is highly affected by SWR, is a crucial conduit of P exports. Rainfall events with high intensity resulted in higher P losses through the surface runoff (McDowell 2012). Water repellency impact on surface runoff volumes (Müller et al., 2018), could contribute drastically to increasing P loads. However, there has been no evidence from field data to support this hypothesis. An increase in runoff volumes effect on P dilution would be difficult to understand in field conditions. Field data is needed to reconcile the understanding of the SWR effect on P loads in surface runoff.

Different trials on P losses in pastures showed that P losses via surface runoff decreased exponentially after P-fertiliser application, starting from the first overland flow event (McDowell et al., 2003; McDowell et al., 2003; Nash et al., 2005). These trials show that P losses are the highest in the early runoff events following fertiliser application and are mainly controlled by the fertilisers' application rate and solubility. However, P concentrations in surface runoff is unrelated to the fertilisers' solubility or application rate after this period (around three months or three important runoff events) (McDowell et al., 2003). Nash et al., (2019) theorised that P exports from the soil surface are dominated by exports of P precipitates from fertiliser granules following fertilisers application. This form of P movement, which is a direct mobilization of the P source itself, has been labelled *incidental* (Gburek et al., 2005; Preedy et al., 2001). Thus, the application rate and fertiliser solubility are the main controlling factors during this period. After this period, P losses are not related to fertiliser application rate and solubility, but soil P status (McDowell and Catto 2005). These background losses were labelled *non-incidental*. McDowell and Condron (2004) reported that P losses in simulated runoff are perfectly correlated with P extractability by water and suggested that H_2O extractable P can be used to estimate non-incidental P losses in runoff simulation. However, estimation and modelling P loads in surface runoff require an understanding of the relationship between P concentration and runoff volumes. Nash et al., (2019) reported that TP concentrations in individual runoff events were unrelated to runoff volumes in field conditions. Obviously, it is difficult to understand the relationship between P concentrations in runoff and runoff magnitude without dealing with incidental and non-incidental P separately. Also, the effect of severe

hydrophobicity on P losses in surface runoff is unknown in post-summer runoff. This study was initiated as a first test of the hypothesis that soil water repellency increases surface runoff volumes and non-incidental phosphorus losses in post-summer rainfall events. Thus, the present work aimed to:

i) Characterise the temporal dynamics of SWR effect on runoff magnitude in post-summer rainfall events.
ii) Understand the relationship between surface runoff, P concentrations in surface runoff, and SWR.

3.3 Material and Methods

3.3.1 Study area

This research was conducted over moderate to steep hill country pasture in Maraetotara, Hawke's Bay region, North Island of New Zealand (39°50'52.72" S, 176°53'02.91" E). The farm includes sheep, beef, and deer production. The area has a mean annual total precipitation of around 1400 mm (2015-2020) (data from Hawke's Bay regional council weather station near the site), mainly falling in winter and spring. The farm's main plant species are perennial ryegrass, white clover, red clover, fescue, brown top, and crested dog's tail. The soil type is Allophanic, derived from the weathering of North Island volcanic ashes. The summer of 2019 was extremely dry as there was no rainfall over the site during January and February. The runoff collectors were installed on dry soil at the end of February. Superphosphate fertiliser was applied on dry soils after runoff collector installation over the whole farm at 200 kg ha^{-1} (18 kg P h^{-1}) using a spreader truck.

3.3.2 Runoff collectors

The runoff collectors design has been adapted from Gillinghm & Gray (2006). Surface runoff was collected by 1.5 m lengths of commercially available plastic roof gutters. The collection area is a 1.5 x 5 m rectangle with plot length down-slope. The collection area was constrained by a rigid plastic wall driven in the soil surface at around 5 cm of the soil surface at the upper and the lateral sides. At the down-slope boundary, the gutter length was set in a trench, and runoff water was conveyed to the gutter by mean of tin length embedded 3 cm below the surface into the upslope wall of the trench. Soil above the tin sheet and the gutter edge was sealed by a silicon glue spray to prevent any associated movement of soil into the gutter. An expanding sealing foam was used to seal the upper and the lateral sides of the collector. The gutter was slightly inclined to one end where a vinyl tube was connected to transfer the collected water to a 20-litter bucket installed at a

level lower than the gutter. A total of seven runoff collectors were installed in areas with different levels of soil water repellency. Three manual plastic rain gauges were placed in each runoff collector to record rainfall. Rainfall data measured with these gauges were equal to data from the weather station installed by the Hawke's Bay regional council nearby the site. After each rainfall event, runoff volumes were measured (bucket emptied), samples from runoff were taken and frozen in the lab for further P analysis. The surface runoff coefficient was determined as the ratio between surface runoff and rainfall for each runoff event.

3.3.3 Soil analysis

Ten samples were collected for each runoff collector using a 7.5 cm depth corer from just outside and around the collection area to avoid soil deterioration inside the collector and maintain the hydrologic properties of the actual runoff plot. Soils were sampled in February (end of summer) and May (end of autumn). Samples were sealed, transferred to the lab, oven-dried for 24 h at 65 °C, and stored for further analysis. On each sample, the water drop penetration test (WDPT) was carried out by placing three water droplets of 40µL on the soil smoothed surface placed in an aluminium tin and measuring the time (s) they took to penetrate the surface (Doerr, 1998). The test's results were used to classify the soils' hydrophobicity status (Bisdom et al., 1993). The median value for the WDPT was used to classify the persistence of SWR into five classes including wettable (<5 s), slightly hydrophobic (5-60 s), strongly hydrophobic (60-600 s), severely hydrophobic (600-3600 s) and extremely hydrophobic (>3600 s). Soils were also tested for pH, Olsen P (Olsen 1954), sulphate sulfur using 0.02M potassium phosphate extraction followed by ion chromatography, and total extractable sulfur using inductively coupled plasma - optical emission spectrometry (ICP-OES).

Runoff samples were transported to the lab and frozen till the day of analysis. For analysis, unfrozen samples were filtered (0.45 mm) and analysed for *dissolved* reactive P (DRP) within 24 h. Total P (TP) was estimated by digesting unfiltered samples using the persulfate oxidation method (Koroleff 1977). Water extractable-P (H_2O-P) was determined using a soil-water ratio of 1:25 and a shaking time of 45 min before measuring DRP in the filtrate (<0.45 µm) (modified from McDowell and Condron, 2004). Different P extracts were analysed using the Murphy & Riley (1962) method. Total C and N were measured using Elementar Vario-Max CN Analyser, Germany. Soil specific surface area was measured using the ethylene glycol monomethyl ether (EGME) method (Cihacek and Bremner 1979).

3.4 Results

The potential SWR remained stable as there was no significant change in the potential SWR from February to May (Table 3-1). Soils in all runoff collectors remained in the same hydrophobicity class over the experiment period, except the collector number 4 where the potential SWR decreased from the "Severely hydrophobic" to "Strongly hydrophobic" class (Table 3-1). Data from (Müller et al., 2014) shows that potential SWR evolution was rather slow over time. Potentially extreme levels of SWR from this study persisted almost one year before dropping to a strong level. The soils' water-extractable P (WEP) varied between 0.04 and 0.29 mg L^{-1}. There were no obvious changes before the P application (February) and three months later (May) except for runoff collector number seven where WEP doubled after the P application. Carbon which ranged from 4.9 to 8.6 %, can be classified as a medium level for New Zealand soils (Webb and Wilson 1995).

Table 3-1 Measured pH, soil C (%), ethylene glycol monomethyl ether (EGME) surface area (m^2/g), Olsen P (mg/L), sulphate sulfur (mg/kg), Extractable Organic sulfur (mg/kg), and Water extractable P (mg/L), and log WDPT(s) measurement in February and May 2020.

Runoff collectors	pH	C (%)	EGME Surface area ($m^2\ g^{-1}$)	Olsen P (mg L^{-1})	Sulphate Sulfur (mg kg^{-1})	Extractable Organic Sulfur (mg kg^{-1})	WEP (mg L^{-1})	Log WDPT (s)	WEP (mg L^{-1})	Log WDPT (s)	SWR Class
							February		May		
1	5.8	4.91	18.3	27	12	6	0.28	0.89	0.29	0.82	Wettable
2	5.8	6.10	25.5	16	20	9	0.09	0.35	0.09	1.61	Wettable
3	5.4	5.86	43.2	21	14	11	0.04	3.53	0.04	3.78	Extremely hydrophobic
4	4.8	5.79	69.2	15	15	14	0.05	3.07	0.05	2.35	Severely hydrophobic
5	5.6	6.68	34.6	13	26	12	0.05	2.08	0.04	2.50	Strongly hydrophobic
6	5.7	8.64	22.8	41	45	15	0.09	2.18	0.10	2.12	Strongly hydrophobic
7	5.3	7.39	22.2	18	44	9	0.06	1.76	0.12	2.22	Strongly hydrophobic

3.4.1 Moisture and Rainfall data

A clear difference in water content was observed between wettable and extremely hydrophobic soils. The extremely hydrophobic collector's moisture was lower than in the wettable soils. This difference in volumetric moisture diminished for the high frequency and intensity rainfall periods (mid-May to early and late June 2020) (Fig. 3-1). The increased amount and frequency of rainfall tightened the gap between moisture levels of the extremely hydrophobic soil and wettable soils (Fig. 3-1). This would be due to the decrease of SWR levels under very wet conditions (Doerr and Thomas 2000).

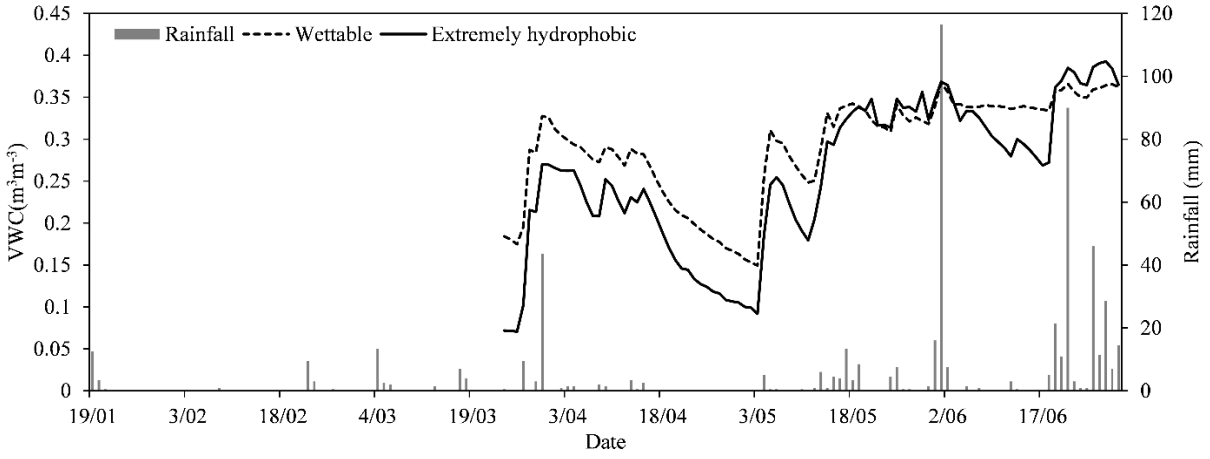

Figure 3-1 Rainfall (mm) from the end of Jan to the end of June 2020 and volumetric water content (VWC) (m^3 m^{-3}) from recorded for the runoff collector 3 (extremely hydrophobic) and collector 2 (wettable).

3.4.2 Surface runoff and P losses

The surface runoff ratio was significantly higher in severely hydrophobic collectors than strongly hydrophobic, which was higher than the wettable collectors. These differences were more important in the period Feb-Mar (Fig. 3-2). Severely hydrophobic soils had runoff ratio between 0.20 and 0.23, strongly hydrophobic soils between 0.16 and 0.17, while wettable soil had ranged between 0.01 and 0.07. After this period, the surface runoff ratio gradually decreased for all runoff collector until no difference was observed by the end of Jun. After mid-January, all soils showed runoff ratios lower than 0.05 (Fig. 3-2). Surface runoff data showed a positive correlation between the potential SWR and the runoff coefficient (R^2=0.46) (Fig. 3-3).

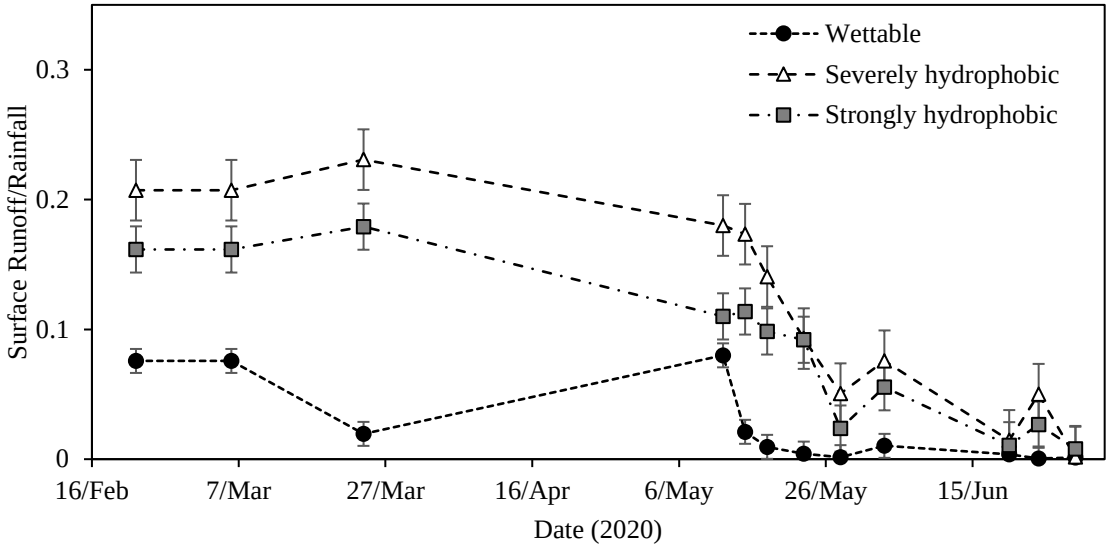

Figure 3-2 Mean surface runoff /rainfall ratio for the three classes of SWR as described and classified in table 1, from February to June 2020.

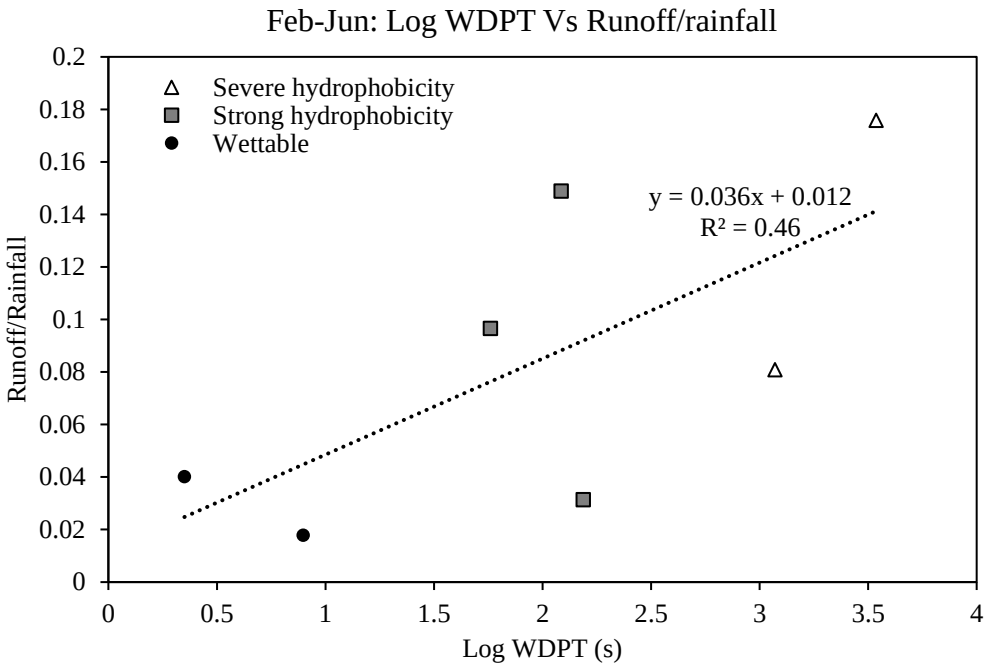

Figure 3-3 Mean surface runoff ratios versus Log WDPT (s) for all the runoff collector during the period between February and June 2020.

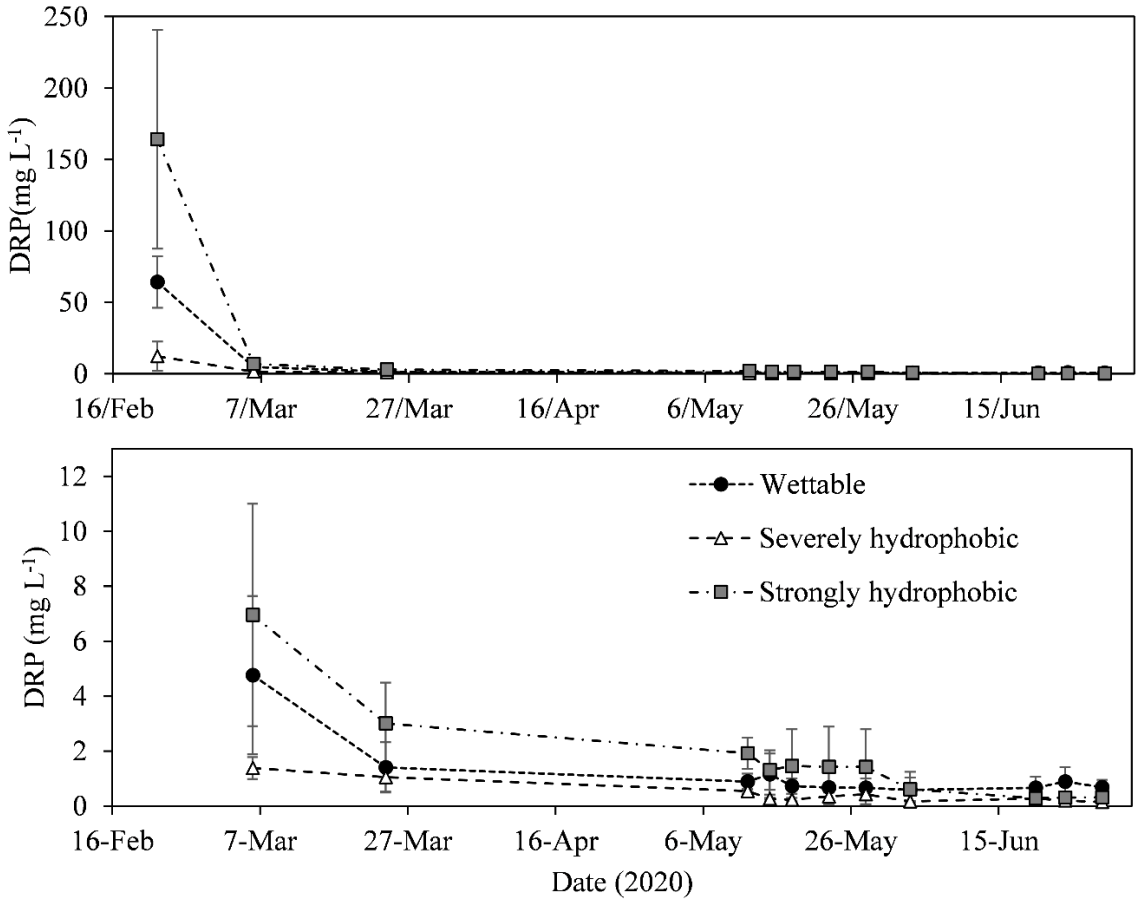

Figure 3-4 Mean dissolved reactive P concentrations (mg L^{-1}) in the surface runoff for wettable, strongly, and severely hydrophobic classes during the period between February and June 2020.

Estimating the amount and the concentrations of DRP mobilised via surface runoff showed an exponential decrease from the first rain event to the experiment's end. The DRP and TP loads in the first event counted for more than 90 % of the losses in the Feb-Jun period (Fig. 3-4, 3-5, 3-6). Total P loads were between 0.2 and 10.4 kg ha^{-1} and DRP loads were between 0.1 and 3.7 kg ha^{-1}, depending on the runoff plots (Fig. 3-6). The DRP loads of the first runoff event counted for between 36 and 73% of the total P loads (Fig. 3-6).

During the March-June period dominated by non-incidental P losses, a strong relationship between DRP concentrations and runoff coefficient have been observed in the different water repellency levels (Fig. 3-7). The R^2 of the regression between runoff coefficient and DRP concentrations were equal to 0.79 and 0.48 for strong and severely hydrophobic soils, respectively. For wettable soils, the runoff coefficient was less than 0.021 during this whole period, except for 12th May, where the runoff coefficient exceeded 0.075. Although wettable soils were dominated by

drainage, the high correlation between DRP and runoff coefficient can still be observed (R^2=0.58) if we exclude the high runoff point of 12th May. The correlation between SWR and TP loads increased progressively when receding from the first runoff events toward the winter period (Fig. 3-8). The determination coefficient of regression between TP loads and SWR (R^2=0.53) was significantly higher in the non-incidental losses period (June 2020) compared to the incidental losses period (Feb 2020) where R^2 was equal to 0.01 (Fig. 3-8).

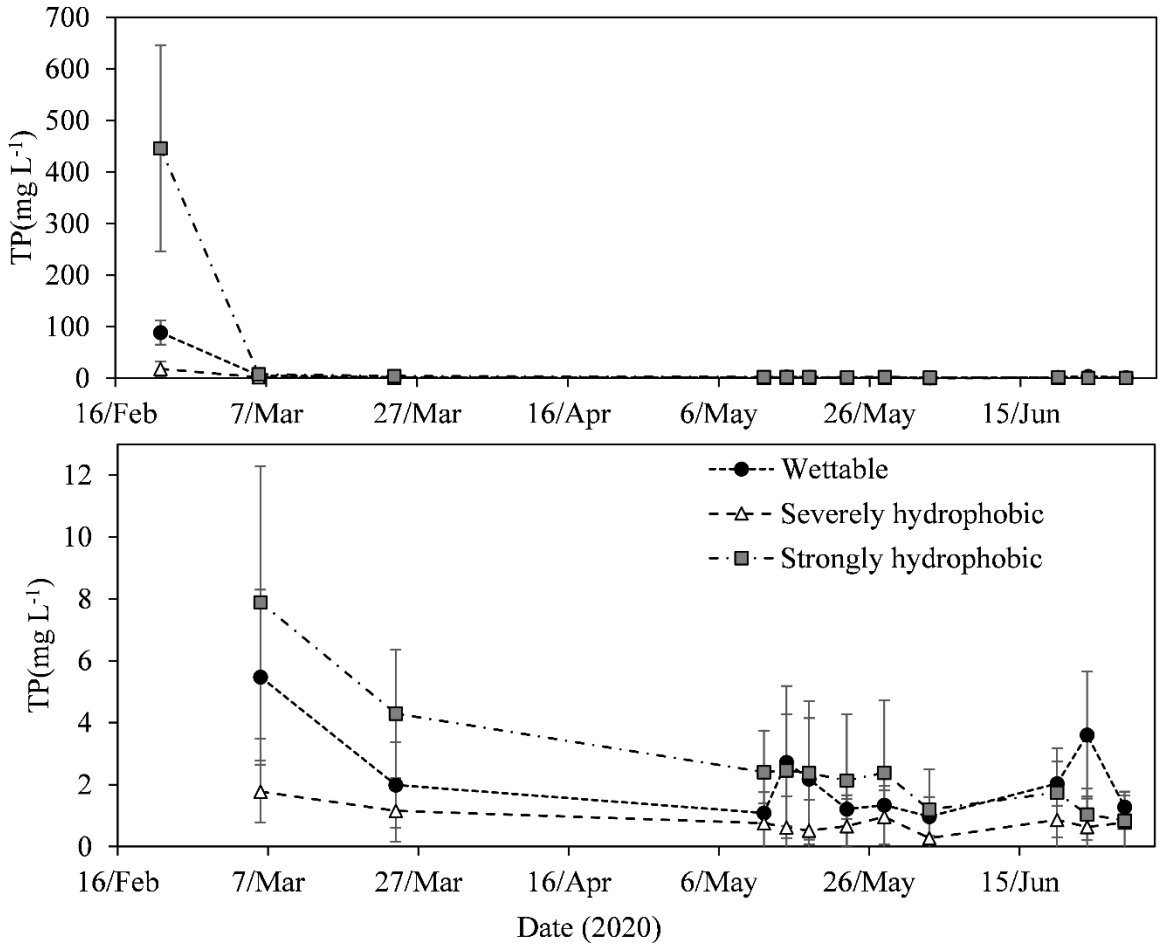

Figure 3-5 Mean total P concentration (mg L^{-1}) per runoff event for the wettable, strongly hydrophobic, and severely hydrophobic classes.

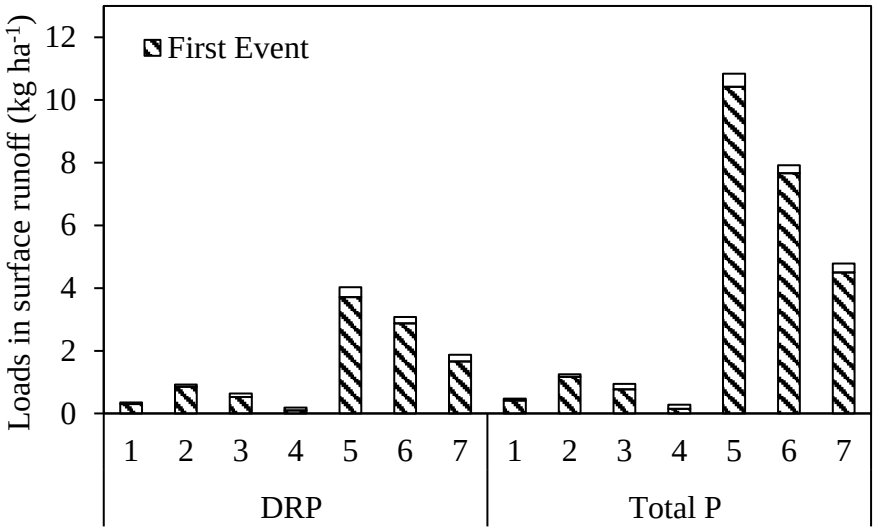

Figure 3-6 Total loads of dissolved reactive P (DRP) and total P in surface runoff (kg/ha) in the seven runoff collectors during the post-summer rain events (Feb-Jun 2020). Hatched areas represent the first runoff event after the dry period and P fertiliser application.

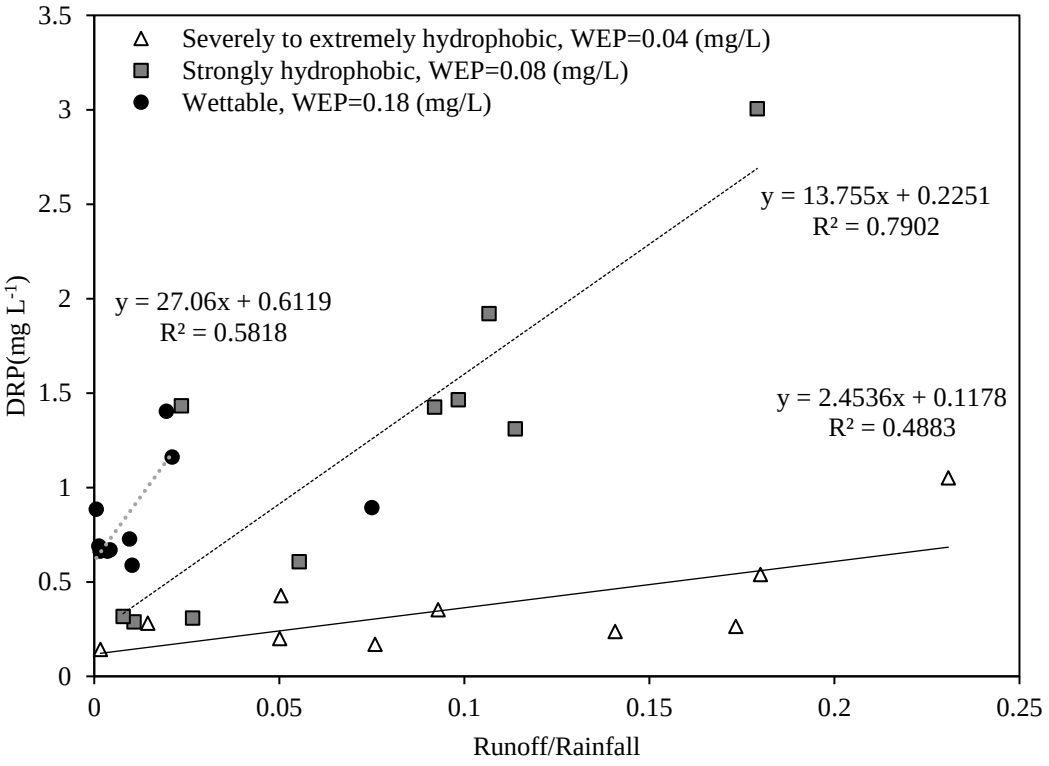

Figure 3.7 Relationship between dissolved reactive P concentration in runoff and runoff ratio for the period March-June. The trendline of wettable plots excludes the date with a 0.075 runoff ratio (12th May 2020).

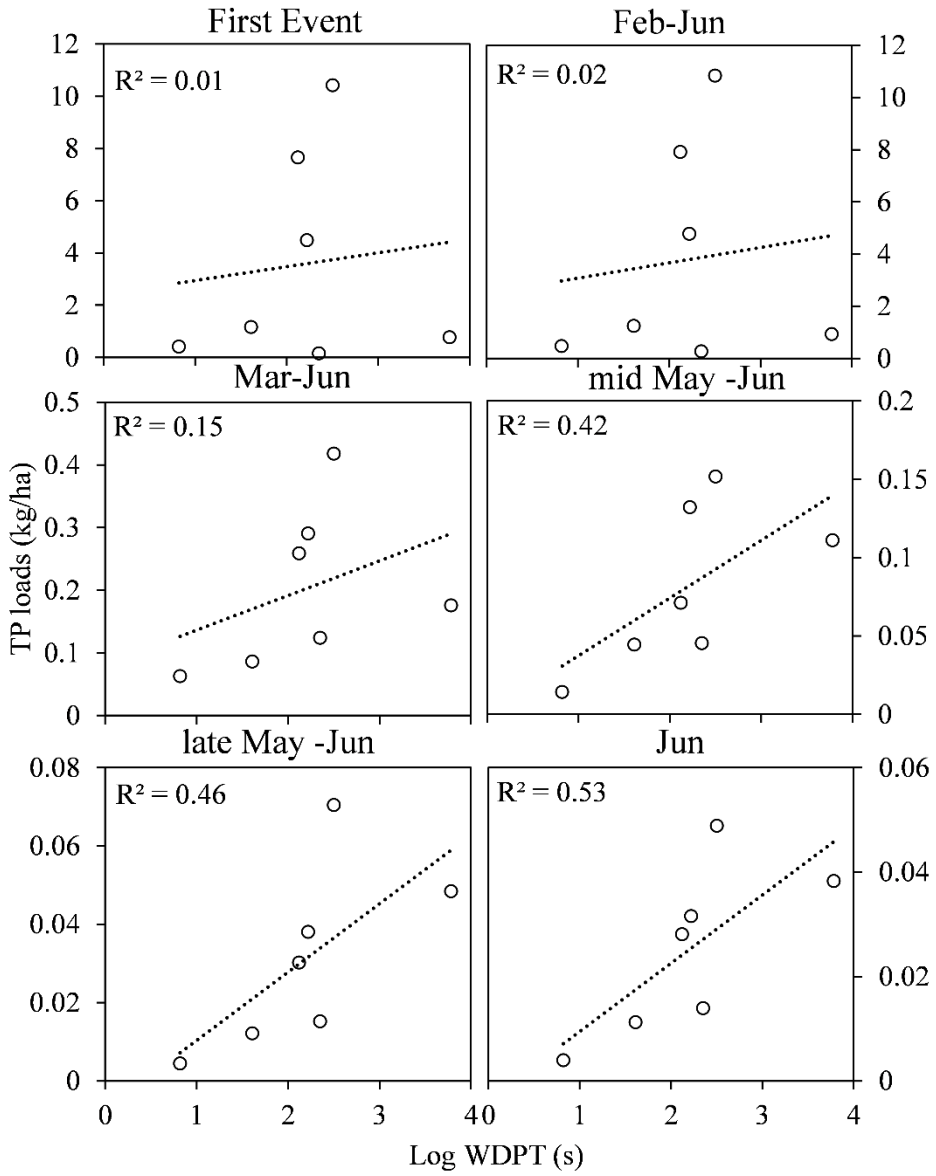

Figure 3.8 Scatter plots of Log WDPT(s) and total P loads (kg ha^{-1}), in the first runoff event, Feb-Jun, Mar-Jun, mid-May-June, late May-June, and June 2020 periods.

3.5 Discussions

As expected, the surface runoff was higher in hydrophobic soils compared to wettable soils, especially in the early runoff event following the dry period (Feb-Mar). The decrease in the actual water repellency during the wet period (Mar-Jun) attenuated the differences in surface runoff ratio between the hydrophobic and wettable soils. Gillingham and Gray (2006) reported that surface runoff was highest from summer to autumn and inversely related to soil moisture in dryland pasture study in Hawke's Bay region. This trend of increasing surface runoff when soil water content decreased was consistent in a two-year study with a correlation coefficient R=-0.38 (Gillingham and

Gray 2006). In another study, Gillingham and Gray (2000) reported that most surface runoffs occurred when surface gravimetric moisture (0-7.5 cm depth) dropped below 10%, while very low runoff was collected when moisture was higher. This is highly likely to be associated with the increase of SWR when moisture drops below a critical water content (Bayad et al., 2020; Chau et al., 2014; Dekker and Ritsema 1994). Similarly, Müller et al., (2014) reported a significant negative correlation between soil moisture and SWR measured by the WDPT test (R=-0.41).

Concentrations and loads of TP and DRP mobilised via surface runoff were the highest in the first runoff event following the dry period and then decreased exponentially in the subsequent events. The DRP and TP loads in the first event represented more than 90 % of the losses of the Feb-Jun period (Fig. 3-4, 3-5, 3-6). These results were comparable to results from McDowell and Catto (2005). The exponential decrease of P losses in superphosphate fertilised soil was reported by McDowell and Catto (2005), who reported that these losses were dictated by fertiliser solubility. However, the proportion of DRP in the subsequent events decreased, and the relationship between DRP and the solubility of fertiliser became insignificant. This indicated the P mobilization's diminishing effect from fertiliser granules as it was lost in the first runoff event or adsorbed to the soils (McDowell et al., 2003). The DRP and TP concentrations and loads were unrelated to SWR, Olsen P, or WEP in the first runoff event. The effect of SWR repellency could not be evaluated in this incidental phase as fertilisers were applied by the farmer using a broadcasting truck over the whole farm. Although the application rate was set to 18 kg P ha^{-1}, a uniform fertiliser application could not be guaranteed.

Phosphorus losses in the March-June period were more likely background losses originated from soils but not from fertiliser granules. During this period, a strong relationship between DRP concentrations and runoff coefficient have been observed in the different SWR levels (Fig. 3-7). The positive correlation between runoff rations and DRP concentrations in all the water repellency categories (R^2 between 0.79 and 0.48) suggest the important implication of runoff in all surface mixing and mobilisation of dissolved phosphorus. In addition to the influence of WEP on P losses (McDowell and Condron 2004), we assume that non-incidental DRP and TP loads after each rain events are also influenced by SWR as the latest has a direct impact on surface runoff ratio. The determination coefficient of regression between TP loads and SWR (R^2=0.53) was significantly higher in the non-incidental losses period (June 2020) compared to the incidental losses period (Feb 2020) (Fig. 3-8). This result represents the first evidence from a field experiment indicating the implication of SWR in increasing non-incidental P loads in surface runoff.

Concentrations of DRP seemed to be influenced by both SWR and WEP of the soils. However, this relationship's slope could be affected by the WEP levels as there is a positive correlation between DRP and WEP. Still, DRP concentration in the wettable soils did not exceed 1.40 ml L^{-1}. McDowell and Condron (2004) reported that DRP concentrations in simulated surface runoff are positively correlated with the WEP. However, Nash et al., (2019) reported that TP concentrations in individual runoff events are unrelated to runoff volumes. Nash and Murdoch (1997) reported that in many cases, within-storm TP concentrations were inversely proportional to the overland flow rate at the time, due to dilution. The surface runoff ratio gives more insight into the dissolution and mobilisation of soil phosphorus on the surface in the mixing surface layer compared to runoff volume which is the output of the runoff process. A higher runoff ratio suggests a higher mixing, dissolution, and mobilization of phosphorus on the surface. Nevertheless, soil water repellency would decrease mixing and dissolution below the wetting front, and thus reducing phosphorus losses from subsurface layers. Hence, we suggest the use of runoff coefficient instead of runoff volume to adequately model DRP concentrations in surface runoff (Fig. 3-7). Nash et al., (2019) demonstrated that overland flow dominated hydrology are associated with a high risk of P losses into waterways and concluded that fertilisers selection is essential in these circumstances. Sparingly soluble P fertiliser would significantly decrease P losses in hydrophobic soils. In an evaluation of two management options in a two-year study to reduce P losses in surface runoff from dairy farms, McDowell (2010) reported that a reactive phosphate rock decreased TP load and DRP concentrations in the runoff by 30 and 58 %, respectively, compared to superphosphate. Data from McDowell et al., 2020 showed that up to 0.5 kg ha^{-1} of DRP was lost in the 21 first days following application in soils with strong repellency that received 40 kg P ha^{-1}. In our study, the incidental DRP losses ranged between 1.7 and 3.7 kg in the same water repellency soil class and where only 18 kg P ha^{-1} was applied (Fig. 3-6). Water repellency was more decisive in the transport of P from the mixing layer (0-3cm) than the water P extractability from the soils.

The DRP losses in the first runoff event are more influenced by P availability (fertiliser application) than P extractability from the soil (McDowell et al., 2007). Phosphorus is directly exported from the fertiliser granules' precipitation zone in the first event following fertilisers application. Then, P mobilization is more dominated by export from the adsorption zone as fertilisers dissolve in the soil.

3.6 Conclusions

The potential SWR had a clear impact on the surface runoff over the rainfall ratio. The surface runoff generated in the summer-autumn period were significantly higher in hydrophobic

soils compared to wettable soils. There was an exponential decrease of DRP and TP concentrations in surface runoff starting from the first runoff event from the dry summer to winter. In the first runoff event following fertiliser application (incidental losses), phosphorus losses were unrelated to SWR or WEP but more likely to the amount of P applied in each plot. The P loads in this event accounted for more than 90 % of the summer-autumn period. While P loads were mainly dominated by incidental losses that are directly related to the amount and the solubility of the P fertilisers applied, the background P losses were strongly controlled by hydrological processes, especially SWR. A strong relationship has been observed between runoff coefficients and DRP concentrations in the surface runoff after the incidental losses period. Besides, non-incidental total P loads in surface runoff seem to be related to SWR. Based on these results, DRP concentrations can be modelled from the surface runoff coefficients, which in turn can be modelled from SWR and soil moisture dynamics. More field data is needed to consolidate these finding and allow modelling P losses in hydrophobic pastoral soils.

Chapter 4

The potential of multispectral satellite data to predict soil water repellency and soil carbon in temperate pastures

4.1 Abstract

Soil water repellency (SWR) is a critical soil property with several implications upon ecosystems functions, including physicochemical and hydrological processes. The occurrence of SWR is governed by the cycling of hydrophobic materials, which are intrinsic constituents of the soil carbon (C) pool. This study aims to explore the capability of multispectral satellite data from Sentinel-2 and Landsat-7 satellites to predict the level of SWR and topsoil C in pastures. Surface reflectance time series data of permanent pastures were filtered using the normalised difference vegetation index (NDVI) to select dates with the least aboveground biomass and acquire topsoil spectra. The potential persistence of SWR was measured using water drop penetration time (WDPT) and the molarity of ethanol droplet (MED) test was used to measure SWR severity. Partial least square regression (PLSR) models were calibrated and validated using topsoil measurements of SWR from 35 and 41 sites matched with topsoil spectra from Sentinel-2 and Landsat-7, respectively. Root mean square error (RMSE), coefficient of determination (R^2), and the ratio of performance to deviation (RPD) were calculated for predictions using leave-one-out cross-validation (v) and for predictions from the calibration set (c). Prediction performance for Log (WDPT) and MED compared was lower than that for soil C. The best prediction for SWR was achieved using Sentinel-2 spectra (R^2_v=0.45; $RMSE_v$=0.98 for Log WDPT) and (R^2_v=0.23; $RMSE_v$=4.95 for MED). Accuracy was improved using the calibration set for predicting Log WDPT (R^2_c=0.64; $RMSE_c$=0.77 with Sentinel-2 spectra), which indicated larger datasets might improve predictions. Soil C showed better predictability with Landsat-7 spectra (R^2_v=0.50; $RMSE_v$=2.58; R^2_c=0.70; $RMSE_c$=1.92) providing a useful model and offering an improvement to the current soil C assessment and mapping in pastoral ecosystems. This will help to quantify the magnitude of soil C to underpin the pastoral soils inventories.

4.2 Introduction

Soil water repellency (SWR) is a natural phenomenon that refers to the delay of soil wetting when water is applied. This transient property is driven by soil moisture and occurs when potentially water-repellent soils dry out below critical soil moisture (Dekker & Ritsema, 1994; Chau et al., 2014),

that is soil and site-specific. With the increasing risks of droughts (Clark et al., 2011), soil moisture may drop below the critical soil moisture more often and thus hindering soil rewetting after precipitation events or irrigation application. Detrimental consequences of SWR include increased surface runoff (Müller et al., 2018) and nutrient losses (Jeyakumar et al., 2014), and decreased soil water storage (Kobayashi & Shimizu, 2007). This dynamic property can be assessed by two different criteria, i) its degree or severity, which is a measure of the initial soil surface tension: and ii) its persistence, which is an estimate of the time taken to break down the repellent character of a soil surface in contact with water. The degree of SWR can be estimated by measuring the contact angle (Carrillo et al., 1999), the molarity of ethanol drop (MED) (Letey, 1969), or sessile drop methods (Chau et al., 2010). The persistence of SWR can be assessed using the water drop penetration time (WDPT) method (Letey et al., 2003). The actual level of SWR persistence as a function of soil moisture can be modelled, for example, using a reversed sigmoidal function that takes into account the potential SWR, the critical soil moisture and a curve shape parameter (Chapter 2). Some previous research in pastoral systems has shown a strong relationship between potential SWR and soil carbon (C). For example, Deurer et al., (2011) and Hermansen et al., (2019) reported significant correlations between SWR and soil C for two soil surveys of New Zealand pastures. Nevertheless, soil texture has an important influence on the occurrence of SWR (Bayad et al., 2020a; Capriel et al., 1995; McKissock et al., 2003).

Conventional methods of SWR measurement are time-consuming and require point scale measurements. Thus, mapping SWR at the farm or regional scale is limited. Remote sensing could provide an effective method for mapping SWR at different scales. Visible, near-infrared (Vis-NIR), and shortwave-infrared (SWIR) hyperspectral remote sensing have opened new opportunities for assessing topsoil properties and producing digital soil maps. Several studies demonstrated that hyperspectral remote sensing can be used to estimate many soil attributes. Examples include soil C (Castaldi et al., 2016; Cécile Gomez et al., 2008; Leone & Escadafal, 2001) soil texture (Casa et al., 2013; Galvão et al., 2008), pH and EC (Ben-Dor et al., 2002). Empirical models were developed to estimate soil properties that are related to chemical chromophores affecting surface reflectance at specific bands (e.g. OH groups in clays) (Ben-Dor et al., 1999) or properties that are consistently correlated with them (soil C and nitrogen). Therefore, correlations of SWR with soil C (Hermansen et al., 2019a) and specific organic materials (Bisdom et al., 1993) could be exploited to predict SWR from surface reflectance signatures. However, no research has investigated the potential of remote sensing surface reflectance data for SWR estimation. Previous attempts used laboratory VNIR/SWIR spectroscopy for estimating the potential SWR (Kim, I. et al., 2014) and predicting the relationship between SWR and soil moisture (Hermansen et al., 2019b; Knadel et al., 2016). However, modelling

SWR using satellite data provides a unique advantage to map soil properties at larger scales, i.e., from farm to regional scale. Bayad et al., 2020b suggested a remote sensing approach using surface biomass (estimated using NDVI) and the temporal dynamics of topsoil water deficits for predicting the occurrence of SWR in pastoral ecosystems. Still, evaluating soil surface reflectance data from satellites for predicting SWR and soil C has not been attempted in permanent pasture systems.

Although hyperspectral remote sensing provides a valuable tool to estimate soil properties, the limited availability of hyperspectral data has restricted its use. Until 2018, Hyperion was the only hyperspectral sensor operational (Folkman et al., 2001). The recently implemented hyperspectral sensor PRISMA (Loizzo et al., 2018) provides a spectral resolution of 10 nm, a spatial resolution of 30 m for VNIR/SWIR bands, 10 m for panchromatic bands, a swath width of 30 km and a revisit time of 7 days. Compared with hyperspectral sensors, multispectral sensors like Landsat-7 have a low spectral resolution. Still, Landsat-7 offers the most important multispectral global archive (Kovalskyy & Roy, 2013). The newly deployed Sentinel-2 satellites by the European Space Agency (ESA) offer multispectral images with high revisit time (2-3 days) that include 13 bands (VNIR/SWIR) and have a spatial resolution between 10 and 60 m (depending on the bands). However, very few studies achieved good accuracy in predicting topsoil physical and chemical properties using multispectral satellite data. Using Sentinel-2 multispectral data, Vaudour et al., (2019) acquired a useful model with an intermediate prediction accuracy for soil C (R^2_v=0.56; $RMSE_v$=1.23), pH (R^2_v=0.51; $RMSE_v$=0.51), and CEC (R^2_v=0.75; $RMSE_v$=1.23) in a temperate region. In terms of comparison between hyperspectral and multispectral remote sensing, Castaldi et al., (2019) showed that there was no substantial difference between the spatial variability of soil C maps derived by Sentinel-2 data and the ones derived by hyperspectral airborne data for a study area dominated by cropping. Similarly, Gomez et al., (2018) reported that there was no significant difference between Sentinel-2 and hyperspectral (airborne and satellite) data in predicting clay content for a semiarid Mediterranean region.

The prediction accuracy of remote sensing approaches depends on the quality of the remote sensing data, modelling approach, and the ground-truthing conducted. Remote sensing using satellite data presents many challenges including the atmospheric interaction with reflected electromagnetic radiation, surface roughness and the nature of the land cover. Ben-Dor, (2002) gives a detailed review of the challenges and the problems influencing quantitative remote sensing of soil properties. Assessing the topsoil properties of pastures is even more challenging because of the additional complexity through the temporal dynamics of the crop canopy and soil moisture. Aboveground biomass in permanent pastures complicates acquiring bare soil surface reflectance. Thus, finding a reliable procedure to deal with this issue is needed. In the present study, topsoil

spectra were acquired by filtering time series data from Landsat-7 and Sentinel-2 to select dates with the least surface biomass. Surface biomass and per cent ground cover are highly correlated with NDVI (Prabhakara et al., 2015). The use of the NDVI threshold to select bare soil areas have been used in several remote sensing studies to estimate topsoil properties. An NDVI threshold could help to select dates with a near bare soil condition from time-series satellite data of a given permanent pasture. When it comes to soil moisture effect on surface reflectance, an increase in water content decreases surface reflectance over the whole VIS-NIR and SWIR spectrum and particularly in 1200, 1400, and 1800 nm wavelengths (Lesaignoux et al., 2013; Lobell & Asner, 2002). Hence, the soil moisture effect could be minimised by considering the higher reflectance spectra from time-series data as dry topsoil spectra.

Soil C was assessed with respectable accuracies (R^2_v=0.56; $RMSE_v$=1.23) (Vaudour et al., 2019) using surface reflectance multispectral data from Sentinel-2 and low accuracies using S-1/2 and digital elevation model (DEM) derivatives (R^2_v=0.44; $RMSE_v$=0.57) (Zhou et al., 2020). Organic matter is a key chromophore across the entire VNIR/SWIR spectral region (Ben-Dor et al., 1999). We assume that relationships between SWR and soil C could be used to indirectly predict SWR using multispectral satellite data.

This research aims to:

i) Retrieve topsoil multispectral surface reflectance from Sentinel-2 and Landsat-7 time series data in permanent pastures;

ii) Investigate the potential of satellite multispectral data in predicting the SWR degree (MED) and persistence (WDPT) and soil C in pastoral soils.

4.3 Materials and methods

4.3.1 Soil sampling and analysis

The present study includes datasets of SWR in pastoral soils from three different surveys. i) The SWR survey conducted in the North Island of New Zealand by Deurer et al., (2011) in 2009; ii) a soil survey from several New Zealand dryland pastures by Whitley et al., (2018) conducted in 2014; and iii) soil samples collected in the Hawke's Bay region in 2019 (Bayad et al., 2020b). The North Island survey (Deurer et al., 2011) examined the influence of drought proneness and soil order on the occurrence of SWR in New Zealand pastures. Sampling in this survey was guided by soil drought-proneness and soil characteristics. The detailed sampling approach and site selection criteria are thoroughly explained in the survey paper by Deurer et al., (2011). The Whitley et al., (2018) survey comprised nine pastoral sites (6 in the South Island and 3 in the North Island). The Hawke's Bay

region sampling in 2019, covered 25 dryland pastoral sites. Combining these soil datasets yielded a varied range of textures from clay to sand. The sampling sites cover a wide selection of soil orders that include Podzol (Spodosols), Allophanic (Andisols), Gley (Aquic groups), Pallic (Inceptisols, Alfisols), Organic (Histosols), Recent (Entisols, Inceptisols), Pumice (Andisols, Vitric), Brown (Inceptisols, Alfisols), Granular (Ultisols), and Ultic (Ultisols) soils (New Zealand soil classification and their taxonomy equivalent (Hewitt, 2010)). Five topsoils (7.5 cm) samples were collected in a star-shaped pattern, 25 m apart in the 2009 survey. Samples were collected at 7.5 cm depth in a cross-shaped pattern and 2 m apart in the 2019 survey. In 2014, soils were collected along 50 m transects at 15 cm depth (Whitley et al., 2020). Soils were sieved at 2 mm and oven-dried at 65 degrees C for the analysis of potential SWR. The WDPT test was carried out by placing three water droplets of 40 µl (50 µl in the 2009 survey) onto a smoothed surface of the soil samples and recording the total infiltration time in seconds (s) (Doerr, 1998). For SWR severity measurements, ethanol concentrations of 0, 3, 5, 8.5, 13, 24, and 36% by volume were prepared, and five droplets of 40 µL were placed on the smoothed soil sample surface. The MED was represented by the ethanol molarity of the droplet that penetrated the soil surface in 5 s (10 s was used in the 2009 survey). The median of the measurements was used instead of the mean since it represents better the tendency in skewed data such as WDPT. Total C was measured using an Elementar Vario-Max CN Analyser, Germany.

4.3.2 Remote sensing data and modelling

Multispectral data were acquired from Landsat-7 and Sentinel-2. Landsat-7 surface reflectance data are provided by the United States Geological Survey (USGS) agency. This dataset is an atmospherically corrected surface reflectance from the Enhanced Thematic Mapper Plus (ETM+) sensor aboard Landsat-7. Atmospheric correction of the raw data was carried out by the USGS using the C Function of Mask (CFMask) algorithm (Foga et al., 2017). The Multi-Spectral Instrument (MSI) aboard the Sentinel-2 satellite provides 13 spectral bands covering VIS-NIR and SWIR region. Surface reflectance data is provided by the Copernicus program, ESA. Atmospheric correction on this dataset was done by the Sen2cor algorithm (Main-Knorn et al., 2017).

Surface reflectance time series from 1999 to 2020 for Landsat-7 and from 2017 to 2020 for Sentinel-2 were filtered for cloud cover (Fig. 4-1. a, b). Cloud-free dates with an atmospheric opacity of less than 10% were used. An NDVI threshold was used to separate dates with bare soil (Gomez et al., 2018). A value of 0.30 was used after considering the lab spectra of 78 soil samples. This threshold was used to identify dates with the bare soil surface and extract reflectance spectra samples (Fig. 4-1. c, d). Surface NDVI was calculated for the whole dataset using the bands B3 and B4

from Landsat-7 (630-690nm and 770-900nm, respectively) and B4, B8 from Sentinel-2 (650-680nm and 785-899nm, respectively).

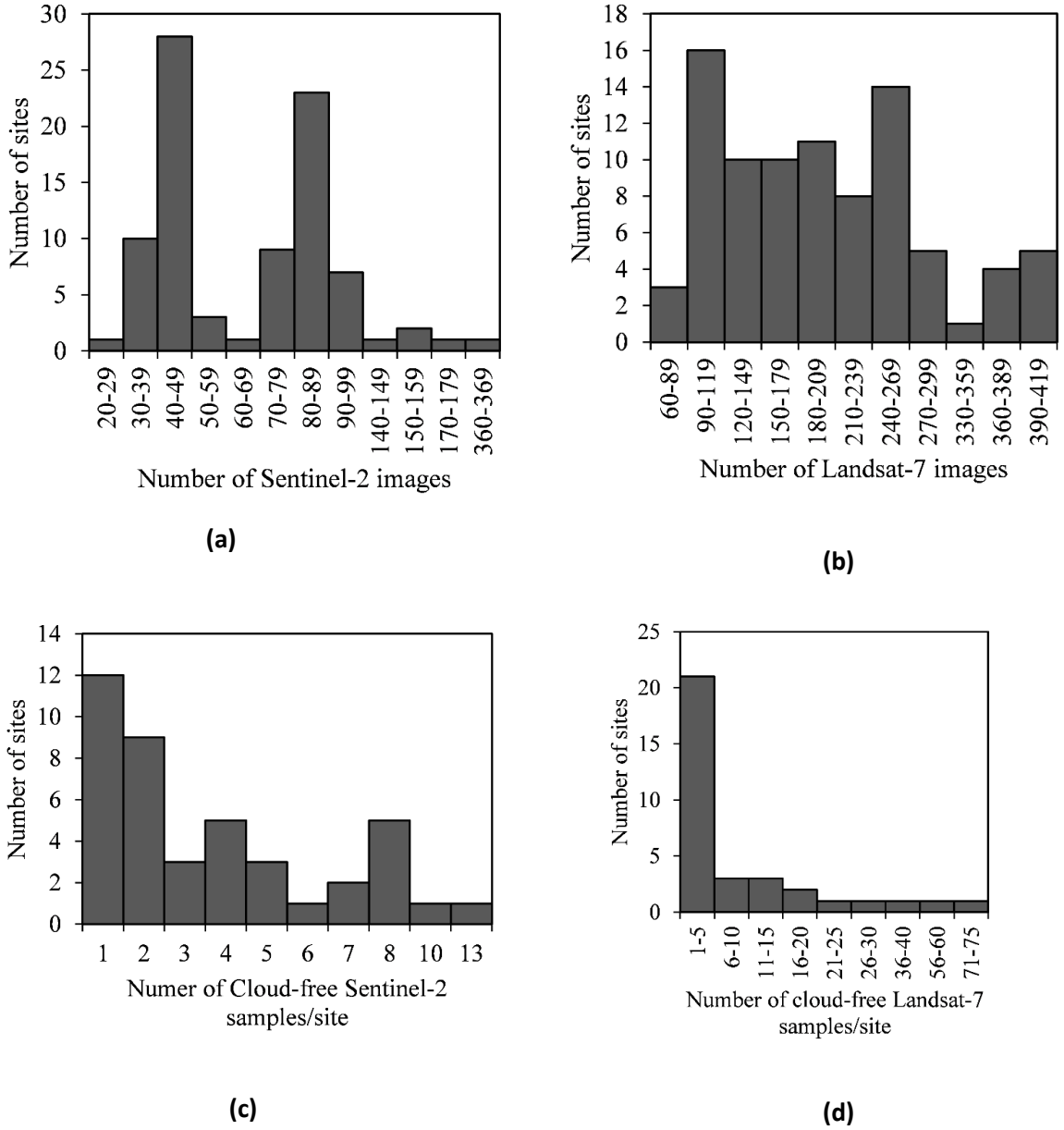

Figure 4-1 Histogram of the number of images per site from a) Sentinel-2, b) Landsat-7; and cloud-free samples of bare soil spectra per site from c) Sentinel-2, and d) Landsat-7. A sample of cloud-free, low atmospheric opacity, and NDVI <0.3 was needed for a pixel to be counted.

Dates with higher reflectance were selected as reflectance samples spectra of dry soils (Lobell & Asner, 2002; Weidong et al., 2002) and were used to build multispectral data inputs. For this purpose, two configurations were tested: i) *Upper spectra,* which had the higher average surface reflectance of MSI and ETM+ bands and, ii) *maximum spectra* that were reconstituted from the

maximum reflectance on each band. An example of a Sentinel-2 time series spectra from a Raw Soil site in Hastings is presented in Figure 4-2. In this example, a cloud-free, low atmospheric opacity, and a 0.3 NDVI threshold were applied. The *Upper spectra*, in this case, correspond to the 15th Feb 2020 and is equal to the *maximum spectra.*

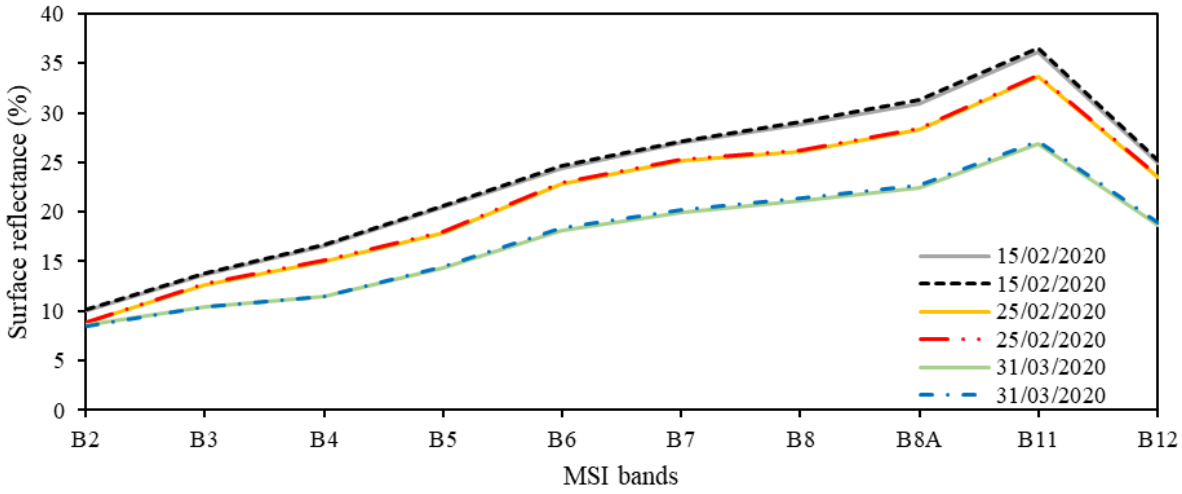

Figure 4-2 Cloud-free surface reflectance samples after application of bare soil threshold for a Raw Soil site located in Hastings, Hawke's Bay, New Zealand.

Separately from the satellite spectra, a set of 78 soil samples were used to get lab spectra using a proximal multispectral sensor. These soils were sampled in 2018 and 2019 from Hastings, and Te Pohu, Hawke's Bay region, New Zealand. The lab spectra were measured using the multispectral sensor Altum, Micasence, USA. For this purpose, the smoothed soil samples were placed near a white reference panel and were evenly illuminated by a halogen lamp. The Altum sensor was positioned at 50 cm height above the sample. The soil reflectance was estimated by multiplying the relative radiance (to the reference panel) with the panel's reflectance. The sensor's spectral bands include blue, green, red, red-edge, and near-IR (475, 560, 668, 717, and 842 nm, respectively). The comparison between MSI, ETM+, and Altum multispectral bands used in this study are presented in Figure 4-3.

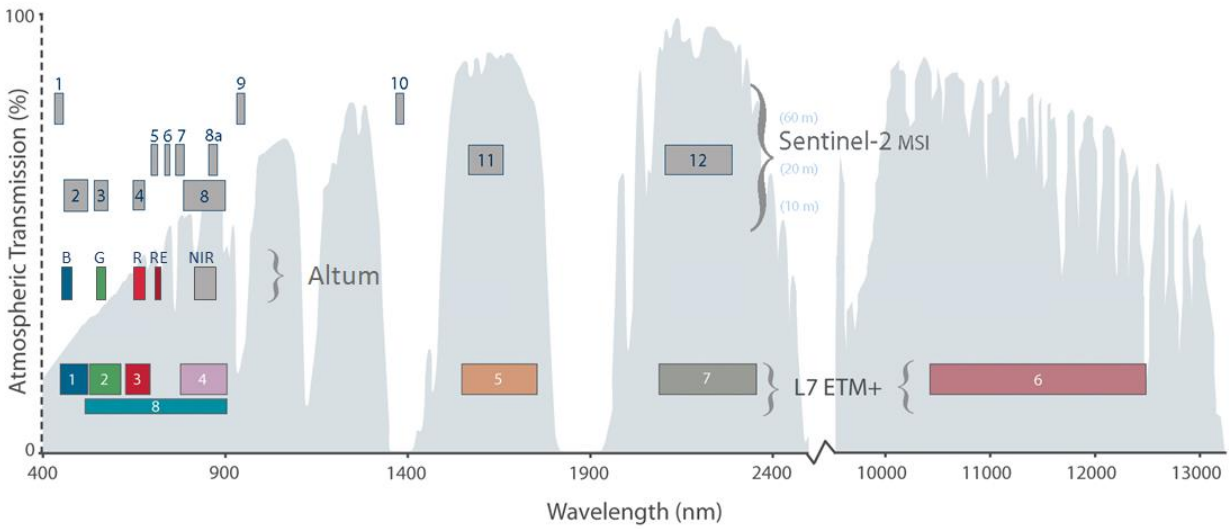

Figure 4-3 Multispectral channels and band-passes different sensors used in the study and atmospheric transmission % (grey background). ETM+ of Landsat-7 (excluding thermal band B6); MSI of Sentinel-2 (excluding B1, B9, and B10); and Altum Micasense sensor (Modified from the source: NASA/Landsat Legacy Project Team and American Society for Photogrammetry and Remote Sensing by adding Altum bands).

The combined soil database contained between 2.49 and 40.5 % C. A peat soil site with soil C equal to 40.5 % was excluded from the ground-truthing data as peat covers merely 0.7 % of New Zealand's land area, with 50 % located in Waikato (Davoren et al., 1978).

Partial least squared regression (PLSR) models were built from the soil spectral and the soil measured data. The PLSR models were developed using all the data (calibration), and using leave-one-out cross-validation (validation).

4.3.3 Measured SWR and soil C matched with soil spectra

After filtering remote sensing data to retrieve soil surface spectra, 41 sites were matched with Sentinel-2 spectra and 34 sites were matched with Landsat-7 spectra. The number of lab spectra was equal to the number of soil samples used in the laboratory (78 samples). Descriptive statistics of the measured soil properties used for calibration and validation of the PLSR model with remote sensing data are presented in Table 4-1. In the three datasets, SWR persistence ranged from wettable to extremely hydrophobic (Table 4-1). The mean Log (WDPT), MED and soil C were within the same range for the three datasets matched with Sentinel-2, Landsat-7, and lab spectra.

Table 4-1 Summary statistics of the dataset used for model calibration with Sentinel-2, Landsat-7, and Laboratory spectra.

		Log (WDPT) (s)	MED (%)	C (%)
Sentinel-2				
n=41	Mean	1.63	4.07	6.58
	Max	4.00	24.00	20.20
	Min	0.00	0.00	2.49
	Std. Deviation	1.30	5.58	3.41
Landsat-7				
n=34	Mean	1.52	4.26	6.81
	Max	3.79	13.00	19.62
	Min	0.00	0.00	2.49
	Std. Deviation	1.26	4.51	3.62
Lab Spectra				
n=78	Mean	1.49	*ND*	6.57
	Max	3.89	*ND*	12.89
	Min	0.00	*ND*	2.49
	Std. Deviation	1.07	*ND*	2.45

(*ND*) not measured.

Partial least square regression (PLSR) method as implemented by (Mevik & Wehrens, 2015) was used to model soil properties based on multispectral and measured SWR and soil C data. The PLSR method provides a robust alternative to multiple linear regression and principal component analysis (Geladi & Kowalski, 1986). The method is one of the most used approaches for multi and hyperspectral data (Viscarra Rossel et al., 2006). It handles better multicollinearities and minimises the effect of data noise. The models' performances were assessed using the root mean squared error (RMSE), the coefficient of determination (R^2) and the ratio of performance to deviation (RPD).

4.4 Results

4.4.1 Measured soil properties

The soil orders Recent, Organic and Pumice had the highest medians of Log (WDPT), while Brown, Organic, and Recent had the highest medians of MED (Fig. 4-4). However, Log (WDPT) values for Pumice and Recent soil orders were more spread around the medians compared to those of the Organic soil order. Raw, Brown, Pallic, Allophanic, and Granular soil orders showed the lowest persistence of SWR. In comparison to SWR data, soil C data were less spread around the median (Fig. 4-4). The positive correlation between soil C and both Log (WDPT) and MED had an R^2 of 0.22. These findings were different to Hermansen et al., (2019a) who found a strong correlation between SWR degree and soil C. However, (Doerr et al., 2006) found no obvious relationship between SWR persistence and soil C in a study covering multiple land-uses in a humid temperate region.

In the soil dataset used for the laboratory spectra analysis, the Pumice and Allophanic had the higher Log (WDPT) and soil C, while Raw and Pallic soil orders showed the lowest Log (WDPT) and soil C. The correlation between soil C and Log (WDPT) in this dataset has an R^2 of 0.28.

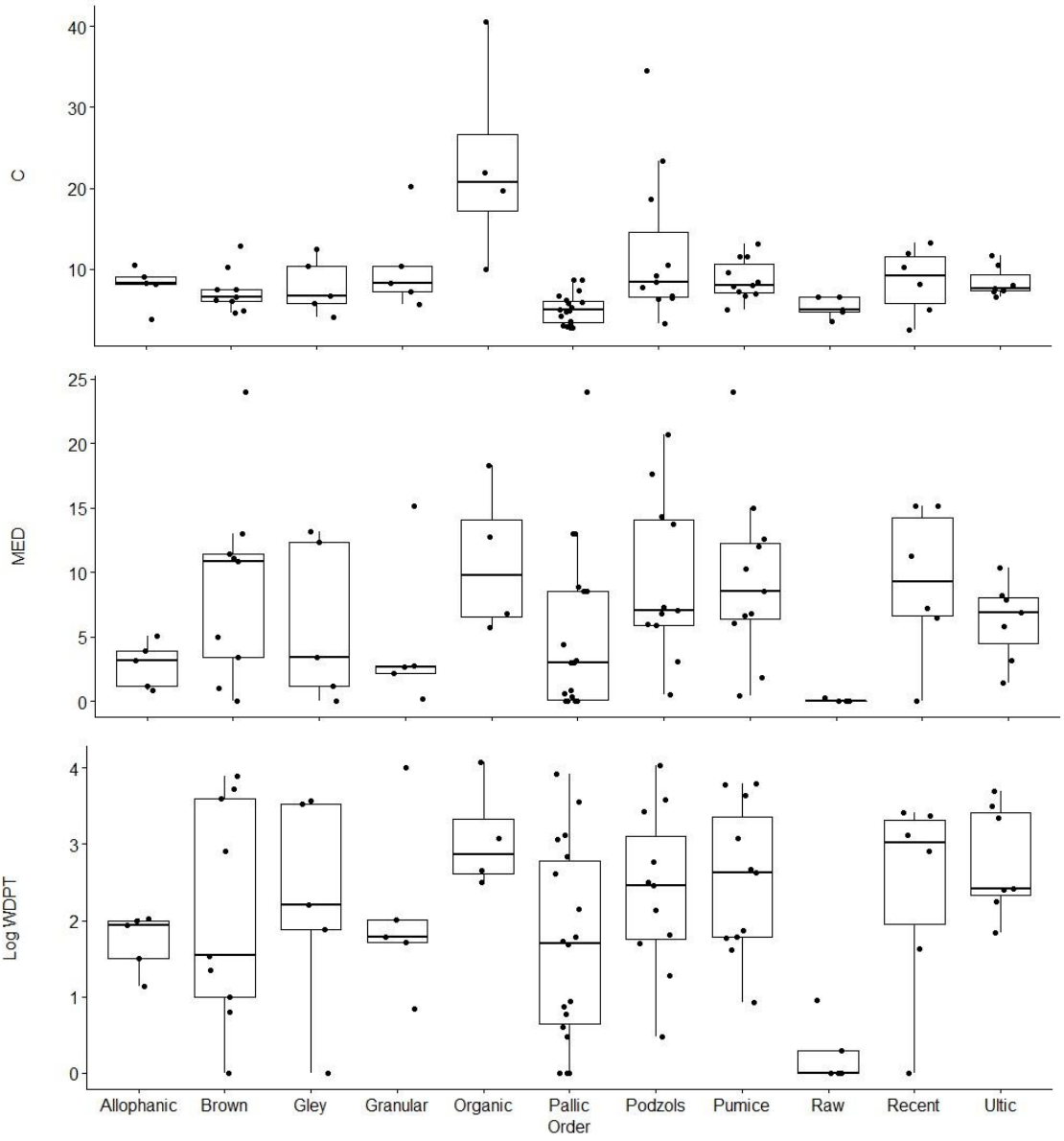

Figure 4-4 Box plots of laboratory analysed soil C (%), water drop penetration time Log (WDPT) (s), and MED (%) (n=41). Points are the outliers, centre lines are median, box limits are lower and upper quartiles; whiskers are 1.5x the interquartile.

4.4.2 Models performance

Performance of models using Sentinel-2, Landsat-7 and lab spectra-derived models are summarised in Table 4-2. The PLSR models performance (R^2 and RMSE) dropped when cross-validation was performed instead of fitting using the calibration set. Generally, the SWR predictions were less accurate than the prediction of soil C. However, the predictions of Log (WDPT) were more accurate than those of MED. The Sentinel-2 derived model performed best for Log (WDPT)

predictions based on the calibration data set ($RMSE_c$=0.77 and R^2_v=0.64) and predictions with cross-validation ($RMSE_v$=0.98; R^2_v=0.44) (Fig. 4-6. a). The Landsat-7 derived model showed the best prediction performance for soil C for both the calibration ($RMSE_c$=1.92; R^2_c=0.71) and the validation data sets ($RMSE_v$=2.58; R^2_v=0.50) (Fig. 4-6. b). The lab spectra derived model showed the best prediction with cross-validation for soil C ($RMSE_v$=1.62; R^2_v=0.52) (Fig. 4-6. c) and the lowest error for log (WDPT) ($RMSE_v$=0.86; R^2=0.35) (Table 4-2 and Fig. 4-6.d). Models built using satellite multispectral data showed comparable performance to models developed using lab multispectral reflectance. The PLSR calibration and cross-validation prediction accuracies can be classified in three levels as described by Vaudour et al., 2019: i) models with intermediate to high predictability (R^2>0.5 and RPD>1.4); ii) models with poor predictability (R^2 of 0.4 – 0.5 and RPD of 1.3); and iii) models with poor to very poor predictive potential (R^2<0.4; RPD<1.3).

Landsat-7 and Sentinel-2 derived models exhibited intermediate prediction accuracies for soil C and Log (WDPT) using the calibration set. However, prediction capacity dropped to poor or very poor for all models (except for soil C with Landsat-7 data), when using leave-one-out cross-validation. Laboratory spectra derived model's performance had no significant drop in performance between calibration and validation sets. This drop in performance could be caused by the limited number of samples in the training set and/or the high variability across the data set (Fig. 4-4). This limits the possibility of adequate training of the model with sufficient redundancy in the predicted features. However, the prediction capacity of the calibration set indicates that using a larger dataset with enough redundancy in the measured features might improve models' performance.

The PLS regression coefficients for prediction of the measured soil properties using Sentinel-2 and Landsat-7 spectra are illustrated in Figure 4-5, a-c. The coefficient's magnitude represents the wavebands contribution in accommodating the measured SWR and soil C data. Thus, the higher the coefficient value, the higher the waveband importance in building the predictive model for the measured property. The green (560 nm) and red-edge bands (703 and 782 nm) had a higher contribution in predicting Log (WDPT) using Sentinel-2 spectra, while the red-edge bands (703-782 nm) and SWIR (1613 nm) all slightly contributed equally to the prediction of Log (WDPT) (Fig. 4-5. c). Red-edge (740 nm) and red (664 nm) bands influenced the prediction of soil C the most (Fig. 4-5. d). When using Landsat-7 spectra, the blue, red and SWIR bands (485, 660, and 1650, respectively) were the most influential bands in determining water repellency and soil C (Fig. 4-5. a, b).

4.4.3 Discussions

The performance of the multispectral data for soil C was comparable to previous studies. Soil C prediction model using the Landsat-7 surface reflectance showed an intermediate performance (R^2

= 0.50, RPD=1.40) (Table 4-2), which is higher than some studies that used Sentinel-2 for soil C prediction (e.g. Zhou et al., 2020) (R^2=0.44, RPD=1.29) or simulated spectra of different multispectral imagers by Castaldi et al., 2016, who found an $R^2 \leq 0.20$ and RPD ≤ 0.13 using soil C data from European Land/Use Cover Area frame Statistical Survey. However, these studies used the top canopy reflectance instead of bare soil reflectance. This might affect the prediction of topsoil attributes in cases where a large number of the training points are covered by surface biomass when the reflectance data is acquired.

The lower performance of the PLSR models in predicting SWR compared to predicting soil C suggests that soil hydrophobicity prediction did not exclusively rely on its spectral chromophore. If the considered property was highly correlated with a strongly expressed spectral property, this might give an advantage in terms of its prediction capability. Soil organic C has a known spectral sensitivity over the whole VNIR-SWIR spectral interval (Ben-Dor et al., 2009). As expected for soil C, loading values were found to have noticeable peaks in the B1, B3, and B5 bands of Landsat-7 corresponding to 470 nm, 660 nm, and 1650 nm, respectively, and B4, B5, and B11 from Sentinel-2 (665 nm, 705 nm, and 1610 nm, respectively) (Fig. 4-5). Similar patterns were observed by Vaudour et al., 2019 who predicted the soil C model based on Sentinel-2 data.

In our study, the correlation between soil C and SWR persistence (Log (WDPT)) in the combined datasets had an R^2 of 0.22. In contrary to the present combined datasets, data from Hermansen et al., 2019a showed a high correlation between soil C and SWR. This could be due to the uniform sampling and a measurement methodology (e.g. same sampling depth and period).

Although soil C was not strongly correlated with SWR persistence, it might contribute to the prediction of SWR. Hydrophobic compounds constitute a very small part of the whole soil C pool (Franco et al., 2003), and hydrophobic compounds derived from different sources will not necessarily dramatically change the reflectance signature of the soil. Still, the occurrence of SWR would be partly influenced by soil order (Fig. 4-4) and soil texture (Bayad et al., 2020a). Clay content, which has intermediate predictability because of the spectral behaviour of OH groups (e.g. R^2_v=0.71; RPD=1.9, in Gomez et al., 2018), could have impacted the predictability of SWR persistence to some extent. Surface reflectance data quality could also have affected the results: aboveground biomass, including dead leaves, could have an important influence on surface reflectance, although the low NDVI threshold was applied.

Table 4-2 Partial least squares regression (PLSR) statistics of prediction from calibration and leave-one-out cross-validation of multispectral data for soil C, the molarity of ethanol droplet test (MED), and water drop penetration time test (Log(WDPT)).

Configuration		Calibration				Validation			
		RMSE	R^2	NF	RPD	RMSE	R^2	NF	RPD
Sentinel-2 (*n*=41)									
Max spectra	Log (WDPT) (s)	**0.77**	**0.64**	**10**	**1.68**	**0.98**	**0.44**	**7**	**1.32**
	MED (%)	4.28	0.39	10	1.30	5.14	0.17	3	1.08
	C (%)	2.20	0.57	10	1.55	3.32	0.07	10	1.02
Upper spectra	Log (WDPT) (s)	0.89	0.52	10	1.46	1.16	0.21	8	1.12
	MED (%)	3.91	0.49	10	1.42	4.95	0.23	4	1.12
	C (%)	2.28	0.54	10	1.49	3.33	0.06	8	1.02
Landsat-7 (*n*=34)									
Max spectra	Log (WDPT) (s)	0.92	0.48	6	1.36	1.15	0.23	5	1.09
	MED (%)	3.81	0.28	6	1.18	4.61	0.00	5	0.97
	C (%)	2.11	0.62	6	1.71	2.86	0.35	6	1.26
Upper spectra	Log (WDPT) (s)	0.94	0.43	6	1.34	1.10	0.25	3	1.14
	MED (%)	3.73	0.29	6	1.20	4.44	0.05	3	1.01
	C (%)	**1.92**	**0.71**	**6**	**1.88**	**2.58**	**0.50**	**6**	**1.40**
Lab Spectra									
	Log (WDPT) (s)	**0.77**	**0.47**	**5**	**1.38**	**0.86**	**0.36**	**5**	**1.24**
	C (%)	**1.45**	**0.64**	**5**	**1.68**	**1.62**	**0.52**	**2**	**1.51**

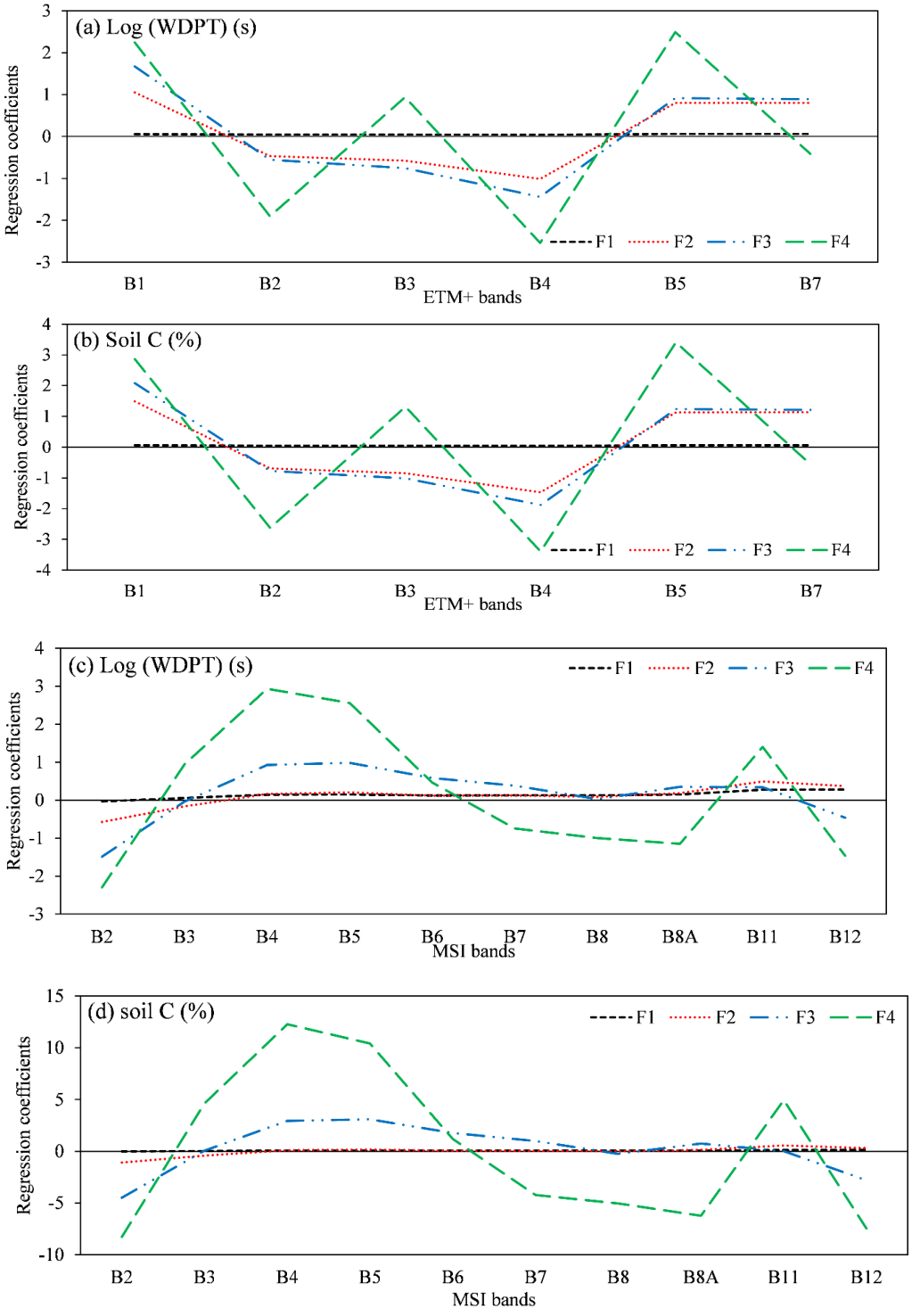

Figure 4-5 Loading plots for Log (WDPT) and soil C for (a) and (b) using ETM+ bands B1 to B7; (c) and (d) using MSI bands (B2 to B12). F1 to F4 are the PLSR components.

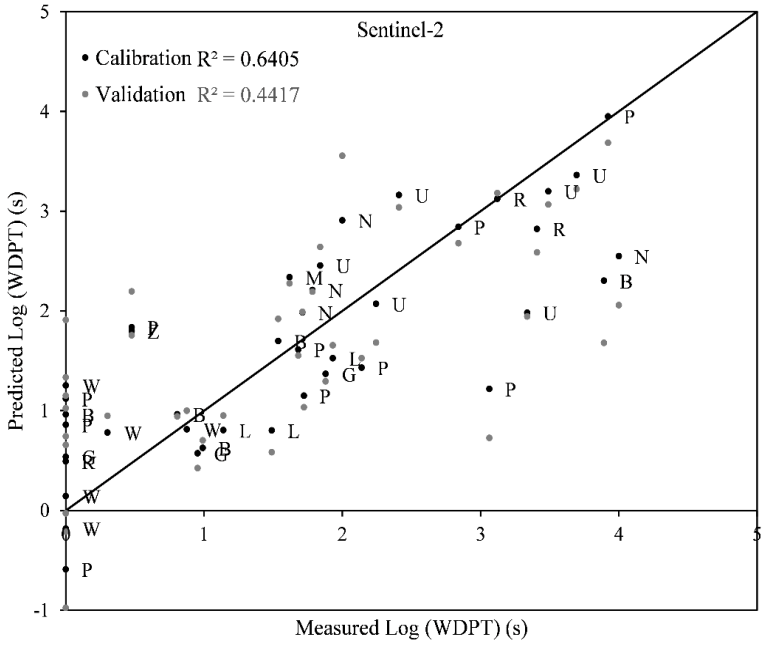
Sentinel-2
• Calibration R² = 0.6405
• Validation R² = 0.4417
Predicted Log (WDPT) (s)
Measured Log (WDPT) (s)
5
4
3
2
1
0
-1
0
1
2
3
4
5

(a)

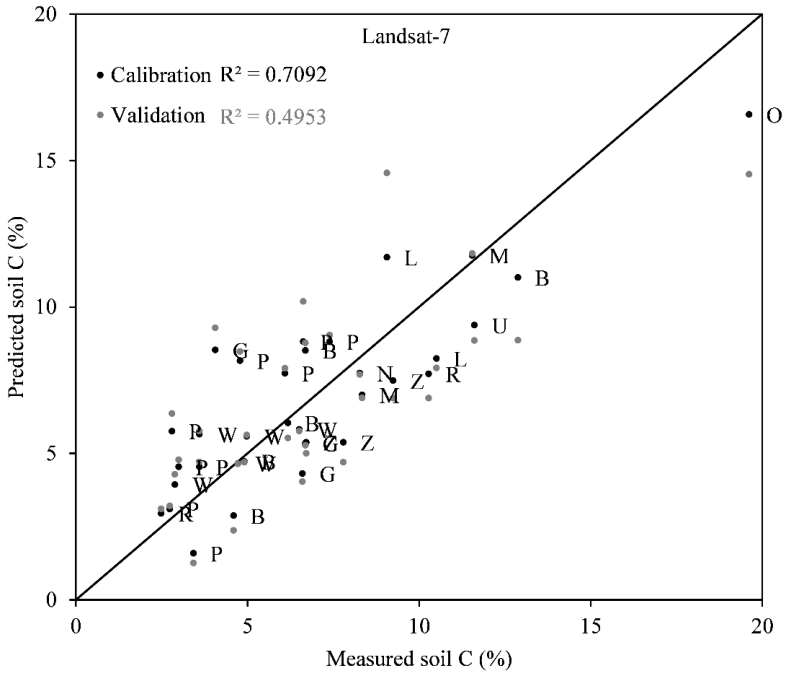
Landsat-7
• Calibration R² = 0.7092
• Validation R² = 0.4953
Predicted soil C (%)
Measured soil C (%)
20
15
10
5
0
0
5
10
15
20

(b)

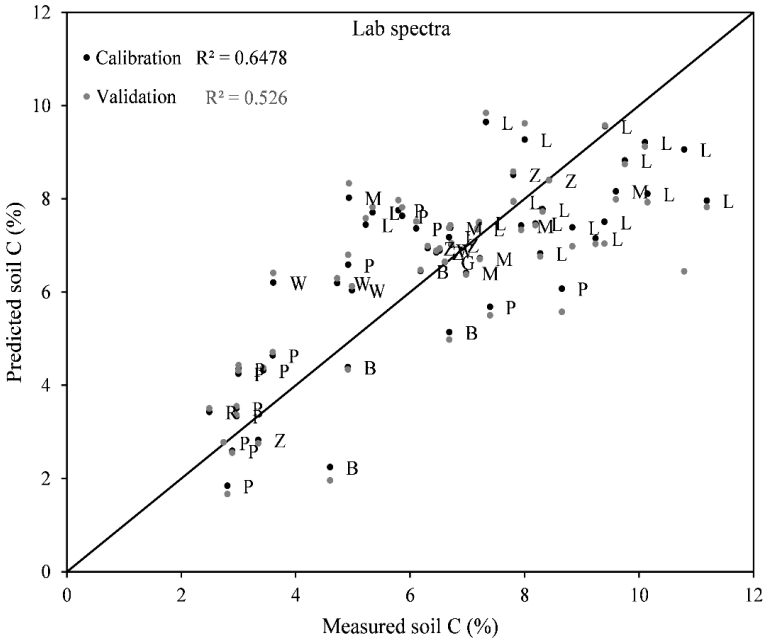
Lab spectra
Calibration R² = 0.6478
Validation R² = 0.526
Predicted soil C (%)
Measured soil C (%)
0
2
4
6
8
10
12

(c)

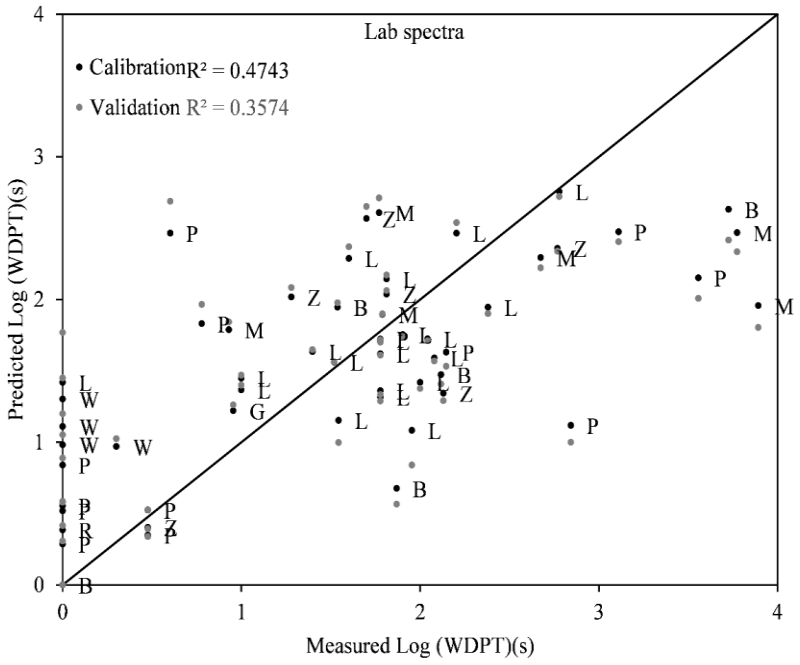

(d)

Figure 4-6 Predicted vs. measured (a) Log (WDPT) using Sentinel-2 data; (b) Soil C using Landsat-7 data; (c) Soil C using lab spectra, and (d) Log (SWR) using lab spectra. The point labels represent the soil orders: Raw (W), Pallic (P), Allophanic (L), Gley (G), Brown (B), Organic (O), Recent (R), Pumice (M), Ultic (U), Podzols (Z), and Granular (N).

4.5 Conclusions

This study investigates the potential of using multispectral satellite time series data to predict SWR and soil C in pastoral systems. It showed that: i) Sentinel-2 and Landsat-7 time series can be used to acquire surface reflectance spectra with low aboveground biomass in permanent pastures, and ii) the extracted surface reflectance data can help in predicting SWR and soil C levels in permanent pastures. Soil C was predicted with an intermediate accuracy (R^2_v=0.50; and RPD=1.4) using Landsat-7 data. However, a lower accuracy was achieved for WDPT prediction (R^2_v=0.45; RPD=1.32 using Sentinel-2). The PLS models trained using multispectral data showed higher accuracy for soil C prediction when predicting values from the calibration dataset compared to when using cross-validation. This indicates the potential of model improvement with a larger training dataset. With the increased availability of multispectral satellite data, the present methodology will help to improve the resolution of soil C inventories in permanent pastures. Further research is needed to understand the effect of SWR on surface reflectance and exploit the full potential of multispectral

satellite data for SWR characterisation. Larger ground truth data could improve the model prediction accuracy and provide a valuable tool for SWR mapping that will guide remediation strategies and reduce the impact of SWR on environmental services.

Chapter 5

Time series of remote sensing and water deficit to predict the occurrence of soil water repellency in New Zealand pastures

This chapter has been published in the ISPRS Journal of Photogrammetry and Remote Sensing.

https://doi.org/10.1016/j.isprsjprs.2020.09.024

5.1 Abstract

Soil water repellency (SWR) is a natural phenomenon occurring in soils throughout the world, which impacts upon ecosystem services at multiple temporal and spatial scales (nano to ecosystem scale). In pastures, the development of SWR is primarily determined by the cycling of hydrophobic materials at the soil surface and is controlled by climate, management, and soil properties. The complex interactions between these factors make it an intricate system to understand and model. Detailed spatiotemporal characterisation of the surface moisture and biomass in pastoral ecosystems would allow for a better understanding of this phenomenon. Normalised Difference Vegetation Index (NDVI) and Synthetic Aperture Radar (SAR) backscatter are good predictors for surface biomass and soil moisture, respectively. Machine learning on remote sensing time series (TS) data shows promise to predict the occurrence of SWR in pastures. This study evaluates the ability of remote sensing TS to predict the occurrence of SWR in New Zealand pastures, using three machine learning algorithms. Soil water repellency data were collected from 58 pastoral sites. Machine learning models were trained and cross-validated on monthly aggregated remote sensing and water deficit TS data to predict SWR level. Prediction output from artificial neural networks (ANN), random forest (RF), and support vector machine (SVM) were compared using root mean squared error (RMSE). When using NDVI TS data from 58 sites as predictors of SWR, the SVM and RF (RMSE= 0.82 and 0.87, respectively) outperformed ANN (RMSE=1.23). Random forest was used to map SWR magnitude over Hawke's Bay region in the North Island of New Zealand, and the overall accuracy was equal to 86%. This study is the first investigation implicating remote sensing TS data to predict the occurrence of SWR at the regional scale. Mapping the potential SWR will aid in identifying critical zones of SWR, to attenuate its effect on pastures through adapted management.

5.2 Introduction

Soil water repellency (SWR) refers to the inability of dry soils to absorb water spontaneously. This phenomenon has been identified in multiple soil types and under a variety of climate conditions (Dekker et al., 2005; Roper et al., 2015). The origin of SWR is due to hydrophobic compounds covering the hydrophilic soil minerals. This issue causes water droplets to ball up on the soil surface and prevent them from infiltration (Doerr et al., 2000). In agroecosystems, water repellency can occur after the decomposition of plants and the release of hydrophobic compounds or because of hydrophobic root exudates. Most grasses have superhydrophobic leaves (Barthlott et al., 2017). Thus, dead leaves decomposition would be a potential source of SWR in pastures. Drought in pastures can significantly contribute to these processes through biomass degradation and the release of hydrophobic compounds. Sudden drought may also contribute to this phenomenon through changes in roots metabolisms resulting in hydrophobic exudates. Many plant species inherently release hydrophobic root exudates (Erickson et al., 2001; Netzly & Butler, 1986; Y. Zhang et al., 2010). Gargallo-Garriga et al., (2014) reported that drought significantly changed root metabolism of two grass species (*Holcus lanatus L. and Alopecurus pratensis L.*). Data from this study showed that drought increased the production of some hydrophobic metabolites (e.g. proline, thymine). However, the effect of root exudate under hydric stress on SWR in not fully understood. There are no systematic studies on how these exudates impact SWR. Microbial communities such as fungi would also have a strong implication in cycling the hydrophobic compounds.

The decrease in water infiltration has significant repercussions for runoff (Müller et al., 2018), reduction in plant growth (Blackwell et al., 1994), and increases in water and nutrient losses (Leitch et al., 1983). In pastoral systems, SWR has negative environmental and economic consequences. In a study of 15 pastoral sites in New Zealand, Müller et al., (2010) reported that SWR caused pastoral growth to decrease between 5 and 20% and significantly increased the risk of herbicide loss via surface runoff. The authors stated that SWR constitutes a risk for New Zealand's pasture production, particularly in the face of future climate change, leading to more periodic summer droughts in some regions of New Zealand. In another study, Müller et al., (2014) demonstrated that a large part of the variability in pasture production was affected by the degree and the persistence of SWR.

To properly understand this problem, adequate characterisation of SWR and its persistence is needed. Knowing the likelihood and severity of SWR in different points of an agricultural field could help reducing water and nutrient losses by advising land managers when and where to use fertilisers and suitable mitigation practices such as surfactant application, lime, and cultivation and resowing (Müller & Deurer, 2011). However, no current method enables the assessment of SWR spatiotemporal dynamics. Although there are different conventional methods for SWR

measurement, such as the water drop penetration time (WDPT) and molarity of ethanol drop (MED) test, these methods are time-consuming and are point scale measurements. Thus, the possibility of constructing spatial and temporal data based on this measurement is limited. To improve the understanding of SWR, we need to investigate SWR occurrence at multiple scales (Mao et al., 2019). Remote sensing provides a promising alternative for SWR characterisation. Abrantes et al., (2017) suggested a method involving the use of infrared thermography and cold water to map soil water repellency at the laboratory scale. In other studies, visible and near-infrared spectroscopy (Kim et al., 2014; Abrantes et al., 2017; Hermansen et al., 2019) was tested for SWR assessment in the lab. These studies showed promising results, indicating the potential for remote sensing in water repellency assessment. Since pasture management and water deficit are important factors controlling surface biomass temporal dynamics, remote sensing and water deficit time series (TS) could provide a valuable tool to predict SWR occurrence in pastures. Still, no experimental approach has been developed to map SWR under field conditions; and more importantly, to predict its occurrence using readily available data.

The recently deployed Sentinel constellation by ESA has opened new horizons for remote sensing applications. These Synthetic Aperture Radar (SAR) and multispectral satellites provide high spatial resolution data, which are required for different remote sensing applications. Another instrument that provides remote sensing data with high temporal frequency (1 to 2 days) is the Moderate Resolution Imaging Spectroradiometer (MODIS). The high temporal resolution is indispensable for tracking surface biomass in highly dynamic agroecosystems like pastures.

Multispectral surface reflectance offers a consistent record of the aboveground biomass, which is directly implicated in the regeneration of hydrophobic materials. The normalised difference vegetation index (NDVI) is highly correlated with surface biomass (Prabhakara et al., 2015). Synthetic Aperture Radar backscatter is highly related to soil surface moisture dynamics (Zhang et al., 1998). Using NDVI, water deficit and SAR TS data would allow the assessment of surface biomass dynamics and thus, reflect the effect on SWR occurrence. These interactions between soil moisture, surface biomass dynamics, and the appearance of water repellency are still poorly understood. Jaramillo et al., (2000) theorised that arid conditions would result in low biomass production rates and, therefore, a lower probability for the development of SWR. While very humid conditions are favourable for biomass production and, thus, for the generation of hydrophobic compounds from decomposed leaves. Based on this theory, soil carbon (C) and hydrophobic compounds share the same cycling dynamics, considering that hydrophobic compounds are a natural constituent of the soil carbon pool in pastoral ecosystems. Soil fungal communities are an additional source of hydrophobic compounds and are profoundly affected by soil moisture dynamics (Castaño et al., 2018; Meisner et al., 2018). Nevertheless, remote sensing TS could be instrumental in tracking soil hydrophobicity

because it allows the assessment of critical components of this complex system, namely, aboveground biomass and moisture dynamics.

Given that the nature and causes of spatial variability in remote sensing data are not fully understood, the analysis of the remote sensing data has been limited to empirical relationships between ground truth data and patterns identified in remotely sensed images, assuming that surface ground truth data are consistently reflected in images (Belgiu et al., 2016; Woodcock et al., 1988). However, the interaction between factors like resolution and the nature of the explored properties makes it difficult to perceive this consistency between ground truth data and images using simple modelling approaches (Marceau, Howarth, and Gratton 1994). Non-parametric supervised algorithms like artificial neural networks (ANN), random forest (RF), and support vector machine (SVM), provide the advantage of deciphering hidden patterns and learning from complex data (Zhu et al., 2017). The present study investigates the potential of these algorithms to predict SWR using remote sensing and water deficit TS as predictors.

The main objectives of this study were to:

i) Explore the potential of remote sensing and water deficit TS in predicting the occurrence of SWR and assessing soil C in pastures;

ii) Understand how surface biomass and soil moisture temporal dynamics affect the SWR occurrence through the use of NDVI and water deficit TS.

5.3 Material and methods

5.3.1 Study area

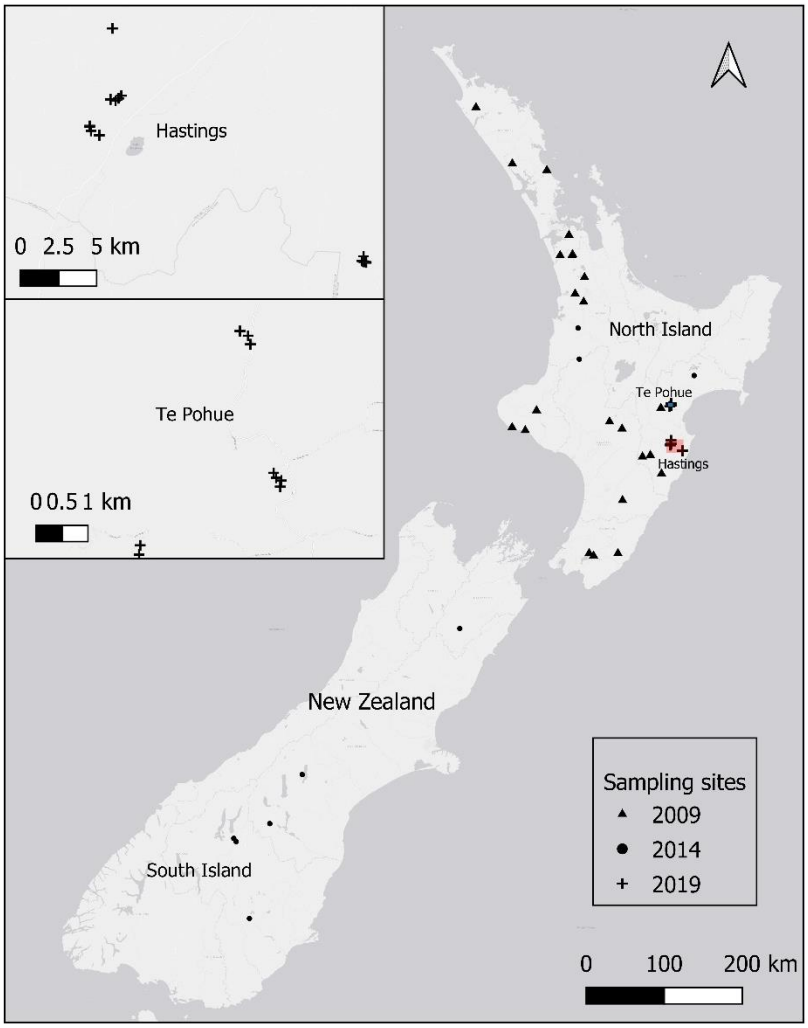

Figure 5-1 The 58 sampling sites, including North Island survey, 2009 Deurer et al., (2011) the 2014 sampling campaign by Whitley et al., (2018), and Hawke's Bay survey, 2019.

This work combines three soil datasets that were collected in three different surveys. New Zealand North Island SWR-survey conducted by Deurer et al., (2011) in 2009. A soil sampling from various New Zealand dryland pastures in 2014 (Whitley 2018) and a soil sampling conducted over Hawke's Bay region in 2019 (Fig. 5-1). The North Island survey (Deurer et al., 2011) had the objective to access the effect of soil order and drought proneness on the occurrence of SWR under pastoral land use. Sampling sites in this survey were selected based on soil order and annual drought-proneness criteria. The detailed soil sampling design is described in the survey paper by Deurer et al., (2011). From the original 50 sites of the survey, 24 suitable sites were selected for our study based

on the homogeneity of the land cover, the absence of trees, buildings and cast shadows in the sites (visually inspected on satellite imagery). Hawke's Bay region sampling in 2019, included 25 dryland pastoral sites and Whitley et al., (2018) sampling included nine different sites (3 in North Island and 6 in South Island). The combined soil dataset represents a wide range of textures including clay, clay loam, silt loam, loam, sandy loam, and sands. The sampling sites represent a wide variety of soil orders, including Allophanic (Andisols), Brown (Inceptisols, alfisols), Granular (Ultisols), Gley (Aquic groups), Pallic (Inceptisols, alfisols), Organic (Histosols), Podzol (Spodosols), Recent (Entisols, inceptisols), Pumice (Andisols, vitric), and Ultic (Ultisols) soils (New Zealand soil classification and Soil Taxonomy equivalent (Hewitt 2010)).

5.3.2 Ground truth data

Soils were sampled from the top 7.5 cm in the 2009 and 2019 samplings and from the top 15 cm in the 2014 sampling. In the 2009 survey, ten soil samples were sampled in a star-shaped pattern, 25 m apart (Deurer et al., 2011). The ten samples include five bulk topsoil (depth, 0-5 cm) and five undisturbed soil cores (0-5 cm). Sampling in Hawke's Bay (2019) was carried out in a cross-shaped pattern with approximately 2 m distance between sampling points. In 2014, ten soils were collected along a transect (minimum 50 m long) (Whitley 2018). Samples were sealed in plastic bags, transferred to the lab, and then oven-dried at 65 °C for 24 h to assess the potential SWR. The potential SWR is the higher level of water repellency a soil can reach when it dries out. For each sample, the WDPT test was carried out by placing three water droplets of 4 µL (5 µL for the 2009 survey) on the smoothed soil surface and measuring the time (s) they took to infiltrate the surface as a measure of the persistence of SWR (Doerr, 1998). The soils were also tested for SWR severity using the MED test. Ethanol concentrations of 0, 3, 5, 8.5, 13, 24, and 36% by volume were prepared, and three droplets of 4µL (5 µL for the 2009 survey) were placed on the smoothed soil surface. The MED was represented by the ethanol molarity of the droplet that entered the soil surface in 5 s (10s for the 2009 survey (Deurer et al., 2011)). The median value for the WDPT was used to classify the persistence of SWR into five classes including wettable (<5s), slightly hydrophobic (5-60s), strongly hydrophobic (60-600s), severely hydrophobic (600-3600s) and extremely hydrophobic (>3600). The median was used instead of the mean since it represents better the central tendency of the WDPT skewed data. The mean value of MED was used to classify SWR severity into seven classes (Doerr, 1998). Total C was measured using Elementar Vario-Max CN Analyser, Germany.

5.3.3 Remote sensing and water deficit data

The present study uses two types of TS data as predictors for the potential SWR. The remote sensing data including Sentinel-1, Sentinel-2 and MODIS and water deficit data from the TerraClimate

dataset (Abatzoglou et al., 2018). The C-band backscatter of single vertical (VV) and dual-polarization (VV+VH). Sentinel-1 data have a spatial resolution of 10 m and a temporal resolution of 12 days. The 12 bands multispectral data from Sentinel-2 including Vis-NIR, shortwave infrared (SWIR) provide a spatial resolution between 10 to 60 m (depending on the bands) and revisit time of 5 days for the combined constellation (10 days for a single satellite). Sentinel-1 A and B images of IW acquisition mode were pre-processed using the SNAP ESA toolbox (Warren et al., 2019). Sentinel-1 data pre-processing included precise orbit application, terrain correction, orthorectification, radiometric calibration, and conversion to logarithmic scale (dB). Moderate Resolution Imaging Spectroradiometer data with 500 m spatial resolution and two days revisit time was used to create monthly NDVI TS. In addition to SAR data, water deficit modelled data (4000 m resolution) from the TerraClimate dataset (Abatzoglou et al., 2018) were tested to verify the consistency of the relationship between temporal moisture dynamics and SWR occurrence. TerraClimate is a global dataset that interpolates high spatial climatological records from the WorldClim dataset to produce a monthly dataset including precipitations, soil moisture, water deficit, and other parameters (Abatzoglou et al., 2018). Although these data have a significantly lower resolution compared to satellite data, we suggest that monthly aggregated soil moisture values of pastoral sites are reasonably homogeneous within the same pixel.

To understand how temporal changes of surface biomass and drought affect SWR occurrence, both remote sensing and water deficit datasets were aggregated on a monthly basis. Monthly data provided higher temporal resolution and allowed a better understanding of drought and biomass relationship compared to seasonal aggregation. The time series configurations included three years of monthly NDVI (MODIS) and monthly water deficit data tested on the 58 sites dataset. This configuration was tested to see explore the potential of remote sensing TS for SWR prediction, regardless of the sampling date. A one year monthly multispectral (S2) NDVI (MODIS and S2), C-band backscatter (VV, VV+VH) and water deficit configuration was tested on 25 sites from the Hawke's Bay region (sampled in 2019). The 25 sites from Hawke's Bay were used to model and map SWR in this region.

5.4 Machine learning and modelling framework

5.4.1 Machine learning algorithms

To build the model and predict SWR and soil C in the studied sites, RF, SVM and ANN models were trained on monthly (12 months) aggregated datasets for 3-years data for the 58 sites and 1-year data from the 25 sites in Hawke's Bay region (2019). A brief introduction of the three used classifies is presented in the next sections.

Random forest

Random forest is an ensemble learning algorithm (Breiman 2001) that has shown big potential for remote sensing application such as land cover classification and cropland mapping (Belgiu and Csillik 2018; Gislason, Benediktsson, and Sveinsson 2006; Ham et al., 2005; Pal 2005). Breiman (2001) defined RF as an ensemble of tree-structured predictors $\{h(\boldsymbol{x}, \Theta_k), k = 1, \dots\}$ where $\{\Theta_k\}$ are autonomous identically distributed vectors and each tree gives an elementary vote for the most popular class at input $\boldsymbol{x}$. In a regression situation, the classifier decision is based on the collective responses of all trees in the forest. The trees are trained on multiple sample combinations form the training dataset. Training sets are created from the input training data using the bootstrap approach. This approach consists of arbitrarily selecting subsets of variables and choosing vectors with a replacement for training. This implies that some vectors arise many times in the trees while would not appear at all. For each trained tree, a random subset of variables is used to determine the best classification. Two parameters need to be tuned for the RF algorithm used in the CARET package (Kuhn 2008): the number of trees and the maximum depth of trees or the number of variables used in tree nodes ramification.

Support vector machine

The original method of SVM developed by Cortes & Vapnik (1995) aims to classify labelled datasets by finding an optimal separating hyperplane that discriminates classes in agreement with the training data with the largest margin. The generalization of this method to construct an optimal hyperplane in non-separable training data became known as the SVMs (Vapnik, 2006). The term optimal hyperplane is used for the decision edge that reduces misclassifications, vis-à-vis the training data. Learning refers to the interactive process of finding this optimal edge that classifies the training patterns and the generalization of this classification for the original data (Zhu et al., 2017). Thus, the cost of misclassification (C parameter) is to be determined for each classification. Pal & Mather (2005) reported that the SVM method showed a higher level of classification accuracy on multispectral and hyperspectral data compared to maximum likelihood and ANN methods. Fukuda & Hirosawa, (2001) performed an efficient land cover classification using an SVM-based classification scheme of SAR data. A detailed review of SVM and its use in remote sensing can be found in Mountrakis et al., (2011).

Artificial neural networks

Artificial neural networks are structurally brain-inspired computational methods. These machine learning algorithms have been used to solve a wide variety of modelling problems. Applications in remote sensing have shown that ANNs are powerful methods for landcover classification (Kussul et al., 2017; Li et al., 2011) and weather forecasting (Abhishek et al., 2012; Zhang et al., 1998). In contrast to the conventional modelling methods, ANNs are data-driven and

independent learning methods with no prior requirement for a conceptual model. Different studies, including land-cover classification methods (Civco, 1993; Yuan et al., 2009). LeCun et al., (2012) provided a detailed explanation of how the ANN algorithm works and how to achieve the best performance using them.

5.4.2 Modelling Framework

To inspect the relationship between measured soil properties, surface biomass and water deficit, the correlation between seasonal NDVI, water deficit, SWR and C were studied. A strong correlation between these variables has been observed in the summer period. A summary of these correlations is presented in the results section (Fig. 5-1). The modelling framework of this study consisted of the following steps:

i) Remote sensing and water deficit TS were aggregated on monthly basis. The final input data are 12 months mean values (instead of seasonal);

ii) Training and validation of the models on Log (WDPT) and soil C datasets as predicted variables and remote sensing TS as predictors using three different classifiers in CARET (Kuhn 2008) and Orfeo ToolBox package (OTB) (Grizonnet et al., 2017);

ii) Evaluation and generalization of the output using the trained models. Training and validation were carried with regression type models in the CARET library and classification type (5 SWR-classes) in the OTB package as implemented by Grizonnet et al., (2017).

A leave-one-out cross-validation was adopted for the training validation process in CARET. This approach allowed building the models using training sets of 57 sites and testing them against the single leftover site. This process is repeated 58 times, ensuring that all sites are used as part of the training and test sets. The RMSE values from each of the 58 runs are then combined to select the model with the least error. The RF algorithm from the OTB package used in this study is a linear kernel. The number of trees was fixed at 100, and the number of variables to be considered in each split of the trees (*mtry* parameter in CARET) was tuned to get the best model. The support vector machine tuning includes the misclassification cost (C parameter). The general accuracy of the models was evaluated using the RMSE in the CARET library and the kappa coefficient (Cohen 1960) in OTB. Sigmoid function has been chosen for the ANN algorithm, and the number of neurons in the hidden layer was tuned to achieve the best performance. To provide more information about the classifiers' quality, OTB output maps are supported by confidence maps. The confidence level for RF is calculated based on the proportion of vote for the majority class. The best performing model on the 58 sites dataset using CARET was selected and used to map SWR classes (as described in Table 2) on the Hawke's Bay region using 25 training sites on OTB. Classification accuracy in the OTB package is further evaluated by precision, recall and F-score for each SWR class.

5.5 Results and discussions

5.5.1 Modelling SWR using remote sensing time series

Potential SWR showed high spatial variability. The persistence of SWR expressed here by the Log (WDPT) values ranged from 0 to 3.9 s. The degree of SWR measured by MED showed values ranging from 0 to 24 % (Table 5-1). Both Log WDPT and MED had high standard deviation, which indicated high spatial variability of SWR across the studied pastoral sites. This variability has already been noticed at the plot scale (20 m^2) and even within individual samples from the Hawke's Bay sampling. Also, the standard deviation was very high within different classes (Table 5-2). This result agreed with previous research indicating a high variability of water repellency at different scales (Deurer et al., 2011; Gerke et al., 2001; Hallett et al., 2004). Classification based on Log (WDPT) (Doerr, 1998) showed that most of the sampled sites were strongly hydrophobic (18 sites). The Log (WDPT) showed a bimodal distribution with a major mode in the strong repellency class and a minor mode in the severe repellency class (Table 5-1 and Fig. 5-2). Total C values were between 2.49 and 13.24%, which can be classified as low to high C contents for New Zealand soils (Webb & Wilson, 1995).

Table 5-1 Summary statistics of the measured soil properties for all samples used in this study.

Soil Property	Mean	Min	Max	Standard deviation
Log WDPT (s)	1.86	0	3.89	1.20
MED (%)	6.24	0	24.00	6.23
C (%)	6.92	2.49	13.24	2.70

Table 5-2 Summary of SWR Classification using Log (WDPT) and number of sites per class.

Classes	Log WDPT (s)	Number of locations	Mean	STDV
Wettable	≤0.69	12	0.15	0.22
Slightly hydrophobic	0.69-1.77	14	1.32	0.35
Strongly hydrophobic	1.77-2.77	18	2.15	0.31
Severely hydrophobic	2.77-3.55	6	3.28	0.23
Extremely hydrophobic	>3.55	8	3.68	0.10

The initial analysis of the soil and remote sensing dataset showed a strong relationship between the measured soil properties, remote sensing, and water deficit data. There was a significant correlation between Log (WDPT), MED and C ($P<0.001$) and a strong correlation between Log (WDPT), summer NDVI and water deficit (December-Mars) (Fig. 5-2). The strong relationship between the potential SWR and C have been observed in a survey on SWR conducted in the South Island, New Zealand (Hermansen et al, 2019). This study, including 26 pastoral sites, found a significant linear correlation between C and MED (Hermansen et al., 2019). Grazing management is a crucial driver of aboveground biomass dynamics. Overgrazed pastures have a higher proportion of actively growing young plant and fewer stem and dead leaves compared to under grazed pastures (Waghorn and Barry 1987). Despite this consistent relationship between C and MED at the regional scale, other factors may control SWR at a farm or even paddock scale. Soil particle size distribution is a crucial factor influencing SWR occurrence. Wallis & Horne (1992) reported that sandy soils are more prone to coating by hydrophobic compounds because of their small specific surface area. In a study of fire-induced SWR, DeBano et al., (1970) reported that the thickness of the hydrophobic layer increased with the decrease of clay content resulting in significantly higher water repellency in sands compared to heavy textured soils. The correlation between NDVI TS data and Log (WDPT) helps to understand the relationship between the surface biomass dynamics and SWR. The strong correlation between summer NDVI, water deficit and SWR supports the assumption of the implication of drought in the generation of hydrophobic compounds from plants in dry periods. The lower the water deficit in the summer periods, the higher the mean NDVI and WDPT, and vice-versa. This suggests that plants were the main source of the hydrophobic compounds in the pastures explored in this study. Jaramillo et al., (2000) suggested that dry conditions would result in low biomass production and, therefore, less SWR occurrence. In contrast, very humid conditions are beneficial for biomass production and, consequently, for the generation of hydrophobic materials from decaying plants when soils dry out. Previous studies showed that root exudate metabolism is affected by drought, and some species can release hydrophobic compound (e.g. leucine and proline) in the drought period (Gargallo-Garriga et al., 2018). Another explanation could be the welting and decomposition of plant leaves in the summer period, which could be the source of hydrophobicity, considering that most grass leaves functional surfaces are naturally superhydrophobic (Barthlott et al., 2017).

A summary of the RMSE of models trained and cross-validated at different dataset configurations using the three classifiers is presented in Table 5-3. Random forest performed better in predicting Log (WDPT) and soil C compared to SVM and ANN (Table 5-3). Except for the one-year MODIS NDVI in Hawke's Bay region, RF had smaller RMSE followed by SVM and ANN. For the New Zealand dataset (n=58), the RMSE for Log (WDPT) was 0.82 when combining MODIS and water deficit

data or when using MODIS data alone. Using water deficit data alone resulted in an RMSE of 0.84. For C prediction, using water deficit TS alone, resulted in RMSE of 1.63%.

The importance of variables in the random forest model using MODIS NDVI showed that the January NDVI was the most influential factor in the model output, followed by February NDVI (Fig. 5-3). January corresponds to the driest month for the aggregated water deficit data, followed by February (Fig. 5-4). This supports the assumption that drought was highly influential in SWR occurrence.

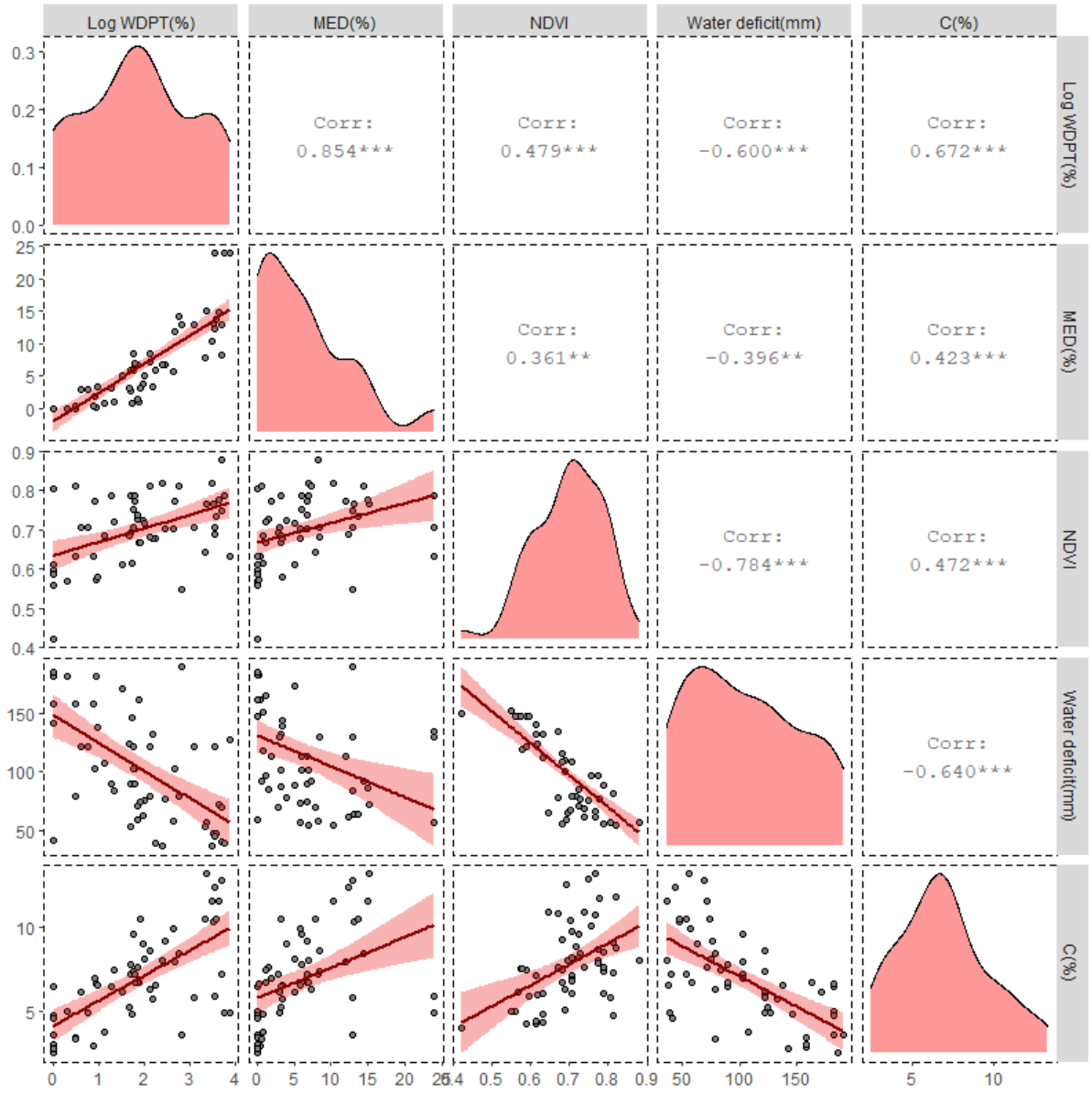

Figure 5-2 Scatter plots and frequency charts of Log (WDPT) (s) MED (%), C (%) mean summer NDVI and water deficit (mm). The shaded band around the regression lines represent a pointwise 95% confidence interval on the fitted values. Pearson Product Moment correlation matrix of P levels: *0.05, **0.01, ***0.001.

Table 5-3 Summary of leave-one-out cross-validation of Log WDPT (s) and C (%) using RF, SVM and ANN on different dataset configurations.

		Log WDPT, RMSE (s)			Carbon, RMSE (%)		
Sites	**Configuration**	**SVM**	**ANN**	**RF**	**SVM**	**ANN**	**RF**
New Zealand (n=58)	Water deficit + MODIS NDVI	0.82	1.24	0.82	2.11	5.92	1.68
Three years	Water deficit	0.84	1.22	0.84	1.80	5.92	1.63
	MODIS NDVI	0.87	1.23	0.82	1.86	5.92	1.75
Hawke's Bay (n=25)	S2 (Multispectral)	0.93	1.13	0.74	1.45	1.76	1.15
One year	S2 (NDVI)	0.93	0.89	0.73	1.42	4.95	1.31
	S1 (VV, VV+VH)	0.87	0.89	0.78	1.79	4.95	1.47
	S1+S2 (NDVI; VV, VV+VH)	0.66	0.89	0.71	1.06	4.95	1.27
	MODIS NDVI	0.60	0.88	0.69	1.27	4.92	1.24

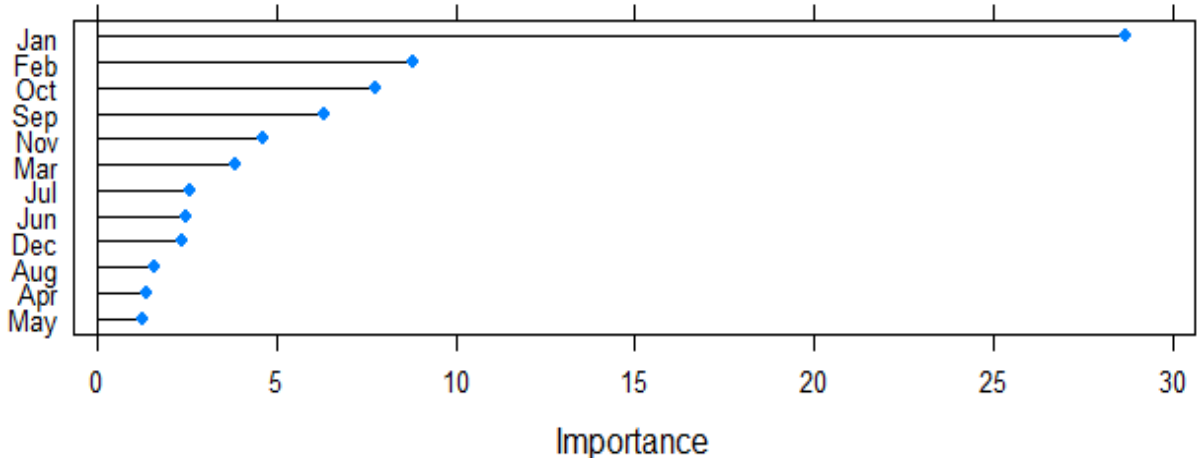

Figure 5-3 Importance of the variables RF model using monthly MODIS NDVI aggregated over 3 years prior sampling dates for all the sites combined.

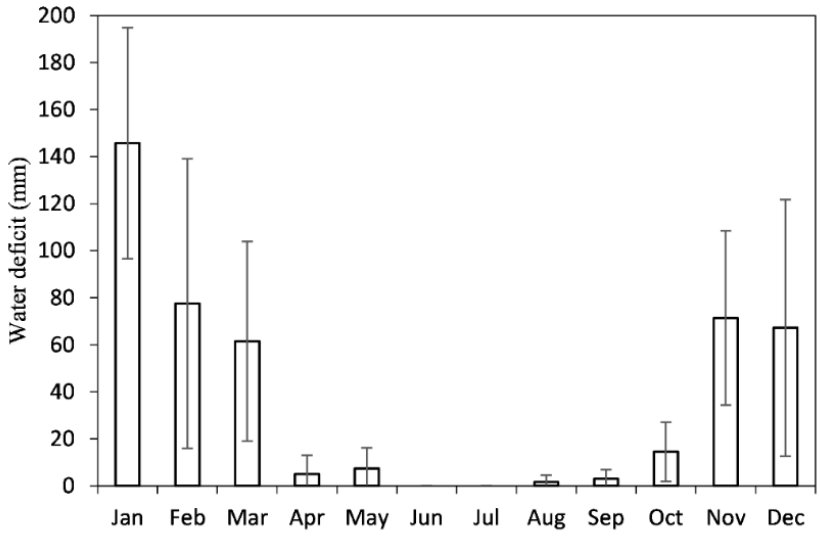

Figure 5-4 Monthly soil water deficit over all the studied sites (n=58) over three years before the sampling dates, retrieved from TerraClimate data (Abatzoglou et al., 2018).

When using the Hawke's Bay dataset alone (n=25), SVM had a higher accuracy for predicting Log (WDPT) when using a one-year monthly MODIS NDVI time series (RMSE=0.60). However, RF had an RMSE of 0.69. Random forest and ANN best predictions for soil C were achieved with Sentinel-2 multispectral time series (RMSE equal to 1.15 and 1.76, respectively). Support vector machine had the lowest RMSE (1.06) for soil C prediction using NDVI and C-band backscatter. The importance of variables of RF using MODIS-NDVI showed that Mars and November mean NDVI were the most important factors for the model output (Fig. 5-5). For the Hawke's Bay region in 2019, these two months were the driest (Fig. 5-6) with over 40 mm-mean water deficit.

Although SVM performed had the least error when working with Hawke's Bay data, its performance decreased when using the larges dataset. The Hawke's Bay data has a clear margin between sites in terms of NDVI and Log (WDPT) compared to the larger dataset (n=58). Support vector machine performs better when clear margin separation between features is present (Sugiyama 2015). Thus, performance may drop with datasets with high noise and overlapping features. Random forest generally provides a reliable importance of variables estimate (Breiman 2001; Liaw and Wiener 2002), which would give a better advantage when working with time series, where some dates are more influential than others. When it comes to ANN, the method had the least error for Log (WDPT) when performing regression type models. Artificial neural networks showed a limited capability to identify casual and explicit relationships between input variables (Tu 1996). For example, in our situation, the high correlations between NDVI and SWR are limited to dry months and ANN would be unlikely to provide any predictive advantage over SVM and FR in this case.

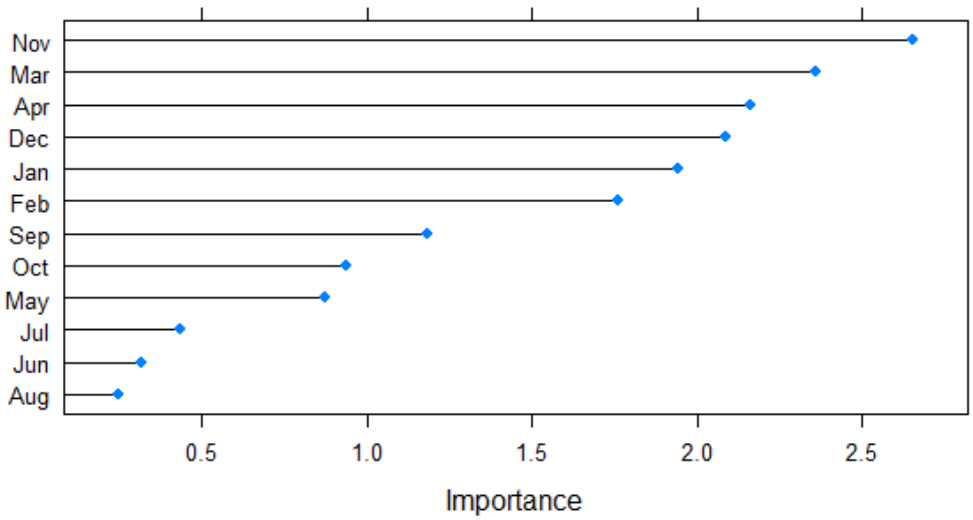

Figure 5-5 Importance of variables RF model using monthly MODIS NDVI for the year 2019 for Hawke's Bay sites (n=25).

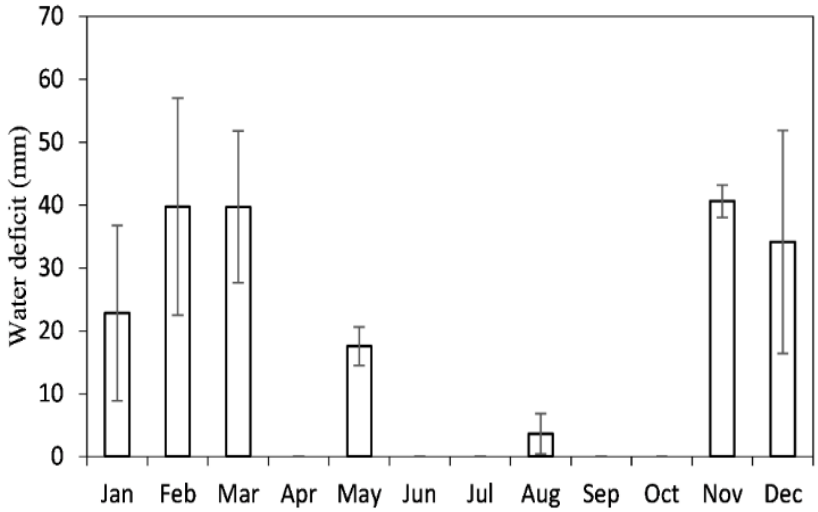

Figure 5-6 Monthly soil water deficit over Hawkes Bay sites (n=25) in 2019 retrieved from TerraClimate data (Abatzoglou et al., 2018).

The time series of Sentinel-2 multispectral configuration showed the lowest error for the prediction of soil C with the RF method (RMSE=1.15). Unlike the NDVI configuration, multispectral data has the additional advantage of including the reflectance of bare soil surface. Indeed, many studies showed the potential of multispectral soil reflectance for the prediction of soil C (Asner and Heidebrecht 2002; Ceddia et al., 2017; Peng et al., 2015). In a farm-scale study (~1km) of soil C mapping using multispectral remote sensing, Žížala et al., (2019) reported a cross-validation RMSE of 0.16 using SVM. Multispectral reflectance also reflects the amount of organic materials on the

surface, including dead leaves and decomposed organic matters. In situations where under grazing is dominant during the summer period, dead leaves' reflectance signature dominates the RS data. Although these areas could potentially be characterised by high levels of hydrophobic compounds derived from decomposed leaves, this would not be registered by using NDVI alone because provides limited information on surface biomass compared to multispectral data.

5.5.2 Mapping SWR in Hawke's Bay region

Using RF and SVM on monthly MODIS-NDVI TS alone provided higher accuracies for predicting potential SWR compared to the ANN model. The RF configuration were used to map the five classes of Log (WDPT) (as described in Table 5-2) for the Hawke's Bay region for the 2019 summer.

The global kappa index for the SWR classification using the RF model was equal to 0.86. The precisions, recalls, and the F-scores of each class for the RF output are presented in Table 5-4. The class "strongly hydrophobic" represented the best precision, recall and F-score (0.91, 1 and 0.95, respectively). The extremely hydrophobic class showed the lowest recall and F-score (0.72 and 0.80, respectively). While the severely hydrophobic class had the least precision (0.76) (Table 5-4).

Table 5-4 Precision, recall and F-score of the RF classification of the five SWR classes for the Hawke's Bay Region. The global Kappa index was equal to 0.86.

SWR class	Precision	Recall	F-score
Wettable	1	0.90	0.95
Slightly hydrophobic	0.90	0.90	0.90
Strongly hydrophobic	0.91	1	0.95
Severely hydrophobic	0.76	0.90	0.83
Extremely hydrophobic	0.88	0.72	0.80

The output of random forest modelling (Fig. 5-7) showed a similar distribution of the five SWR classes compared to the ground truth data (Fig. 5-8), with the strong hydrophobic class as the most abundant class and severely hydrophobic class as the least abundant class. However, the strong hydrophobic class showed the highest bias between the generalization map and the measured data (Fig. 5-8). This is obviously due to the limited number of samples that are not covering the entire Hawke's bay region. Still, the strong hydrophobicity class showed higher confidence level compared to other classes (Fig. 5-7).

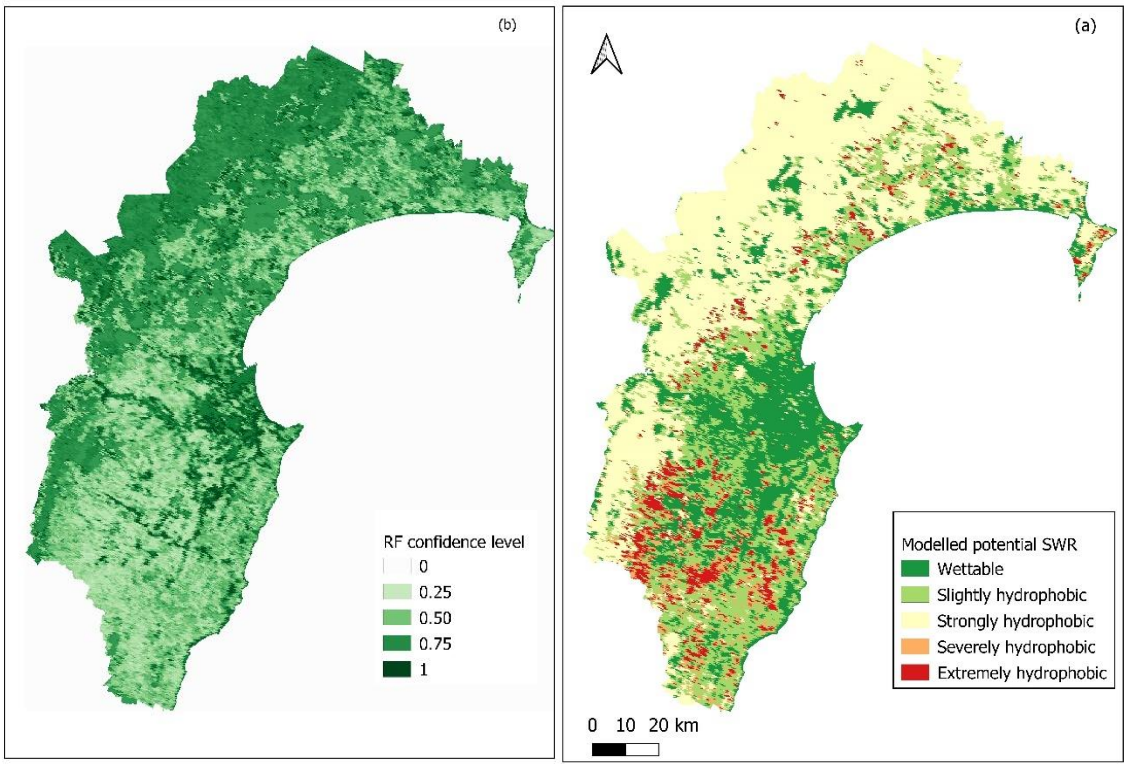

Figure 5-7 Random forest model classification output (a) and classification confidence (b) of the five potential SWR classes for the Hawke's Bay region using monthly MODIS NDVI TS as predictors in 25 sampling sites as ground truth data for training.

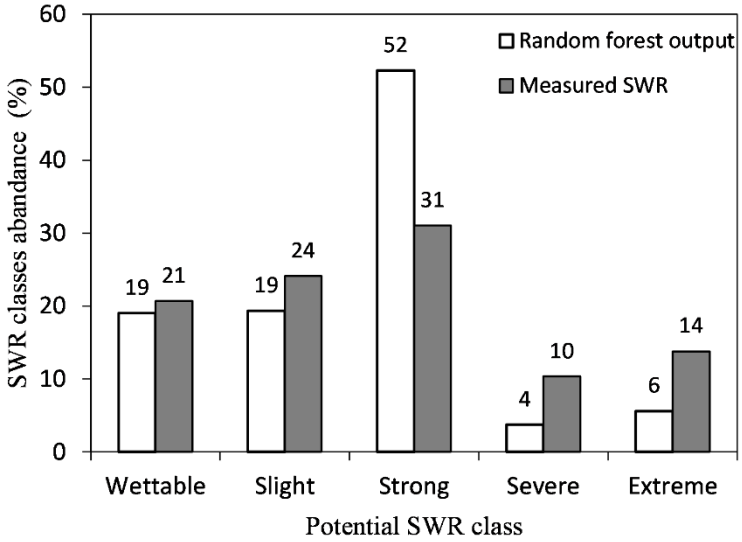

Figure 5-8 The abundance SWR five classes (wettable, slightly hydrophobic, strongly hydrophobic, severely hydrophobic, and extremely hydrophobic) of the Hawke's Bay region calculated based on RF output map (surface area distribution) and the number of sites per class from measured data.

5.6 Conclusion

Soil water repellency is a dynamic property that has many repercussions on the agroecosystems. The impact of SWR on hydrological processes is hard to predict using conventional point measurements. In this study, we tested the potential of remote sensing and water deficit TS in predicting the persistence SWR level in New Zealand pastures using three different machine learning algorithms; namely RF, SVM, and ANN. Models were trained and cross-validated using measured SWR at 58 pastoral sites. This approach improved the understanding of how surface biomass, soil moisture and their temporal dynamics affect the persistence of SWR and also allowed the mapping of the SWR using remote sensing data.

Training and validating the machine learning algorithms on SWR data from 58 sites, remote sensing, and water deficit TS showed strong capability of predicting the persistence of SWR and soil C levels. Generally, RF and SVM models outperformed ANN in predicting SWR and C levels. The monthly NDVI TS resulted in the best prediction of SWR with the RF model (RMSE=0.82). For soil C, water deficit TS data with the RF model showed the lowest error (RMSE=1.63).

Prediction models and maps will help in understanding the spatio-temporal dynamics of SWR and how they might impact hydrological processes. In addition, mapping the potential SWR will aid in identifying critical zones for remediation and attenuating its effect on the agroecosystems through adapted local management (e.g. grazing, fertilisers application, and surfactant treatment).

Chapter 6

Hyperspectral satellite data to assess topsoil water repellency and carbon content in permanent pastures

6.1 Abstract

Previous work using lab visible and near-infrared (VIS-NIR) spectroscopy and satellite broadband multispectral surface reflectance showed large potential for predicting topsoil carbon and soil water repellency (SWR) persistence. A higher spectral resolution in some hyperspectral sensors such as Hyperion could allow better estimation of soil carbon (C) and water repellency persistence in permanent pastures. The present study tested the predictability of both topsoil carbon and water repellency in permanent pastures using hyperspectral satellite data. Measurements of water repellency and topsoil carbon content were paired with Hyperion sensor data to train and cross-validate partial least squared regression (PLSR) models. The paired ground-truth included measurements from 16 and 22 pastoral sites for SWR and soil C, respectively. This approach showed an important capability for water repellency persistence prediction. The PLSR had high predictability for Log (WDPT) with R^2_v=0.78, $RMSE_v$=0.54, and RPD_v=2.01. Prediction for topsoil carbon had an R^2_v=0.47, $RMSE_v$=1.96, and RPD_v=2.01. The present work is the first investigation of the suitability of hyperspectral satellite data for water repellency estimation. The results consolidated previous work using lab spectra and supporting the possibility for implementing large scale mapping of SWR using the existing measured datasets, and the hyperspectral data from current and future sensors.

6.2 Introduction

The comprehension of the spatial and temporal dynamics of soil physicochemical properties are vital for the sustainable management of agroecosystems. The current soil repositories and maps are often unsatisfactory to meet the need for integrated sustainable farming practices. The benefits of quantitative soils information include the possibility to support the precision agricultural approach and helps to understand the long term repercussions on the ecosystems. However, sustainable and site-specific management of agroecosystems requires accurate quantitative information on key soil properties such as texture, carbon, nitrogen content, and moisture dynamics. The remote sensing approach opens unprecedented opportunities for upgrading the existing soil inventories (Barnes et al., 2003).

In the past three decades, a substantial amount of work has been done on the use of remote sensing for soil properties assessment (Wang & Qu, 2009; Ge et al., 2011). Examples included soil texture (Ben-Dor et al., 2002; Castaldi et al., 2016; C. Gomez et al., 2018; Lagacherie et al., 2008), soil carbon (Castaldi et al., 2019; Castaldi et al., 2019; Gholizadeh et al., 2018; Gomez et al., 2008; Hbirkou et al., 2012), salinity (Mougenot et al., 1993; VERMA et al., 1994), pH (Zhang et al., 2018), soil moisture (Mohanty et al., 2017).

Previous work on soil attributes retrieval used topsoil multispectral and hyperspectral imagers. Numerous studies used multispectral satellite data to retrieve soil properties with intermediate accuracy. For example, Vaudour et al., (2019) used Sentinel-2 to assess soil carbon, texture, pH, EC, $CaCO_3$, CEC with different accuracies in the Mediterranean region. Castaldi et al., (2014) obtained reasonable accuracy for clay content prediction using Advanced Land Imager (ALI) multispectral data. Because of their lower spatial resolution, multispectral satellite data, theoretically provide inferior results compared to hyperspectral. Still, many case studies showed no significant difference between hyperspectral and multispectral satellite data for assessing key soil properties.

When it comes to hyperspectral data, both space and airborne hyperspectral imagers provide higher spectral resolution, which theoretically improves the prediction capabilities compared to multispectral sensors. However, their performance can be hampered by the low signal to noise ratio (Castaldi et al., 2014). To date, only three hyperspectral imagers were available for remote sensing application; namely, Hyperion onboard earth observer one (EO-1) launched by NASA (Folkman et al., 2001), the Compact High-Resolution Imaging Spectrometer (CHRIS) onboard PROBA satellite launched by the European Space Agency (Barnsley et al., 2004), and PRISMA sensor lunched by the Italian space program (Loizzo et al., 2018).

Soil water repellency (SWR) is a crucial soil property that controls water absorption dynamics at the soil surface. It is caused by amphiphilic compounds inducing soil hydrophobicity. Whether this property can be estimated using soil reflectance signature was inspected by (Kim, I. et al., 2014) who used lab VIS-NIR spectroscopy. Their results showed that the visible bands around 457, 622, and 670 nm had a high influence on SWR repellency prediction. For the infrared bands, 1364, 1765, 1936, 2167, 2381, and 2356 nm were the most influential in predicting the degree of SWR measured by the molarity of the ethanol test. The coefficients pattern of the partial least square regression (PLSR) in their study showed that soil carbon and water repellency degree were generally different. Nevertheless, these two properties shared common active spectral regions around 1364, 1740, and 2164 nm. Soil carbon characteristic expressed in the 2100 to 2437 wavebands were speculated to be associated with aliphatic C-H bonds. Many workers reported that these compounds contributed to soil hydrophobicity (Capriel et al., 1995; McKissock et al., 2003).

Since its launch by the National Aeronautics and Space Administration (NASA) in the year 2000, Hyperion sensor acquired more than 89000 hyperspectral images globally in 2017 (decommissioning year) (Middleton et al., 2017). However, full global coverage is not achieved with the existing hyperspectral imagers. The increasing availability of hyperspectral satellite data with existing sensors such as Hyperion (Folkman et al., 2001) and Prisma (Loizzo et al., 2018) and the upcoming spaceborne sensors such as Hyperspectral Imager Suite (HISUI) (Tanii et al., 2012), EnMap (Sang et al., 2008), HyspIRI (Lee et al., 2015), and HypXIM (Michel et al., 2011) will open a broad range of opportunities for quantitative soil information mapping.

The present study was initiated to test the hypothesis that soils with different levels of topsoil water repellency and carbon have distinguishable reflectance features that can be characterised using Hyperion reflectance data. Thus, the objective of this study was to estimate soil water repellency and soil C in permanent pastures using Hyperion satellite data.

6.3 Materials and methods

6.3.1 Remote sensing data

Radiometrically calibrated and orthorectified radiance data published by the United States Geological Survey (USGS) were used. The data is a 30 meters spatial resolution for all 220 bands with 10 nm bandwidth. This top of atmosphere radiance data was used as input to train and cross-validate partial least square regression (PLSR). Radiance data for each site were filtred for cloud cover and NDVI index to select dates with the nearest possible state to bare soil. Different preprocessing operations were conducted on the calibrated radiance data including the pseudo-absorbance transformation Log (1/R), Savitzky Golay (SG), and first derivative (D) (Fig. 6-1). Saviszky Golay filter allows noise reduction and derivative transformation enhances differences between peaks separation in overlapping bands (Castaldi et al., 2016).

Soil water repellency and topsoil carbon data were acquired in surveys conducted by (Bayad et al., 2020) and (Deurer et al., 2011) (Chapter 5) in addition to the South Island of New Zeland survey on SWR by (Hermansen et al., 2019) and carbon data in multiple pastoral sites published by (Schipper et al., 2010). Sampling sites from these surveys that have been scanned by Hyperion satellite were used for training and cross-validation of PLSR models. The PLSR calibration and cross-validation prediction accuracies could be classified in three classes as described by some workers (e.g. Vaudour et al., 2019): i) models with intermediate to high predictability (R^2>0.5 and RPD>1.4); ii) models with poor to intermediate predictability (R^2 of 0.4 – 0.5 and

RPD between 1.3 and 1.4); and iii) models with poor to very poor predictive potential (R^2<0.4; RPD<1.3).

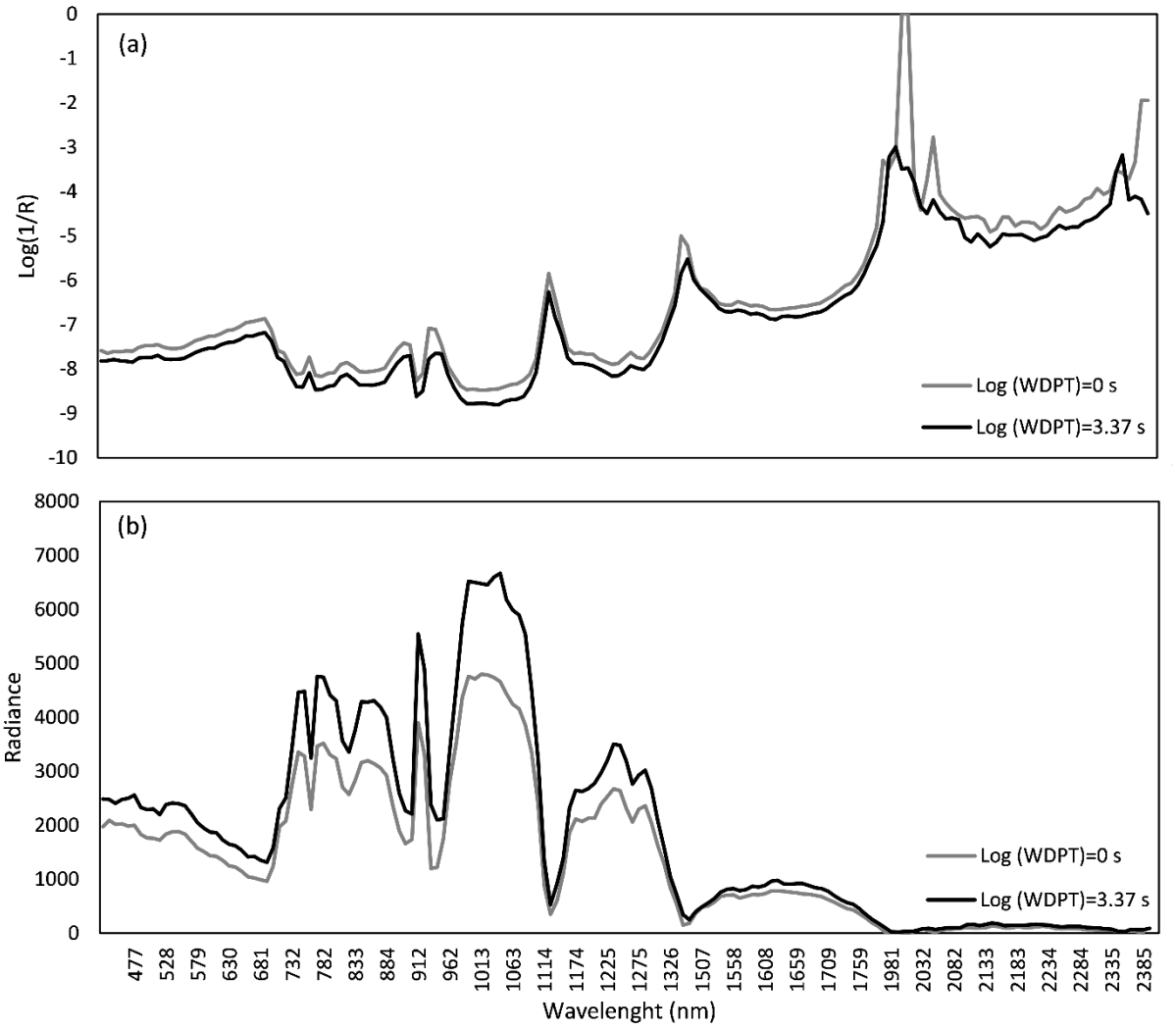

Figure 6-1 The pre-processed Hyperion spectral of wettable (Log (WDPT)=0 s) and hydrophobic spectra (Log (WDPT)=3.37 s) using a) pseudo-absorbance Log (1/R) and b) raw radiance data calibrated.

6.4 Results

For the studies sites, soil water repellency persistence ranged from *wettable* to *severely hydrophobic*. The log (WDPT)(s) at the 16 sites matched with Hyperion data ranged between 0 and 3.37 s (Table 6-1). The 22 sites matched with Hyperion data had a wide soil carbon range (1.17 to 13.2 %; Table 6-1).

Table 6-1 Summary statistics of the topsoil carbon and Log (WDPT) dataset matched with Hyperion data.

	Nb. sites	Min	Max	Mean	Stdv.
Log (WDPT)(s)	16	0	3.37	1.19	1.09
Soil C (%)	22	1.17	13.2	4.36	2.58

The performance of models trained and cross-validated using Hyperion calibrated radiance, measured topsoil soil C, and Log (WDPT) (s) are presented in Table 6-2. The PLSR models' performance for both water repellency persistence and soil C varied depending on whether calibration or validation sets were used and on the spectral data preprocessing used. Soil water repellency persistence estimated using Log (WDPT) had an $RMSE_v$ of 0.54, R^2_v of 0.78, and RPD_v of 5.73 when Log(1/R) transformation was used. The highest carbon content prediction model ($RMSE_v$ of 1.96, R^2_v of 0.47, and RPD_v of 1.31) was acquired with Savitsky Golay transformation and first derivative. The calibration model had high predictability within the used dataset for both soil C and Log (WDPT) (R^2_c =0.98 and 0.99, respectively) (Table 6-2).

Table 6-2 Partial least squares regression (PLSR) prediction statistics for calibration and leave-one-out cross-validation of Hyperion data for topsoil carbon and Log (WDPT).

			Calibration				Validation			
	No. Sites	**Tr.**	**RMSE**	**R^2**	**RPD**	**NF**	**RMSE**	**R^2**	**RPD**	**NF**
C (%)	22	R	0.81	0.90	3.18	7	2.34	0.43	1.10	5
		Log (1/R)	0.73	0.92	3.53	7	2.23	0.31	1.15	3
		SG+D	**0.30**	**0.98**	**8.6**	**7**	**1.96**	**0.47**	**1.31**	**5**
		D	0.30	0.98	8.6	7	1.96	0.47	1.31	5
Log (WDPT) (s)	16	R	0.19	0.96	5.73	7	1.76	NA*	0.61	7
		Log(1/R)	**0.13**	**0.98**	**8.38**	**7**	**0.54**	**0.78**	**2.01**	**6**
		SG+D	0.08	0.99	13.62	7	1.30	NA	0.83	3
		D	0.08	0.99	13.62	7	1.30	NA	0.83	3

NA*: The R^2 had a negative value. Spectra transformations (Tr.) include calibrated radiance (R), standard normal variate (SNV), and pseudo-absorbance Log (1/R).

For topsoil carbon, the explained variability of the prediction model exceeded 20% at the second factor and reached its peak at the fifth factor (47 %) (Fig. 6-2, a). The explained variability of the PLSR model for Log (WDPT) exceeded 40% starting from the second factor to reach its peak (78 %) with the sixth factor (Fig. 6-2, b). Explained variability in the calibration model of soil C increased gradually with the number of factors used. However, the water repellency persistence calibration model explained more than 70 % with the first factor (Fig. 6-2; a,b).

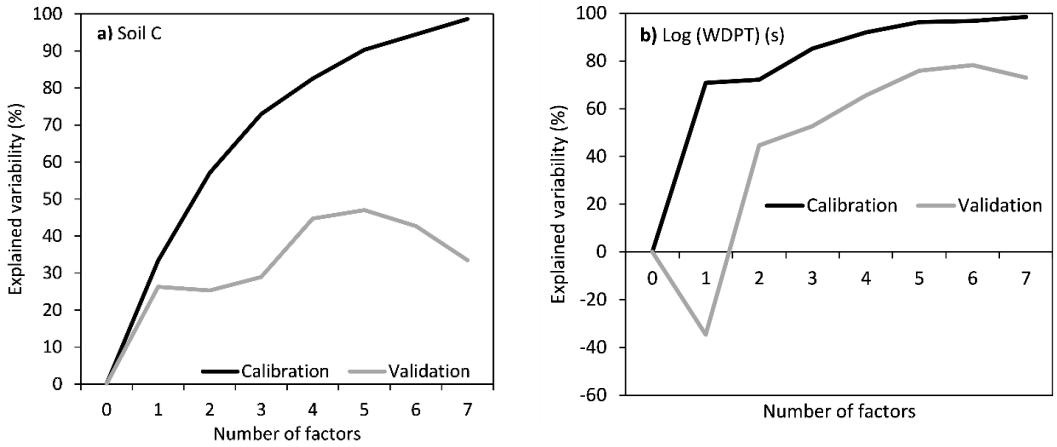

Figure 6-2 Explained variability in the PLSR calibration and validation models for topsoil carbon and Log (WDPT) as a function of the number of factors used for calibration and validation on the model.

Weighted coefficients of the PLSR models for topsoil carbon and SWR persistence prediction using Hyperion spectra are illustrated in Figure 6-3. The wavebands coefficients' magnitude represents their contribution in explaining Log (WDPT) and soil C data. Accordingly, important wavelengths have high regressions weighted coefficients. For soil C, the bands 426 nm and 752 nm, 915, 1023, and 1164, 1316-1326 nm were the most important bands for the PLSR models (Fig. 6-3, a). The bands 426-447 nm, 942 nm, 1124 nm, 1487 nm, 1981-2052 nm were the most important factors for predicting SWR persistence (Fig. 6-3, b).

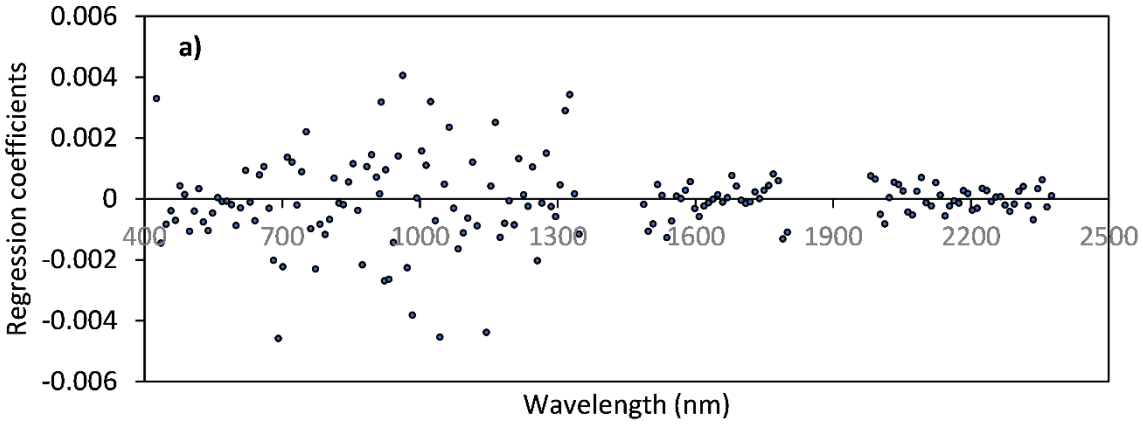

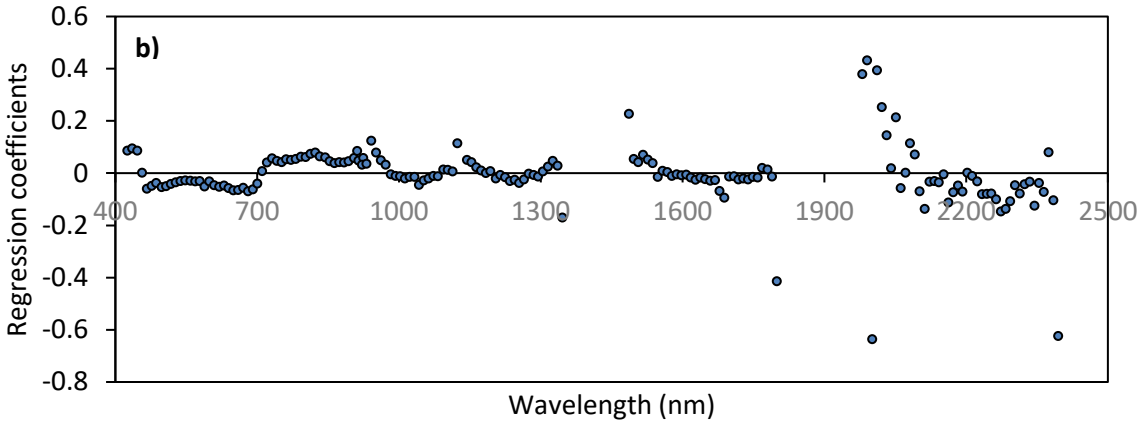

Figure 6-3 Weighted PLSR regression coefficients for a) topsoil carbon model using Savitzky Golay plus first derivative pre-processing and b) Log (WDPT) prediction model using Log (1/R) transformation.

6.5 Discussions

Bases on ground-truth data from 16 permanent pastoral sites matched with Hyperion data, the PLSR models showed a high prediction capability for SWR resistance and poor predictability for soil C (Figure 6-3). Whereas data transformation had no impact on the calibration PLSR models, cross-validation models performance was affected by the type of preprocessing used. After testing several preprocessing methods, the first derivative showed the highest performance for carbon content prediction models. For, water repellency persistence, Log (1/R) was the only transformation to yield a reliable cross-validated model (R^2_v=0.78) (Table 6-2). Prediction capability dropped significantly when switching from training to cross-validation datasets for topsoil carbon (Fig. 6-3, a). However, SWR persistence prediction showed high accuracy with both training and cross-validation datasets (Fig. 6-3, b).

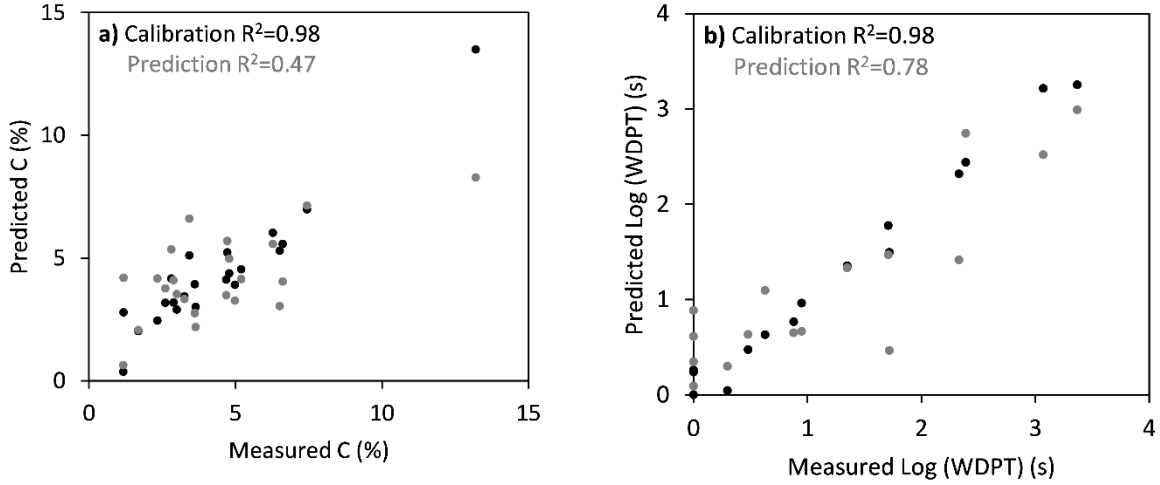

Figure 6-4 Scatter plots of the measured versus predicted a) soil carbon and b) Log (WDPT) calibration and cross-validation PLSR models.

Topsoil carbon prediction accuracy levels acquired within the used soil dataset are comparable with previous studies that used Hyperion data (Chapter 1; Table 1-1). Using a dataset of over 700 data points, Castaldi et al., (2016) evaluated the prediction capabilities of soil C using simulated Hyperion spectra. The result from this simulation showed poor prediction capabilities with the used dataset (R^2_v=0.27; $RMSE_v$=0.46, RPD=1.23). The present result showed relatively higher prediction accuracy compared to this study (R^2_v=0.47; $RMSE_v$=1.96, RPD=1.31), but lower accuracy compared to numerous studies that reported intermediate to high accuracies for soil C (e.g. Gomez et al., 2008; Minu et al., 2017; Peón et al., 2017; T. Zhang et al., 2013). In terms of comparison with multispectral data, Hyperion models showed similar accuracy for soil C prediction compared to the PLSR model developed using Landsat-7 in Chapter 5 (R^2_v=0.50; $RMSE_v$=2.58, RPD=1.40). Although hyperspectral data supposedly provides better performance compared to multispectral broadband data, Castaldi et al., (2014) found no remarkable difference between the Advanced land imager (ALI) multispectral broadband data and Hyperion narrowband data, for soil C prediction. The authors speculated that this could be attributed to the low signal to noise ratio of the Hyperion sensor, particularly in the SWIR region which is highly important for soil C estimation. Another reason for this drop in accuracy for soil C would be the atmospheric effect (Goetz et al., 2002). The lack of atmospheric correction may have an impact on the quality of the multispectral data in the present study.

Prediction capability for water repellency persistence of model developed with Hyperion (R^2_v=0.78; $RMSE_v$=0.54, RPD=5.73) had higher prediction capability than the best performance of multispectral PLSR models (Sentinel-2; R^2_v=0.44; $RMSE_v$=0.98, RPD=1.32) developed in Chapter 5. This is highly likely attributed to the capabilities of hyperspectral data to exploit the higher spectral resolution in accomodating soil water repellency. The clear contribution of both VIS, NIR, and SWIR specific bands in assisting SWR prediction suggest that key soil chromophores have an important influence on SWR. Topsoil reflectance bands around 426 nm and 752 nm importance indicated that kye colour compounds contribute to the estimation of water repellency persistence. Kim, I. et al., 2014 who used lab spectra to assess water repellency levels reported that wavelengths around 447, 622, and 670 nm have large coefficients for SWR severity (MED test). The change in visible bands reflectance can be related to key soil properties such as organic C, iron oxides, clay minerals (Rossel & Behrens, 2010). The important NIR bands in Log (WDPT) estimation were 1487, 1487, 1981, 2012, 2375 nm. These bands are quite similar to the lab spectra coefficient for MED estimation from Kim, I. et al., (2014) who reported a high importance at 1364, 1765, 1936, 2167, 2381, and 2356 nm. Radiation absorbance at 1487 and 1981 nm were attributed to O-H bonds groups. The bands around

2012 nm were attributed to absorption by organic compounds, clay and polysaccharides by Rossel & Behrens, (2010). They specifically identified 2307–2496 nm to be related to methyls (C-H) and 2381 nm to be related to carbohydrates (C-O). The wavelength 2200-2300 nm were reported to have high absorbance by phenolic O-H and aliphatic C-H compounds (Cozzolino & Moron, 2003). We suggest that these compounds have contributed to the prediction of SWR persistence in the present study.

6.6 Conclusion

Soil reflectance data from different satellite sensors showed important potential for predicting multiples soil properties. The present studies revealed that Hyperion sensor data allowed reliable prediction of water repellency persistence in permanent pastors. Training and cross-validating PLSR models using hyperspectral radiance from Hyperion and measured SWR and soil C as inputs yielded a high accuracy model for SWR and but low accuracy for soil C. For water repellency persistence, the PLSR model had an R^2_v=0.78 and $RMSE_v$=0.54. Topsoil carbon had an R^2_v=0.47 and $RMSE_v$=1.96. However, calibration models had an R^2_v=0.90 and $RMSE_v$=0.81 indicating the possibility of improvement for bigger datasets. Variables importance analysis of the PLSR showed that many wavebands were related to water repellency persistence in VIS and NIR spectrum. The present results demonstrated the feasibility of estimating topsoil water repellency persistence using satellite hyperspectral data. The increasing availability of hyperspectral data from current and future space sensors will allow larger surface coverage providing unprecedented opportunities for mapping water repellency at the farm to regional scales.

Chapter 7

Summary

The present thesis attempted to 1) model the relationship between SWR persistence and soil moisture in drying hydrophobic soils; 2) investigate the effect of SWR on surface water runoff and phosphorus losses in surface runoff; and 3) testing for the first time the assessment and map SWR in permanent pastures using remote sensing data from multiple satellites using multiple approaches. The relationship between soil water repellency persistence and soil moisture was assessed in air-drying hydrophobic soils (Chapter 2). The actual soil water repellency persistence increased with decreasing water content in sigmoidal patterns. We suggested a simple sigmoidal equation to model the actual repellency persistence as a function of soil moisture, the potential repellency and two curve shape parameters. The potential water repellency was controlled by soil carbon and soil texture in the pastoral soils investigated in this study. The suggested model can be used to simulate the evolution of water repellency in drying soils. Thus, the actual water repellency spatial dynamics could be estimated in real-time in dry seasons using i) available soils moisture data and ii) the potential SWR data which in turn could be estimated using the remote sensing approaches tested in Chapters 4, 5, and 6. The results provide an unprecedented opportunity for mapping the spatiotemporal dynamics of SWR at the farm and regional scales.

In terms of the environmental impact of soil water repellency, surface runoff and phosphorus losses in surface runoff we measured in a field trial in hydrophobic and wettable soils during post-summer rainfall event; when water repellency is in full swing (Chapter 3). The surface runoff engendered at the post-summer period was considerably higher in hydrophobic soils compared to wettable soils. The P loads in the first runoff following phosphorus application accounted for more than 90 % of the total losses in the summer-autumn period. These first loads after phosphorus application, which are considered incidental losses, are mainly controlled by the amount and the solubility of the fertiliser per se. Still, a strong liaison has been observed between phosphorus loads and water repellency beyond the incidental losses period (background losses). This was the first evidence from a pastoral trial implicating SWR on non-incidental phosphorus losses in surface runoff. The results provide new insight into the implication of SWR in phosphorus losses dynamics in pastoral ecosystems. This understanding is indispensable for modelling and quantification of phosphorus losses dynamics in hydrophobic losses.

The first remote sensing approach implemented in this thesis consists of the use of temporal dynamics of surface biomass estimated through NDVI and water deficit time series as predictors of

SWR occurrence in permanent pastures and topsoil carbon content. Assuming that the occurrence of water repellency is controlled by the cycling of hydrophobic compounds within the soil carbon pool. The surface biomass, which is mainly controlled by the management and climate (e.g. rainfall), plays a vital role in the cycling of these compounds. The approach adopted in Chapter 5 aimed to understand how surface biomass, soil moisture and their temporal dynamics affect soil water repellency occurrence and topsoil carbon contents permanent pastures. This novel method bypasses the need for the topsoil surface reflectance data to estimate the studied properties. The studied soil attributes are the results of the temporal dynamic of climate and agricultural practices directly impacting surface biomass (e.g., grazing). To test this approach, machine learning algorithms were trained and validated on measurement of soil water repellency from 58 sites, and time-series of remote sensing, and water deficit. Random forest algorithm showed the strong capability of predicting the persistence of SWR and soil C levels using these time series data. Prediction models were used to generate the first soil water repellency map in Hawke's Bay region, New Zealand. The next step of this research would be the improvement of these maps using larger ground truth datasets. The suggested approach would also help monitor long term carbon stocks changes in pastures. To achieve this, longer remote sensing time-series should be tested (ten to twenty years) should be used (e.g. Landsat-7); and measurements of soil carbon stock (e.g. at one-metre depth) long term evolution could be used. The advances in computation power and the tremendous amount of remote sensing data allow unmatched possibilities for assessing not only SWR and soil carbon, but also additional properties such as soil fertility, microbial communities, and carbon stocks long term changes.

This thesis provides the first evaluation of the multispectral topsoil reflectance from satellites such as Sentinel-2 and Landsat-7 (Chapter 4) and hyperspectral data from Hyperion sensor (Chapter 6) for water repellency and soil carbon estimation in permanent pastures. Results showed that soil carbon can be predicted with intermediate accuracy using Landsat-7 spectra, while water repellency showed a lower prediction accuracy using Sentinel-2. Hyperspectral data from the Hyperion sensor provided a better prediction accuracy for topsoil water repellency prediction compared to multispectral data. With the overwhelming accessibility of multispectral and hyperspectral satellite data, the suggested methodology could help to ameliorate the accuracy and the spatial resolution of the existing soil carbon inventories in permanent pastures. Larger soil water repellency measured datasets could improve the prediction models' accuracy for soil water repellency, and thus provide an additional layer consisting of water repellency spatial dynamics to the current soil inventories. The soil water repellency spatial data is indispensable for guiding the remediation strategies and attenuating the impact of soil water repellency on environmental services.

7.1 References

Aamlid, T. S., Espevig, T., & Kvalbein, A. (2009). The potential of a surfactant to restore turfgrass quality on a severely water-repellent golf green. Biologia, 64(3), 620–623. https://doi.org/10.2478/s11756-009-0071-1

Abatzoglou, J. T., Dobrowski, S. Z., Parks, S. A., & Hegewisch, K. C. (2018). TerraClimate, a high-resolution global dataset of monthly climate and climatic water balance from 1958–2015. Scientific Data, 5(1), 1–12. https://doi.org/10.1038/sdata.2017.191

Abhishek, K., Singh, M. P., Ghosh, S., & Anand, A. (2012). Weather forecasting model using artificial neural network. Procedia Technology, 4, 311–318. https://doi.org/10.1016/j.protcy.2012.05.047

Abrantes, J. R. C. B., de Lima, J. L. M. P., Prats, S. A., & Keizer, J. J. (2017). Assessing soil water repellency spatial variability using a thermographic technique: An exploratory study using a small-scale laboratory soil flume. Geoderma, 287(Supplement C), 98–104. https://doi.org/10.1016/j.geoderma.2016.08.014

Adamson, A. W. (1982). Physical Chemistry of Surfaces. J. Wiley.

Adamson, A. W., & Gast, A. P. (1967). *Physical chemistry of surfaces* (Vol. 15). New York: Interscience publishers.

Ahn, S., Doerr, S. H., Douglas, P., Bryant, R., Hamlett, C. A. E., McHale, G., Newton, M. I., & Shirtcliffe, N. J. (2013). Effects of hydrophobicity on splash erosion of model soil particles by a single water drop impact. Earth Surface Processes and Landforms, 38(11), 1225–1233. https://doi.org/10.1002/esp.3364

Albert, R., & Köhn, M. (1926). Investigations into the resistance of sandy soils to wetting. Proceedings of the International Society of Soil Science, 2, 139–145.

Asner, G. P., & Heidebrecht, K. B. (2002). Spectral unmixing of vegetation, soil and dry carbon cover in arid regions: Comparing multispectral and hyperspectral observations. International Journal of Remote Sensing, 23(19), 3939–3958. https://doi.org/10.1080/01431160110115960

Bachmann, J., Ellies, A., & Hartge, K. H. (2003). Sessile drop contact angle method. In Soil Water Repellency: occurrence, consequences and amelioration, 57-65. Elsevier. https://doi.org/10.1016/B978-0-444-51269-7.50008-4

Bajwa, S. G., & Tian, L. F. (2005). Soil fertility characterization in agricultural fields using hyperspectral remote sensing. Transactions of the ASAE, 48(6), 2399–2406.

Barnes, E. M., Sudduth, K. A., Hummel, J. W., Lesch, S. M., Corwin, D. L., Yang, C., Daughtry, C. S. T., & Bausch, W. C. (2003). Remote- and Ground-Based Sensor Techniques to Map Soil Properties. Photogrammetric Engineering & Remote Sensing, 69(6), 619–630. https://doi.org/10.14358/PERS.69.6.619

Barnsley, M. J., Settle, J. J., Cutter, M. A., Lobb, D. R., & Teston, F. (2004). The PROBA/CHRIS mission: A low-cost smallsat for hyperspectral multiangle observations of the Earth surface and atmosphere. IEEE Transactions on Geoscience and Remote Sensing, 42(7), 1512–1520. https://doi.org/10.1109/TGRS.2004.827260

Barthlott, W., Mail, M., Bhushan, B., & Koch, K. (2017). Plant Surfaces: Structures and Functions for Biomimetic Innovations. Nano-Micro Letters, 9(2), 23. https://doi.org/10.1007/s40820-016-0125-1

Bayad, M., Chau, H. W., Trolove, S., Moir, J., Condron, L., & Bouray, M. (2020). The Relationship between Soil Moisture and Soil Water Repellency Persistence in Hydrophobic Soils. Water, 12(9), 2322. https://doi.org/10.3390/w12092322

Bayad, M., Chau, H. W., Trolove, S., Müller, K., Condron, L., Moir, J., & Yi, L. (2020). Time series of remote sensing and water deficit to predict the occurrence of soil water repellency in New Zealand pastures. ISPRS Journal of Photogrammetry and Remote Sensing, 169, 292–300. https://doi.org/10.1016/j.isprsjprs.2020.09.024

Belgiu, M., & Csillik, O. (2018). Sentinel-2 cropland mapping using pixel-based and object-based time-weighted dynamic time warping analysis. Remote Sensing of Environment, 204, 509–523. https://doi.org/10.1016/j.rse.2017.10.005

Ben-Dor, E. (2002). Quantitative remote sensing of soil properties. Advances in Agronomy, 75, 173–243. https://doi.org/10.1016/S0065-2113(02)75005-0

Ben-Dor, E., Irons, J. R., & Epema, G. F. (1999). Soil reflectance. Remote Sensing for the Earth Sciences: Manual of Remote Sensing, 3, 111–188.

Ben-Dor, E., Patkin, K., Banin, A., & Karnieli, A. (2002). Mapping of several soil properties using DAIS-7915 hyperspectral scanner data: A case study over clayey soils in Israel. International Journal of Remote Sensing, 23(6), 1043–1062. https://doi.org/10.1080/01431160010006962

Bisdom, E. B. A., Dekker, L. W., & Schoute, J. F. Th. (1993). Water repellency of sieve fractions from sandy soils and relationships with organic material and soil structure. Geoderma, 56(1), 105–118. https://doi.org/10.1016/0016-7061(93)90103-R

Blackwell, P., Morrow, G., Webster, A., & Nicholson, D. (1994). Improvement to crop production from wide furrow sowing in water repellent sand; a comparison to level sowing methods. Proceedings of the 2nd National Water Repellency Workshop. 106–113. Dept. of Agriculture, Perth, W.Aust.

Breiman, L. (2001). Random forests. Machine Learning, 45(1), 5–32.

Buczko, U., Bens, O., & Hüttl, R. F. (2005). Variability of soil water repellency in sandy forest soils with different stand structure under Scots pine (Pinus sylvestris) and beech (Fagus sylvatica). Geoderma, 126(3), 317–336. https://doi.org/10.1016/j.geoderma.2004.10.003

Burch, G. J., Moore, I. D., & Burns, J. (1989). Soil hydrophobic effects on infiltration and catchment runoff. Hydrological Processes, 3(3), 211–222. https://doi.org/10.1002/hyp.3360030302

Burnham, J. H., & Sletten, R. S. (2010). Spatial distribution of soil organic carbon in northwest Greenland and underestimates of high Arctic carbon stores. Global Biogeochemical Cycles, 24(3). https://doi.org/10.1029/2009GB003660

Cann, M. A. (2003). Clay spreading on water repellent sands. In Soil Water Repellency (pp. 273–280). Elsevier. https://doi.org/10.1016/B978-0-444-51269-7.50027-8

Capriel, P., Beck, T., Borchert, H., Gronholz, J., & Zachmann, G. (1995). Hydrophobicity of the organic matter in arable soils. Soil Biology and Biochemistry, 27(11), 1453–1458. https://doi.org/10.1016/0038-0717(95)00068-P

Carrillo, M. L. K., Yates, S. R., & Letey, J. (1999). Measurement of Initial Soil-Water Contact Angle of Water Repellent Soils. Soil Science Society of America Journal, 63(3), 433–436. https://doi.org/10.2136/sssaj1999.03615995006300030002x

Casa, R., Castaldi, F., Pascucci, S., Palombo, A., & Pignatti, S. (2013). A comparison of sensor resolution and calibration strategies for soil texture estimation from hyperspectral remote sensing. Geoderma, 197–198, 17–26. https://doi.org/10.1016/j.geoderma.2012.12.016

Castaldi, F., Casa, R., Castrignanò, A., Pascucci, S., Palombo, A., & Pignatti, S. (2014). Estimation of soil properties at the field scale from satellite data: A comparison between spatial and non-spatial techniques. European Journal of Soil Science, 65(6), 842–851. https://doi.org/10.1111/ejss.12202

Castaldi, F., Hueni, A., Chabrillat, S., Ward, K., Buttafuoco, G., Bomans, B., Vreys, K., Brell, M., & van Wesemael, B. (2019). Evaluating the capability of the Sentinel 2 data for soil organic carbon prediction in croplands. ISPRS Journal of Photogrammetry and Remote Sensing, 147, 267–282. https://doi.org/10.1016/j.isprsjprs.2018.11.026

Castaldi, F., Palombo, A., Santini, F., Pascucci, S., Pignatti, S., & Casa, R. (2016). Evaluation of the potential of the current and forthcoming multispectral and hyperspectral imagers to estimate soil texture and organic carbon. Remote Sensing of Environment, 179, 54–65. https://doi.org/10.1016/j.rse.2016.03.025

Castaldi, F., Chabrillat, S., Don, A., & van Wesemael, B. (2019). Soil Organic Carbon Mapping Using LUCAS Topsoil Database and Sentinel-2 Data: An Approach to Reduce Soil Moisture and Crop Residue Effects. Remote Sensing, 11(18), 2121. https://doi.org/10.3390/rs11182121

Castaldi, F., Chabrillat, S., Jones, A., Vreys, K., Bomans, B., & Van Wesemael, B. (2018). Soil Organic Carbon Estimation in Croplands by Hyperspectral Remote APEX Data Using the LUCAS Topsoil Database. Remote Sensing, 10(2), 153. https://doi.org/10.3390/rs10020153

Castaldi, F., Hueni, A., Chabrillat, S., Ward, K., Buttafuoco, G., Bomans, B., Vreys, K., Brell, M., & van Wesemael, B. (2019). Evaluating the capability of the Sentinel 2 data for soil organic carbon prediction in croplands. ISPRS Journal of Photogrammetry and Remote Sensing, 147, 267–282. https://doi.org/10.1016/j.isprsjprs.2018.11.026

Castaldi, F., Palombo, A., Santini, F., Pascucci, S., Pignatti, S., & Casa, R. (2016). Evaluation of the potential of the current and forthcoming multispectral and hyperspectral imagers to estimate soil texture and organic carbon. Remote Sensing of Environment, 179, 54–65. https://doi.org/10.1016/j.rse.2016.03.025

Castaño, C., Lindahl, B. D., Alday, J. G., Hagenbo, A., Aragón, J. M. de, Parladé, J., Pera, J., & Bonet, J. A. (2018, December 1). Soil microclimate changes affect soil fungal communities in a Mediterranean pine forest. New Phytologist. https://doi.org/10.1111/nph.15205

Ceddia, M. B., Gomes, A. S., Vasques, G. M., & Pinheiro, É. F. (2017). Soil carbon stock and particle size fractions in the central Amazon predicted from remotely sensed relief, multispectral and radar data. Remote Sensing, 9(2), 124. https://doi.org/10.3390/rs9020124

Chau, H. W., Biswas, A., Vujanovic, V., & Si, B. C. (2014). Relationship between the severity, persistence of soil water repellency and the critical soil water content in water repellent soils. Geoderma, 221(Supplement C), 113–120. https://doi.org/10.1016/j.geoderma.2013.12.025

Chau, H. W., Goh, Y. K., Si, B. C., & Vujanovic, V. (2010). Assessment of alcohol percentage test for fungal surface hydrophobicity measurement. Letters in Applied Microbiology, 50(3), 295–300. https://doi.org/10.1111/j.1472-765X.2009.02791.x

Cihacek, L. J., & Bremner, J. M. (1979). A Simplified Ethylene Glycol Monoethyl Ether Procedure for Assessment of Soil Surface Area. Soil Science Society of America Journal, 43(4), 821–822. https://doi.org/10.2136/sssaj1979.03615995004300040045x

Cisar, J. L., Williams, K. E., Vivas, H. E., & Haydu, J. J. (2000). The occurrence and alleviation by surfactants of soil-water repellency on sand-based turfgrass systems. Journal of Hydrology, 231–232, 352–358. https://doi.org/10.1016/S0022-1694(00)00207-9

Civco, D. L. (1993). Artificial neural networks for land-cover classification and mapping. International Journal of Geographical Information Systems, 7(2), 173–186. https://doi.org/10.1080/02693799308901949

Clark, A., Mullan, B., & Porteous, A. (2011). Scenarios of regional drought under climate change. National Institute of Water & Atmospheric Research.

Cohen, J. (1960). A coefficient of agreement for nominal scales. Educational and Psychological Measurement, 20(1), 37–46. https://doi.org/10.1177/001316446002000104

Comino, F., Aranda, V., Domínguez-Vidal, A., & Ayora-Cañada, M. J. (2017). Thermal destruction of organic waste hydrophobicity for agricultural soils application. Journal of Environmental Management, 202(Pt 1), 94–105. https://doi.org/10.1016/j.jenvman.2017.07.024

Condron, L. M., Turner, B. L., & Cade-Menun, B. J. (2005). Chemistry and Dynamics of Soil Organic Phosphorus. In Phosphorus: Agriculture and the Environment (pp. 87–121). John Wiley & Sons, Ltd. https://doi.org/10.2134/agronmonogr46.c4

Conley, D. J., Paerl, H. W., Howarth, R. W., Boesch, D. F., Seitzinger, S. P., Havens, K. E., Lancelot, C., & Likens, G. E. (2009). Controlling eutrophication: Nitrogen and phosphorus. Science, 323(5917), 1014–1015. https://www.science.org/doi/10.1126/science.1167755

Cortes, C., & Vapnik, V. (1995). Support-vector networks. Machine Learning, 20(3), 273–297. https://doi.org/10.1007/BF00994018

Cozzolino, D., & Moron, A. (2003). The potential of near-infrared reflectance spectroscopy to analyse soil chemical and physical characteristics. The Journal of Agricultural Science, 140(1), 65–71. https://doi.org/10.1017/S0021859602002836

DeBano, L. F. (2000). Water repellency in soils: A historical overview. Journal of Hydrology, 231–232, 4–32. https://doi.org/10.1016/S0022-1694(00)00180-3

DeBano, L. F., Mann, L. D., & Hamilton, D. A. (1970). Translocation of Hydrophobic Substances into Soil by Burning Organic Litter. Soil Science Society of America Journal, 34(1), 130–133. https://doi.org/10.2136/sssaj1970.03615995003400010035x

Dekker, L. W., & Ritsema, C. J. (1994). How water moves in a water repellent sandy soil: 1. Potential and actual water repellency. Water Resources Research, 30(9), 2507–2517. https://doi.org/10.1029/94WR00749

Dekker, L. W., Oostindie, K., & Ritsema, C. J. (2005). Exponential increase of publications related to soil water repellency. Australian Journal of Soil Research, 43(3), 403–441. https://doi.org/10.1071/SR05007

Dekker, L. W., Oostindie, K., Kostka, S. J., & Ritsema, C. J. (2003). Treating water repellent surface layer with surfactant. In Soil Water Repellency (pp. 281–289). Elsevier. https://doi.org/10.1016/B978-0-444-51269-7.50028-X

Dekker, L. W., & Ritsema, C. J. (1996). Preferential Flow Paths in a Water Repellent Clay Soil with Grass Cover. Water Resources Research, 32(5), 1239–1249. https://doi.org/10.1029/96WR00267

Dekker, L. W., Doerr, S. H., Oostindie, K., Ziogas, A. K., & Ritsema, C. J. (2001). Water Repellency and Critical Soil Water Content in a Dune Sand. Soil Science Society of America Journal, 65(6), 1667–1674. https://doi.org/10.2136/sssaj2001.1667

Dekker, L. W., Ritsema, C. J., Oostindie, K., & Boersma, O. H. (1998). Effect of drying temperature on the severity of soil water repellency. Soil Science, 163(10), 780–796.

Dekker, L. W., Ritsema, C. J., Oostindie, K., Wesseling, J. G., & Geissen, V. (2019). Effects of a soil surfactant on grass performance and soil wetting of a fairway prone to water repellency. Geoderma, 338, 481–492. https://doi.org/10.1016/j.geoderma.2018.09.016

DeTar, W. R., Chesson, J. H., Penner, J. V., & Ojala, J. C. (2008). Detection of soil properties with airborne hyperspectral measurements of bare fields. Transactions of the ASABE, 51(2), 463–470.

Deurer, M., & Müller, K. (2010). Towards a better understanding of the causes, effects and remediation of soil hydrophobicity. A report by Plant & Food Research to Regional Councils. PFR Client Report,

10(38016), 94. http://envirolink.govt.nz/assets/Envirolink/814-HBRC115-Workshop-Towards-a-better-understanding-of-soil-hydrophobicity.pdf

Deurer, M., Müller, K., Van Den Dijssel, C., Mason, K., Carter, J., & Clothier, B. E. (2011). Is soil water repellency a function of soil order and proneness to drought? A survey of soils under pasture in the North Island of New Zealand. European Journal of Soil Science, 62(6), 765–779. https://doi.org/10.1111/j.1365-2389.2011.01392.x

Doerr, S. H., & Thomas, A. D. (2000). The role of soil moisture in controlling water repellency: New evidence from forest soils in Portugal. Journal of Hydrology, 231–232, 134–147. https://doi.org/10.1016/S0022-1694(00)00190-6

Doerr, S. H., Ferreira, A. J. D., Walsh, R. P. D., Shakesby, R. A., Leighton-Boyce, G., & Coelho, C. O. A. (2003). Soil water repellency as a potential parameter in rainfall-runoff modelling: Experimental evidence at point to catchment scales from Portugal. Hydrological Processes, 17(2), 363–377. https://doi.org/10.1002/hyp.1129

Doerr, S. H., Shakesby, R. A., & Walsh, R. P. D. (2000). Soil water repellency: Its causes, characteristics and hydro-geomorphological significance. Earth-Science Reviews, 51(1), 33–65. https://doi.org/10.1016/S0012-8252(00)00011-8

Doerr, S. H., Shakesby, R. A., Dekker, L. W., & Ritsema, C. J. (2006). Occurrence, prediction and hydrological effects of water repellency amongst major soil and land-use types in a humid temperate climate. European Journal of Soil Science, 57(5), 741–754. https://doi.org/10.1111/j.1365-2389.2006.00818.x

Doerr, S. H. (1998). On standardizing the 'water drop penetration time' and the 'molarity of an ethanol droplet' techniques to classify soil hydrophobicity: A case study using medium textured soils. Earth Surface Processes and Landforms: The Journal of the British Geomorphological Group, 23(7), 663–668. https://doi.org/10.1002/(SICI)1096-9837(199807)23:7<663::AID-ESP909>3.0.CO;2-6

Doerr, S. H., & Thomas, A. D. (2000). The role of soil moisture in controlling water repellency: New evidence from forest soils in Portugal. Journal of Hydrology, 231, 134–147. https://doi.org/10.1016/S0022-1694(00)00190-6

Domingo, W. R. (1950). Some notes on irreversibly-dried, diñicultly-wettable soils. Landbouwkundig Tijdschrift, 62, 252–260.

Eisele, A., Lau, I., Hewson, R., Carter, D., Wheaton, B., Ong, C., Cudahy, T. J., Chabrillat, S., & Kaufmann, H. (2012). Applicability of the Thermal Infrared Spectral Region for the Prediction of Soil Properties Across Semi-Arid Agricultural Landscapes. Remote Sensing, 4(11), 3265–3286. https://doi.org/10.3390/rs4113265

Erickson, J., Schott, D., Reverri, T., Muhsin, W., & Ruttledge, T. (2001). GC-MS analysis of hydrophobic root exudates of sorghum and implications on the parasitic plant Striga asiatica. Journal of Agricultural and Food Chemistry, 49(11), 5537–5542. https://pubs.acs.org/doi/10.1021/jf0111099

Ferreira, R. V., Serpa, D., Cerqueira, M. A., & Keizer, J. J. (2016). Short-time phosphorus losses by overland flow in burnt pine and eucalypt plantations in north-central Portugal: A study at micro-plot scale. Science of The Total Environment, 551–552, 631–639. https://doi.org/10.1016/j.scitotenv.2016.02.036

Foga, S., Scaramuzza, P. L., Guo, S., Zhu, Z., Dilley, R. D., Beckmann, T., Schmidt, G. L., Dwyer, J. L., Joseph Hughes, M., & Laue, B. (2017). Cloud detection algorithm comparison and validation for operational Landsat data products. Remote Sensing of Environment, 194, 379–390. https://doi.org/10.1016/j.rse.2017.03.026

Folkman, M. A., Pearlman, J., Liao, L. B., & Jarecke, P. J. (2001). EO-1/Hyperion hyperspectral imager design, development, characterization, and calibration. Hyperspectral Remote Sensing of the Land and Atmosphere, 4151, 40–51.

Franceschini, M. H. D., Demattê, J. A. M., da Silva Terra, F., Vicente, L. E., Bartholomeus, H., & de Souza Filho, C. R. (2015). Prediction of soil properties using imaging spectroscopy: Considering fractional vegetation cover to improve accuracy. International Journal of Applied Earth Observation and Geoinformation, 38, 358–370. https://doi.org/10.1016/j.jag.2015.01.019

Franco, C. M. M., Clarke, P. J., Tate, M. E., & Oades, J. M. (2003). Chapter 4—Chemical characterisation of water repellent materials in Australian sands. In Soil Water Repellency (pp. 37–48). Elsevier. https://doi.org/10.1016/B978-0-444-51269-7.50006-0

Fukuda, S., & Hirosawa, H. (2001). Support vector machine classification of land cover: Application to polarimetric SAR data. IGARSS 2001. Scanning the Present and Resolving the Future. Proceedings. IEEE 2001 International Geoscience and Remote Sensing Symposium (Cat. No. 01CH37217), 1, 187–189. https://doi.org/10.1109/IGARSS.2001.976097

Galvão, L. S., Formaggio, A. R., Couto, E. G., & Roberts, D. A. (2008). Relationships between the mineralogical and chemical composition of tropical soils and topography from hyperspectral remote sensing data. ISPRS Journal of Photogrammetry and Remote Sensing, 63(2), 259–271. https://doi.org/10.1016/j.isprsjprs.2007.09.006

Gargallo-Garriga, A., Sardans, J., Pérez-Trujillo, M., Rivas-Ubach, A., Oravec, M., Vecerova, K., Urban, O., Jentsch, A., Kreyling, J., Beierkuhnlein, C., Parella, T., & Peñuelas, J. (2014). Opposite metabolic responses of shoots and roots to drought. Scientific Reports, 4(1), 1–7. https://doi.org/10.1038/srep06829

Gburek, W. J., Barberis, E., Haygarth, P. M., Kronvang, B., & Stamm, C. (2005). Phosphorus Mobility in the Landscape. Phosphorus: Agriculture and the Environment, agronomymonogra(phosphorusagric), 941–979. https://doi.org/10.2134/agronmonogr46.c29

Ge, Y., Thomasson, J. A., & Sui, R. (2011). Remote sensing of soil properties in precision agriculture: A review. Frontiers of Earth Science, 5(3), 229–238. https://doi.org/10.1007/s11707-011-0175-0

Geladi, P., & Kowalski, B. R. (1986). Partial least-squares regression: A tutorial. Analytica Chimica Acta, 185, 1–17. https://doi.org/10.1016/0003-2670(86)80028-9

Gerighausen, H., Menz, G., & Kaufmann, H. (2012). Spatially explicit estimation of clay and organic carbon content in agricultural soils using multi-annual imaging spectroscopy data. Applied and Environmental Soil Science, 2012. https://doi.org/10.1155/2012/868090

Gerke, H. H., Hangen, E., Schaaf, W., & Hüttl, R. F. (2001). Spatial variability of potential water repellency in a lignitic mine soil afforested with Pinus nigra. Geoderma, 102(3), 255–274. https://doi.org/10.1016/S0016-7061(01)00036-2

Gholizadeh, A., Žižala, D., Saberioon, M., & Borůvka, L. (2018). Soil organic carbon and texture retrieving and mapping using proximal, airborne and Sentinel-2 spectral imaging. Remote Sensing of Environment, 218, 89–103. https://doi.org/10.1016/j.rse.2018.09.015

Gillingham, A. G., & Gray, M. H. (2000). Strategies for fertiliser use on dry hill country. Proceedings of the New Zealand Fertiliser Manufacturers' Research Asssociation Technical Conference, 26, 38–45.

Gillingham, A. G., & Gray, M. H. (2006). Measurement and modelling of runoff and phosphate movement from seasonally dry hill-country pastures. New Zealand Journal of Agricultural Research, 49(3), 233–245. https://doi.org/10.1080/00288233.2006.9513714

Gislason, P. O., Benediktsson, J. A., & Sveinsson, J. R. (2006). Random Forests for land cover classification. Pattern Recognition Letters, 27(4), 294–300. https://doi.org/10.1016/j.patrec.2005.08.011

Goetz, A. F., Ferri, M., Kindel, B., & Qu, Z. (2002). Atmospheric correction of Hyperion data and techniques for dynamic scene correction. IEEE International Geoscience and Remote Sensing Symposium, 3, 1408–1410.

Gomez, C., Adeline, K., Bacha, S., Driessen, B., Gorretta, N., Lagacherie, P., Roger, J. M., & Briottet, X. (2018). Sensitivity of clay content prediction to spectral configuration of VNIR/SWIR imaging data, from multispectral to hyperspectral scenarios. Remote Sensing of Environment, 204, 18–30. https://doi.org/10.1016/j.rse.2017.10.047

Gomez, C., Lagacherie, P., & Coulouma, G. (2012). Regional predictions of eight common soil properties and their spatial structures from hyperspectral Vis–NIR data. Geoderma, 189–190, 176–185. https://doi.org/10.1016/j.geoderma.2012.05.023

Gomez, C., Rossel, R. A. V., & McBratney, A. B. (2008). Soil organic carbon prediction by hyperspectral remote sensing and field vis-NIR spectroscopy: An Australian case study. Geoderma, 146(3–4), 403–411. https://doi.org/10.1016/j.geoderma.2008.06.011

Gomez, C., Viscarra Rossel, R. A., & McBratney, A. B. (2008). Soil organic carbon prediction by hyperspectral remote sensing and field vis-NIR spectroscopy: An Australian case study. Geoderma, 146(3), 403–411. https://doi.org/10.1016/j.geoderma.2008.06.011

Granged, A. J. P., Jordán, A., Zavala, L. M., & Bárcenas, G. (2011). Fire-induced changes in soil water repellency increased fingered flow and runoff rates following the 2004 Huelva wildfire. Hydrological Processes, 25(10), 1614–1629. https://doi.org/10.1002/hyp.7923

Grizonnet, M., Michel, J., Poughon, V., Inglada, J., Savinaud, M., & Cresson, R. (2017). Orfeo ToolBox: Open source processing of remote sensing images. Open Geospatial Data, Software and Standards, 2(1), 15. https://doi.org/10.1186/s40965-017-0031-6

Hallett, P. D., Nunan, N., Douglas, J. T., & Young, I. M. (2004). Millimeter-scale spatial variability in soil water sorptivity. Soil Science Society of America Journal, 68(2), 352–358. https://doi.org/10.2136/sssaj2004.3520

Ham, J. S., Chen, Y., Crawford, M. M., & Ghosh, J. (2005). Investigation of the random forest framework for classification of hyperspectral data. IEEE Transactions on Geoscience and Remote Sensing, 43(3), 492–501. https://doi.org/10.1109/TGRS.2004.842481

Haygarth, P. M., & Jarvis, S. C. (1999). Transfer of Phosphorus from Agricultural Soil. In D. L. Sparks (Ed.), Advances in Agronomy (Vol. 66, pp. 195–249). Academic Press. https://doi.org/10.1016/S0065-2113(08)60428-9

Haygarth, P. M., Condron, L. M., Heathwaite, A. L., Turner, B. L., & Harris, G. P. (2005). The phosphorus transfer continuum: Linking source to impact with an interdisciplinary and multi-scaled approach. Science of The Total Environment, 344(1), 5–14. https://doi.org/10.1016/j.scitotenv.2005.02.001

Hbirkou, C., Pätzold, S., Mahlein, A.-K., & Welp, G. (2012). Airborne hyperspectral imaging of spatial soil organic carbon heterogeneity at the field-scale. Geoderma, 175–176, 21–28. https://doi.org/10.1016/j.geoderma.2012.01.017

Hermansen, C., Moldrup, P., Müller, K., Jensen, P. W., van den Dijssel, C., Jeyakumar, P., & de Jonge, L. W. (2019). Organic carbon content controls the severity of water repellency and the critical moisture level across New Zealand pasture soils. Geoderma, 338, 281–290. https://doi.org/10.1016/j.geoderma.2018.12.007

Hermansen, C., Moldrup, P., Müller, K., Knadel, M., & Jonge, L. W. de. (2019). The Relation between Soil Water Repellency and Water Content Can Be Predicted by Vis-NIR Spectroscopy. Soil Science Society of America Journal, 83(6), 1616–1627. https://doi.org/10.2136/sssaj2019.03.0092

Hewitt, A. E. (2010). New Zealand soil classification. Landcare Research Science Series, 1.

Hillel, D. (2013). Fundamentals of soil physics. Academic press.

Hively, W. D., McCarty, G. W., Reeves, J. B., Lang, M. W., Oesterling, R. A., & Delwiche, S. R. (2011). Use of airborne hyperspectral imagery to map soil properties in tilled agricultural fields. Applied and Environmental Soil Science, 2011. https://doi.org/10.1155/2011/358193

Horne, D. J., & McIntosh, J. C. (2003). Chapter 3—Hydrophobic compounds in sands from New Zealand. In Soil Water Repellency (pp. 25–35). Elsevier. https://doi.org/10.1016/B978-0-444-51269-7.50005-9

Imeson, A. C., Verstraten, J. M., van Mulligen, E. J., & Sevink, J. (1992). The effects of fire and water repellency on infiltration and runoff under Mediterranean type forest. CATENA, 19(3), 345–361. https://doi.org/10.1016/0341-8162(92)90008-Y

Jaber, S. M., Lant, C. L., & Al-Qinna, M. I. (2011). Estimating spatial variations in soil organic carbon using satellite hyperspectral data and map algebra. International Journal of Remote Sensing, 32(18), 5077–5103. https://doi.org/10.1080/01431161.2010.494637

Jamison, V. C. (1947). Resistance to wetting in the surface of sandy soils under citrus trees in central Florida and its effect upon penetration and the efficiency of irrigation. Soil Science Society of America Journal, 11(C), 103–109. https://doi.org/10.2136/sssaj1947.036159950011000C0020x

Jaramillo, D. F., Dekker, L. W., Ritsema, C. J., & Hendrickx, J. M. H. (2000). Occurrence of soil water repellency in arid and humid climates. Journal of Hydrology, 231–232, 105–111. https://doi.org/10.1016/S0022-1694(00)00187-6

Jeyakumar, P., Müller, K., Deurer, M., van den Dijssel, C., Mason, K., Le Mire, G., & Clothier, B. (2014). A novel approach to quantify the impact of soil water repellency on run-off and solute loss. Geoderma, 221–222(Supplement C), 121–130. https://doi.org/10.1016/j.geoderma.2014.01.008

Jonge, L. W. de, Moldrup, P., & Schjønning, P. (2009). Soil Infrastructure, Interfaces & Translocation Processes in Inner Space ("Soil-it-is"): Towards a road map for the constraints and crossroads of soil architecture and biophysical processes. Hydrology and Earth System Sciences, 13(8), 1485–1502. https://doi.org/10.5194/hess-13-1485-2009

Kaiser, M., Kleber, M., & Berhe, A. A. (2015). How air-drying and rewetting modify soil organic matter characteristics: An assessment to improve data interpretation and inference. Soil Biology and Biochemistry, 80, 324–340. https://doi.org/10.1016/j.soilbio.2014.10.018

Kanning, M., Siegmann, B., & Jarmer, T. (2016). Regionalization of Uncovered Agricultural Soils Based on Organic Carbon and Soil Texture Estimations. Remote Sensing, 8(11), 927. https://doi.org/10.3390/rs8110927

Karnok, K. J., & Tucker, K. A. (2001). Wetting agent treated hydrophobic soil and its effect on color, quality and root growth of creeping bentgrass. International Turfgrass Society Research Journal, 9(2), 537–541. http://kkarnok.com/pubs/WettingAgentTreatedHydrophobicSoils.pdf

Karunarathna, A. K., Moldrup, P., Kawamoto, K., Jonge, L. W. de, & Komatsu, T. (2010). Two-Region Model for Soil Water Repellency as a Function of Matric Potential and Water Content. Vadose Zone Journal, 9(3), 719–730. https://doi.org/10.2136/vzj2009.0124

Kawamoto, K., Moldrup, P., Komatsu, T., de Jonge, L. W., & Oda, M. (2007). Water Repellency of Aggregate Size Fractions of a Volcanic Ash Soil. https://pubag.nal.usda.gov/catalog/712118

Kenyon, S. A. (1929). The "ironclad" or artificial catchment. Journal Department Agriculture of Victoria, 27, 86–91.

Kim, I., Pullanagari, R. R., Deurer, M., Singh, R., Huh, K. Y., & Clothier, B. E. (2014). The use of visible and near-infrared spectroscopy for the analysis of soil water repellency. Blackwell Publishing Ltd. http://onlinelibrary.wiley.com/doi/10.1111/ejss.12138/full

King, P. M. (1981). Comparison of methods for measuring severity of water repellence of sandy soils and assessment of some factors that affect its measurement. Soil Research, 19(3), 275–285. https://doi.org/10.1071/sr9810275

Knadel, M., Masís-Meléndez, F., de Jonge, L. W., Moldrup, P., Arthur, E., & Greve, M. H. (2016). Assessing soil water repellency of a sandy field with visible near infrared spectroscopy. Journal of near Infrared Spectroscopy, 24(3), 215–224. https://doi.org/10.1255/jnirs.1188

Kobayashi, M., & Shimizu, T. (2007). Soil water repellency in a Japanese cypress plantation restricts increases in soil water storage during rainfall events. Hydrological Processes, 21(17), 2356–2364. https://doi.org/10.1002/hyp.6754

Koptsik, S., Strand, L., & Clarke, N. (2003). On the calculation of the surface area of different soil size fractions. Applied Geochemistry, 18(5), 629–651. https://doi.org/10.1016/S0883-2927(02)00160-9

Koroleff, F. (1977). Simultaneous persulphate oxidation of phosphorus and nitrogen compounds in water. Report of the Baltic Intercalibration Worshop, 52–53.

Kostka, S. J. (2000). Amelioration of water repellency in highly managed soils and the enhancement of turfgrass performance through the systematic application of surfactants. Journal of Hydrology, 231–232, 359–368. https://doi.org/10.1016/S0022-1694(00)00208-0

Kovalskyy, V., & Roy, D. P. (2013). The global availability of Landsat 5 TM and Landsat 7 ETM+ land surface observations and implications for global 30m Landsat data product generation. Remote Sensing of Environment, 130, 280–293. https://doi.org/10.1016/j.rse.2012.12.003

Kuhn, M. (2008). Building predictive models in R using the caret package. Journal of Statistical Software, 28(5), 1–26. https://doi.org/10.18637/jss.v028.i05

Kussul, N., Lavreniuk, M., Skakun, S., & Shelestov, A. (2017). Deep learning classification of land cover and crop types using remote sensing data. IEEE Geoscience and Remote Sensing Letters, 14(5), 778–782. https://doi.org/10.1109/LGRS.2017.2681128

Lagacherie, P., Baret, F., Feret, J.-B., Madeira Netto, J., & Robbez-Masson, J. M. (2008). Estimation of soil clay and calcium carbonate using laboratory, field and airborne hyperspectral measurements. Remote Sensing of Environment, 112(3), 825–835. https://doi.org/10.1016/j.rse.2007.06.014

Larsen, I. J., MacDonald, L. H., Brown, E., Rough, D., Welsh, M. J., Pietraszek, J. H., Libohova, Z., de Dios Benavides-Solorio, J., & Schaffrath, K. (2009). Causes of post-fire runoff and erosion: Water repellency, cover, or soil sealing? Soil Science Society of America Journal, 73(4), 1393–1407. https://doi.org/10.2136/sssaj2007.0432

LeCun, Y. A., Bottou, L., Orr, G. B., & Müller, K.-R. (2012). Efficient BackProp. In G. Montavon, G. B. Orr, & K.-R. Müller (Eds.), Neural Networks: Tricks of the Trade: Second Edition (pp. 9–48). Springer Berlin Heidelberg. https://doi.org/10.1007/978-3-642-35289-8_3

Lee, C. M., Cable, M. L., Hook, S. J., Green, R. O., Ustin, S. L., Mandl, D. J., & Middleton, E. M. (2015). An introduction to the NASA Hyperspectral InfraRed Imager (HyspIRI) mission and preparatory activities. Remote Sensing of Environment, 167, 6–19. https://doi.org/10.1016/j.rse.2015.06.012

Leighton-Boyce, G., Doerr, S. H., Shakesby, R. A., & Walsh, R. P. D. (2007). Quantifying the impact of soil water repellency on overland flow generation and erosion: A new approach using rainfall simulation and wetting agent on in situ soil. Hydrological Processes, 21(17), 2337–2345. https://doi.org/10.1002/hyp.6744

Leinauer, B., Karcher, D., Barrick, T., Ikemura, Y., Hubble, H., & Makk, J. (2007). Water Repellency Varies with Depth and Season in Sandy Rootzones Treated With Ten Wetting Agents. Applied Turfgrass Science, 4(1), 1–9. https://doi.org/10.1094/ATS-2007-0221-01-RS

Leitch, C. J., Flinn, D. W., & Graaff, R. H. M. van de. (1983). Erosion and nutrient loss resulting from Ash Wednesday (February 1983) wildfires a case study. Australian Forestry, 46(3), 173–180. https://doi.org/10.1080/00049158.1983.10674396

Lemmnitz, C., Kuhnert, M., Bens, O., Güntner, A., Merz, B., & Hüttl, R. F. (2008). Spatial and temporal variations of actual soil water repellency and their influence on surface runoff. Hydrological Processes, 22(12), 1976–1984. https://doi.org/10.1002/hyp.6782

Leone, A. P., & Escadafal, R. (2001). Statistical analysis of soil colour and spectroradiometric data for hyperspectral remote sensing of soil properties (example in a southern Italy Mediterranean ecosystem). International Journal of Remote Sensing, 22(12), 2311–2328. https://doi.org/10.1080/01431160120522

Lesaignoux, A., Fabre, S., & Briottet, X. (2013). Influence of soil moisture content on spectral reflectance of bare soils in the 0.4–14 µm domain. International Journal of Remote Sensing, 34(7), 2268–2285. https://doi.org/10.1080/01431161.2012.743693

Letey, J. (1969). Measurement of contact angle, water drop penetration time, and critical surface tension.

Letey, J., Carrillo, M. L. K., & Pang, X. P. (2003). Chapter 5—Characterizing the degree of repellency. In Soil Water Repellency (pp. 51–55). Elsevier. https://doi.org/10.1016/B978-0-444-51269-7.50007-2

Letey, J., Osborn, J., & Pelishek, R. E. (1962). Measurement of liquid-solid contact angles in soil and sand. *Soil Science*, *93*(3), 149-153.

Li, G., Lu, D., Moran, E., & Hetrick, S. (2011). Land-cover classification in a moist tropical region of Brazil with Landsat Thematic Mapper imagery. International Journal of Remote Sensing, 32(23), 8207–8230. https://doi.org/10.1080/01431161.2010.532831

Li, Y., Wang, X., Cao, Z., & Si, B. (2016). Soil water repellency characteristic curve influenced by drying and wetting processes. Canadian Journal of Soil Science, 97(2), 226–240. https://doi.org/10.1139/cjss-2016-0003

Liaw, A., & Wiener, M. (2002). Classification and regression by randomForest. R News, 2(3), 18–22. https://cogns.northwestern.edu/cbmg/LiawAndWiener2002.pdf

Lindsay, W. L., & Moreno, E. C. (1960). Phosphate Phase Equilibria in Soils 1. Soil Science Society of America Journal, 24(3), 177–182. https://doi.org/10.2136/sssaj1960.03615995002400030016x

Lobell, D. B., & Asner, G. P. (2002). Moisture effects on soil reflectance. Soil Science Society of America Journal, 66(3), 722–727. https://doi.org/10.2136/sssaj2002.7220

Loizzo, R., Guarini, R., Longo, F., Scopa, T., Formaro, R., Facchinetti, C., & Varacalli, G. (2018). PRISMA: The Italian hyperspectral mission. IGARSS 2018-2018 IEEE International Geoscience and Remote Sensing Symposium, 175–178. https://doi.org/10.1109/IGARSS.2018.8518512

Lu, P., Wang, L., Niu, Z., Li, L., & Zhang, W. (2013). Prediction of soil properties using laboratory VIS–NIR spectroscopy and Hyperion imagery. Journal of Geochemical Exploration, 132, 26–33. https://doi.org/10.1016/j.gexplo.2013.04.003

Main-Knorn, M., Pflug, B., Louis, J., Debaecker, V., Müller-Wilm, U., & Gascon, F. (2017). Sen2Cor for sentinel-2. Image and Signal Processing for Remote Sensing XXIII, 10427, 1042704. https://doi.org/10.1117/12.2278218

Makkonen, L. (2016). Young's equation revisited. Journal of Physics: Condensed Matter, 28(13), 135001. https://doi.org/10.1088/0953-8984/28/13/135001

Mao, J., Nierop, K. G. J., Sinninghe Damsté, J. S., & Dekker, S. C. (2014). Roots induce stronger soil water repellency than leaf waxes. Geoderma, 232–234, 328–340. https://doi.org/10.1016/j.geoderma.2014.05.024

Marceau, D. J., Howarth, P. J., & Gratton, D. J. (1994). Remote sensing and the measurement of geographical entities in a forested environment. 1. The scale and spatial aggregation problem. Remote Sensing of Environment, 49(2), 93–104. https://doi.org/10.1016/0034-4257(94)90046-9

McDowell, R. W. (2010). Evaluation of two management options to improve the water quality of Lake Brunner, New Zealand. New Zealand Journal of Agricultural Research, 53(1), 59–69. https://doi.org/10.1080/00288231003606351

McDowell, R. W. (2012). Challenges and opportunities to decrease phosphorus losses from land to water. https://www.massey.ac.nz/~flrc/workshops/12/Manuscripts/McDowell_2012.pdf

McDowell, R. W., & Catto, W. (2005). Alternative fertilisers and management to decrease incidental phosphorus loss. Environmental Chemistry Letters, 2(4), 169–174. https://doi.org/10.1007/s10311-005-0099-6

McDowell, R. W., & Condron, L. M. (2004). Estimating phosphorus loss from New Zealand grassland soils. New Zealand Journal of Agricultural Research, 47(2), 137–145. https://doi.org/10.1080/00288233.2004.9513581

McDowell, R. W., Catto, W., & McDowell, N. L. S. (2020). The mitigation of phosphorus losses from a water-repellent soil used for grazed dairy farming. Geoderma, 362, 114125. https://doi.org/10.1016/j.geoderma.2019.114125

McDowell, R. W., Monaghan, R. M., & Carey, P. L. (2003). Potential phosphorus losses in overland flow from pastoral soils receiving long-term applications of either superphosphate or reactive phosphate rock. New Zealand Journal of Agricultural Research, 46(4), 329–337. https://doi.org/10.1080/00288233.2003.9513561

McDowell, R. W., Nash, D. M., & Robertson, F. (2007). Sources of Phosphorus Lost from a Grazed Pasture Receiving Simulated Rainfall. Journal of Environmental Quality, 36(5), 1281–1288. https://doi.org/10.2134/jeq2006.0347

Mcghie, D. A., & Posner, A. M. (1980). Water repellence of a heavy textured Western Australian surface soil. Soil Research, 18(3), 309–323. https://doi.org/10.1071/sr9800309

McKissock, I., Gilkes, R. J., & Bronswijk, W. van. (2003). The relationship of soil water repellency to aliphatic C and kaolin measured using DRIFT. Soil Research, 41(2), 251–265. https://doi.org/10.1071/sr01091

Meisner, A., Jacquiod, S., Snoek, B. L., ten Hooven, F. C., & van der Putten, W. H. (2018). Drought Legacy Effects on the Composition of Soil Fungal and Prokaryote Communities. Frontiers in Microbiology, 9. https://doi.org/10.3389/fmicb.2018.00294

Mevik, B.H., & Wehrens, R. (2015). Introduction to the pls Package. Help Section of The “Pls” Package of R Studio Software; R Foundation for Statistical Computing: Vienna, Austria, 1–23. https://cran.r-project.org/web/packages/pls/vignettes/pls-manual.pdf

Michel, J.C. (2009). Influence of Clay Addition on Physical Properties and Wettability of Peat-growing Media. HortScience, 44(6), 1694–1697. https://doi.org/10.21273/HORTSCI.44.6.1694

Michel, S., Gamet, P., & Lefevre-Fonollosa, M.-J. (2011). HYPXIM — A hyperspectral satellite defined for science, security and defence users. 2011 3rd Workshop on Hyperspectral Image and Signal Processing: Evolution in Remote Sensing (WHISPERS), 1–4. https://doi.org/10.1109/WHISPERS.2011.6080864

Middleton, E. M., Campbell, P. K. E., Ong, L., Landis, D. R., Zhang, Q., Neigh, C. S., Huemmrich, K. F., Ungar, S. G., Mandl, D. J., Frye, S. W., Ly, V. T., Cappelaere, P. G., Chien, S. A., Franks, S., & Pollack, N. H. (2017). Hyperion: The first global orbital spectrometer, earth observing-1 (EO-1) satellite (2000–2017). 2017 IEEE International Geoscience and Remote Sensing Symposium (IGARSS), 3039–3042. https://doi.org/10.1109/IGARSS.2017.8127639

Minu, S., Shetty, A., Minasny, B., & Gomez, C. (2017). The role of atmospheric correction algorithms in the prediction of soil organic carbon from Hyperion data. International Journal of Remote Sensing, 38(23), 6435–6456. https://doi.org/10.1080/01431161.2017.1354265

Miyata, S., Kosugi, K., Gomi, T., Onda, Y., & Mizuyama, T. (2007). Surface runoff as affected by soil water repellency in a Japanese cypress forest. Hydrological Processes, 21(17), 2365–2376. https://doi.org/10.1002/hyp.6749

Mohanty, B. P., Cosh, M. H., Lakshmi, V., & Montzka, C. (2017). Soil Moisture Remote Sensing: State-of-the-Science. Vadose Zone Journal, 16(1), vzj2016.10.0105. https://doi.org/10.2136/vzj2016.10.0105

Mougenot, B., Pouget, M., & Epema, G. F. (1993). Remote sensing of salt affected soils. Remote Sensing Reviews, 7(3–4), 241–259. https://doi.org/10.1080/02757259309532180

Mountrakis, G., Im, J., & Ogole, C. (2011). Support vector machines in remote sensing: A review. ISPRS Journal of Photogrammetry and Remote Sensing, 66(3), 247–259. https://doi.org/10.1016/j.isprsjprs.2010.11.001

Müller, K., Deurer, M., Slay, M., Aslam, T., Carter, J. A., & Clothier, B. E. (2010). Environmental and economic consequences of soil water repellency under pasture. Proceedings of the New Zealand Grassland Association, 72, 207–210.

Müller, K., Mason, K., Strozzi, A. G., Simpson, R., Komatsu, T., Kawamoto, K., & Clothier, B. (2018). Runoff and nutrient loss from a water-repellent soil. Geoderma, 322, 28–37. https://doi.org/10.1016/j.geoderma.2018.02.019

Müller, K., & Deurer, M. (2011). Review of the remediation strategies for soil water repellency. Agriculture, Ecosystems & Environment, 144(1), 208–221. https://doi.org/10.1016/j.agee.2011.08.008

Müller, K., Mason, K., Strozzi, A. G., Simpson, R., Komatsu, T., Kawamoto, K., & Clothier, B. (2018). Runoff and nutrient loss from a water-repellent soil. Geoderma, 322, 28–37. https://doi.org/10.1016/j.geoderma.2018.02.019

Murphy, J., & Riley, J. P. (1962). A modified single solution method for the determination of phosphate in natural waters. Analytica Chimica Acta, 27, 31–36. https://doi.org/10.1016/S0003-2670(00)88444-5

Nadav, I., Tarchitzky, J., & Chen, Y. (2013). Water Repellency Induced by Organic Matter (OM) in Treated Wastewater (TWW) Infiltration Ponds and Irrigation. In Functions of Natural Organic Matter in Changing Environment (pp. 883–887). Springer, Dordrecht. https://doi.org/10.1007/978-94-007-5634-2_161

Nash, D. M., McDowell, R. W., Condron, L. M., & McLaughlin, M. J. (2019). Direct Exports of Phosphorus from Fertilizers Applied to Grazed Pastures. Journal of Environmental Quality, 48(5), 1380–1396. https://doi.org/10.2134/jeq2019.02.0085

Nash, D., Clemow, L., Hannah, M., Barlow, K., & Gangaiya, P. (2005). Modelling phosphorus exports from rain-fed and irrigated pastures in southern Australia. Soil Research, 43(6), 745–755. https://doi.org/10.1071/SR04119

Nash, David, & Murdoch, C. (1997). Phosphorus in runoff from a fertile dairy pasture. Soil Research, 35(2), 419–429. https://doi.org/10.1071/s96039

Netzly, D. H., & Butler, L. G. (1986). Roots of sorghum exude hydrophobic droplets containing biologically active components 1. Crop Science, 26(4), 775–778.

Nowkandeh, S. M., Noroozi, A. A., & Homaee, M. (2018). Estimating soil organic matter content from Hyperion reflectance images using PLSR, PCR, MinR and SWR models in semi-arid regions of Iran. Environmental Development, 25, 23–32. https://doi.org/10.1016/j.envdev.2017.10.002

Olsen, S. R. (1954). Estimation of available phosphorus in soils by extraction with sodium bicarbonate (No. 939). US Department of Agriculture. http://archive.org/details/estimationofavai939olse

Oostindie, K., Dekker, L. W., Wesseling, J. G., & Ritsema, C. J. (2008). Soil surfactant stops water repellency and preferential flow paths. Soil Use and Management, 24(4), 409–415. https://doi.org/10.1111/j.1475-2743.2008.00185.x

Osborn, J., Letey, J., DeBano, F., & Terry, E. (1967). Seed Germination and Establishment as Affected by Non-Wettable Soils and Wetting Agents. Ecology, 48(3), 494–497. https://doi.org/10.2307/1932685

Pal, M. (2005). Random forest classifier for remote sensing classification. International Journal of Remote Sensing, 26(1), 217–222. https://doi.org/10.1080/01431160412331269698

Parfitt, R. L. (1989). Phosphate reactions with natural allophane, ferrihydrite and goethite. Journal of Soil Science, 40(2), 359–369. https://doi.org/10.1111/j.1365-2389.1989.tb01280.x

Pascucci, S., Casa, R., Belviso, C., Palombo, A., Pignatti, S., & Castaldi, F. (2014). Estimation of soil organic carbon from airborne hyperspectral thermal infrared data: A case study. European Journal of Soil Science, 65(6), 865–875. https://doi.org/10.1111/ejss.12203

Patzold, S., Mertens, F. M., Bornemann, L., Koleczek, B., Franke, J., Feilhauer, H., & Welp, G. (2008). Soil heterogeneity at the field scale: A challenge for precision crop protection. Precision Agriculture, 9(6), 367–390. https://doi.org/10.1007/s11119-008-9077-x

Peng, Y., Xiong, X., Adhikari, K., Knadel, M., Grunwald, S., & Greve, M. H. (2015). Modeling Soil Organic Carbon at Regional Scale by Combining Multi-Spectral Images with Laboratory Spectra. PLOS ONE, 10(11), e0142295. https://doi.org/10.1371/journal.pone.0142295

Peón, J., Fernández, S., Recondo, C., Calleja, J. F., Peón, J., Fernández, S., Recondo, C., & Calleja, J. F. (2017). Evaluation of the spectral characteristics of five hyperspectral and multispectral sensors for soil organic carbon estimation in burned areas. International Journal of Wildland Fire, 26(3), 230–239. https://doi.org/10.1071/WF16122

Peón, J., Recondo, C., Fernández, S., F. Calleja, J., De Miguel, E., & Carretero, L. (2017). Prediction of Topsoil Organic Carbon Using Airborne and Satellite Hyperspectral Imagery. Remote Sensing, 9(12), 1211. https://doi.org/10.3390/rs9121211

Prabhakara, K., Hively, W. D., & McCarty, G. W. (2015). Evaluating the relationship between biomass, percent groundcover and remote sensing indices across six winter cover crop fields in Maryland, United States. International Journal of Applied Earth Observation and Geoinformation, 39, 88–102. https://doi.org/10.1016/j.jag.2015.03.002

Preedy, N., McTiernan, K., Matthews, R., Heathwaite, L., & Haygarth, P. (2001). Rapid Incidental Phosphorus Transfers from Grassland. Journal of Environmental Quality, 30(6), 2105–2112. https://doi.org/10.2134/jeq2001.2105

Regalado, C. M., & Ritter, A. (2006). Geostatistical Tools for Characterizing the Spatial Variability of Soil Water Repellency Parameters in a Laurel Forest Watershed. Soil Science Society of America Journal, 70(4), 1071–1081. https://doi.org/10.2136/sssaj2005.0177

Ritsema, C. J., & Dekker, L. W. (1994). How water moves in a water repellent sandy soil: 2. Dynamics of fingered flow. Water Resources Research, 30(9), 2519–2531. https://doi.org/10.1029/94WR00750

Ritsema, C. J., & Dekker, L. W. (1995). Distribution Flow: A General Process in the Top Layer of Water Repellent Soils. Water Resources Research, 31(5), 1187–1200. https://doi.org/10.1029/94WR02979

Roper, M. M., Davies, S. L., Blackwell, P. S., Hall, D. J. M., Bakker, D. M., Jongepier, R., & Ward, P. R. (2015). Management options for water-repellent soils in Australian dryland agriculture. Soil Research, 53(7), 786–806. https://doi.org/10.1071/SR14330

Rossel, R. V., & Behrens, T. (2010). Using data mining to model and interpret soil diffuse reflectance spectra. Geoderma, 158(1), 46–54. https://doi.org/10.1016/j.geoderma.2009.12.025

Rossel, R. V., Walvoort, D. J. J., McBratney, A. B., Janik, L. J., & Skjemstad, J. O. (2006). Visible, near infrared, mid infrared or combined diffuse reflectance spectroscopy for simultaneous assessment of various soil properties. Geoderma, 131(1), 59–75. https://doi.org/10.1016/j.geoderma.2005.03.007

Rye, C. F., & Smettem, K. R. J. (2017). The effect of water repellent soil surface layers on preferential flow and bare soil evaporation. Geoderma, 289(Supplement C), 142–149. https://doi.org/10.1016/j.geoderma.2016.11.032

Sang, B., Schubert, J., Kaiser, S., Mogulsky, V., Neumann, C., Förster, K.-P., Hofer, S., Stuffler, T., Kaufmann, H., Müller, A., Eversberg, T., & Chlebek, C. (2008). The EnMAP hyperspectral imaging spectrometer: Instrument concept, calibration, and technologies. Imaging Spectrometry XIII, 7086, 708605. https://doi.org/10.1117/12.794870

Schindler, D. W., & Vallentyne, J. R. (2008). The Algal Bowl: Overfertilization of the World's Freshwaters and Estuaries. University of Alberta Press.

Schipper, L. A., Parfitt, R. L., Ross, C., Baisden, W. T., Claydon, J. J., & Fraser, S. (2010). Gains and losses in C and N stocks of New Zealand pasture soils depend on land use. Agriculture, Ecosystems & Environment, 139(4), 611–617. https://doi.org/10.1016/j.agee.2010.10.005

Schoeneberger, P. J., Wysocki, D. A., & Benham, E. C. (2012). Field book for describing and sampling soils. Government Printing Office.

Schreiner, O., & Shorey, E. C. (1910). Chemical nature of soil organic matter. US Government Printing Office.

Schwanghart, W., & Jarmer, T. (2011). Linking spatial patterns of soil organic carbon to topography—A case study from south-eastern Spain. Geomorphology, 126(1), 252–263. https://doi.org/10.1016/j.geomorph.2010.11.008

Selige, T., Böhner, J., & Schmidhalter, U. (2006). High resolution topsoil mapping using hyperspectral image and field data in multivariate regression modeling procedures. Geoderma, 136(1), 235–244. https://doi.org/10.1016/j.geoderma.2006.03.050

Sharpley, A. N., McDowell, R. W., & Kleinman, P. J. A. (2001). Phosphorus loss from land to water: Integrating agricultural and environmental management. Plant and Soil, 237(2), 287–307. https://doi.org/10.1023/A:1013335814593

Shen, J., Yuan, L., Zhang, J., Li, H., Bai, Z., Chen, X., Zhang, W., & Zhang, F. (2011). Phosphorus Dynamics: From Soil to Plant1. Plant Physiology, 156(3), 997–1005. https://doi.org/10.1104/pp.111.175232

Simpson, R. M., Mason, K., Robertson, K., & Müller, K. (2019). Relationship between soil properties and enzyme activities with soil water repellency. Soil Research, 57(6), 689–702. https://doi.org/10.1071/SR18199

Steinberg, A., Chabrillat, S., Stevens, A., Segl, K., & Foerster, S. (2016). Prediction of Common Surface Soil Properties Based on Vis-NIR Airborne and Simulated EnMAP Imaging Spectroscopy Data: Prediction Accuracy and Influence of Spatial Resolution. Remote Sensing, 8(7), 613. https://doi.org/10.3390/rs8070613

Stevens, A., Udelhoven, T., Denis, A., Tychon, B., Lioy, R., Hoffmann, L., & van Wesemael, B. (2010). Measuring soil organic carbon in croplands at regional scale using airborne imaging spectroscopy. Geoderma, 158(1), 32–45. https://doi.org/10.1016/j.geoderma.2009.11.032

Stevens, A., Wesemael, B. van, Vandenschrick, G., Touré, S., & Tychon, B. (2006). Detection of Carbon Stock Change in Agricultural Soils Using Spectroscopic Techniques. Soil Science Society of America Journal, 70(3), 844–850. https://doi.org/10.2136/sssaj2005.0025

Stoof, C. R., Moore, D., Ritsema, C. J., & Dekker, L. W. (2011). Natural and fire-induced soil water repellency in a Portuguese shrubland. Soil Science Society of America Journal, 75(6), 2283–2295. https://doi.org/10.2136/sssaj2011.0046

Sugiyama, M. (2015). Introduction to statistical machine learning. Morgan Kaufmann. https://doi.org/10.1016/C2014-0-01992-2

Tanii, J., Iwasaki, A., Kawashima, T., & Inada, H. (2012). Results of evaluation model of Hyperspectral Imager Suite (HISUI). 2012 IEEE International Geoscience and Remote Sensing Symposium, 131–134. https://doi.org/10.1109/IGARSS.2012.6351619

Tschapek, M. (1984). Criteria for Determining the hydrophilicity-hydrophobicity of Soils. Zeitschrift Für Pflanzenernährung Und Bodenkunde, 147(2), 137–149. https://doi.org/10.1002/jpln.19841470202

Tu, J. V. (1996). Advantages and disadvantages of using artificial neural networks versus logistic regression for predicting medical outcomes. Journal of Clinical Epidemiology, 49(11), 1225–1231. https://doi.org/10.1016/S0895-4356(96)00002-9

Uno, Y., Prasher, S. O., Patel, R. M., Strachan, I. B., Pattey, E., & Karimi, Y. (2005). Development of field-scale soil organic matter content estimation models in Eastern Canada using airborne hyperspectral imagery. Canadian Biosystems Engineering, 47(1.9), 1–14.

Vapnik, V. (2006). Estimation of Dependences Based on Empirical Data. Springer-Verlag. https://www.springer.com/gp/book/9780387308654

Vaudour, E., Gomez, C., Fouad, Y., & Lagacherie, P. (2019). Sentinel-2 image capacities to predict common topsoil properties of temperate and Mediterranean agroecosystems. Remote Sensing of Environment, 223, 21–33. https://doi.org/10.1016/j.rse.2019.01.006

Verma, K. S., Saxena, R. K., Barthwal, A. K., & Deshmukh, S. N. (1994). Remote sensing technique for mapping salt affected soils. International Journal of Remote Sensing, 15(9), 1901–1914. https://doi.org/10.1080/01431169408954215

Vohland, M., Ludwig, M., Thiele-Bruhn, S., & Ludwig, B. (2017). Quantification of Soil Properties with Hyperspectral Data: Selecting Spectral Variables with Different Methods to Improve Accuracies and Analyze Prediction Mechanisms. Remote Sensing, 9(11), 1103. https://doi.org/10.3390/rs9111103

Waghorn, G. C., & Barry, T. N. (1987). Pasture as a nutrient source. Livestock Feeding on Pasture, 10, 21–38.

Wallis, M. G., & Horne, D. J. (1992). Soil Water Repellency. In Advances in Soil Science (pp. 91–146). Springer, New York, NY. https://doi.org/10.1007/978-1-4612-2930-8_2

Wallis, M. G., Scotter, D. R., & Horne, D. J. (1991). An evaluation of the intrinsic sorptivity water repellency index on a range of New Zealand soils. Soil Research, 29(3), 353–362. https://doi.org/10.1071/sr9910353

Wang, L., & Qu, J. J. (2009). Satellite remote sensing applications for surface soil moisture monitoring: A review. Frontiers of Earth Science in China, 3(2), 237–247. https://doi.org/10.1007/s11707-009-0023-7

Wang, S., Zhuang, Q., Wang, Q., Jin, X., & Han, C. (2017). Mapping stocks of soil organic carbon and soil total nitrogen in Liaoning Province of China. Geoderma, 305, 250–263. https://doi.org/10.1016/j.geoderma.2017.05.048

Warren, M. A., Simis, S. G., Martinez-Vicente, V., Poser, K., Bresciani, M., Alikas, K., Spyrakos, E., Giardino, C., & Ansper, A. (2019). Assessment of atmospheric correction algorithms for the Sentinel-2A MultiSpectral Imager over coastal and inland waters. Remote Sensing of Environment, 225, 267–289. https://doi.org/10.1016/j.rse.2019.03.018

Watson, C. L., & Letey, J. (1970). Indices for characterizing soil water repellency based upon contact angle surface tension relationships. Soil Science Society of America Journal, 34(6), 841–844. https://doi.org/10.2136/sssaj1970.03615995003400060011x

Webb, T. H., & Wilson, A. D. (1995). A manual of land characteristics for evaluation of rural land: Landcare Research Science Series. Manaaki Whenua Press. http://doi.org/10.7931/DL1-LRSS-10

Weidong, L., Baret, F., Xingfa, G., Qingxi, T., Lanfen, Z., & Bing, Z. (2002). Relating soil surface moisture to reflectance. Remote Sensing of Environment, 81(2), 238–246. https://doi.org/10.1016/S0034-4257(01)00347-9

Whitley, A. E. (2018). Investigations of soil extractable aluminium and toxicity in New Zealand soils. [Doctoral thesis, Lincoln University]. Lincoln University research archive. https://hdl.handle.net/10182/10473

Wijewardana, N. S., Müller, K., Moldrup, P., Clothier, B., Komatsu, T., Hiradate, S., de Jonge, L. W., & Kawamoto, K. (2016). Soil-water repellency characteristic curves for soil profiles with organic carbon gradients. Geoderma, 264, 150–159. https://doi.org/10.1016/j.geoderma.2015.10.020

Woodcock, C. E., Strahler, A. H., & Jupp, D. L. B. (1988). The use of variograms in remote sensing: I. Scene models and simulated images. Remote Sensing of Environment, 25(3), 323–348. https://doi.org/10.1016/0034-4257(88)90108-3

Woudt, B. D. V. T. (1959). Particle coatings affecting the wettability of soils. Journal of Geophysical Research (1896-1977), 64(2), 263–267. https://doi.org/10.1029/JZ064i002p00263

Young, T. (1805). An essay on the cohesion of fluids. Philosophical Transactions of the Royal Society of London, 95, 65–87. https://doi.org/10.1098/rstl.1805.0005

Yuan, H., Van Der Wiele, C. F., & Khorram, S. (2009). An Automated Artificial Neural Network System for Land Use/Land Cover Classification from Landsat TM Imagery. Remote Sensing, 1(3), 243–265. https://doi.org/10.3390/rs1030243

Zhang, G., Eddy Patuwo, B., & Y. Hu, M. (1998). Forecasting with artificial neural networks: The state of the art. International Journal of Forecasting, 14(1), 35–62. https://doi.org/10.1016/S0169-2070(97)00044-7

Zhang, T., Li, L., & Zheng, B. (2013). Estimation of agricultural soil properties with imaging and laboratory spectroscopy. Journal of Applied Remote Sensing, 7(1), 073587. https://doi.org/10.1117/1.JRS.7.073587

Zhang, Y., Gu, M., Shi, K., Zhou, Y. H., & Yu, J. Q. (2010). Effects of aqueous root extracts and hydrophobic root exudates of cucumber (Cucumis sativus L.) on nuclei DNA content and expression of cell cycle-

related genes in cucumber radicles. Plant and Soil, 327(1), 455–463. https://doi.org/10.1007/s11104-009-0075-1

Zhang, Y., Guo, L., Chen, Y., Shi, T., Luo, M., Ju, Q., Zhang, H., & Wang, S. (2019). Prediction of Soil Organic Carbon based on Landsat 8 Monthly NDVI Data for the Jianghan Plain in Hubei Province, China. Remote Sensing, 11(14), 1683. https://doi.org/10.3390/rs11141683

Zhang, Y., Sui, B., Shen, H., & Wang, Z. (2018). Estimating temporal changes in soil pH in the black soil region of Northeast China using remote sensing. Computers and Electronics in Agriculture, 154, 204–212. https://doi.org/10.1016/j.compag.2018.09.005

Zhou, T., Geng, Y., Chen, J., Pan, J., Haase, D., & Lausch, A. (2020). High-resolution digital mapping of soil organic carbon and soil total nitrogen using DEM derivatives, Sentinel-1 and Sentinel-2 data based on machine learning algorithms. Science of The Total Environment, 729, 138244. https://doi.org/10.1016/j.scitotenv.2020.138244

Zhu, X. X., Tuia, D., Mou, L., Xia, G.-S., Zhang, L., Xu, F., & Fraundorfer, F. (2017). Deep learning in remote sensing: A comprehensive review and list of resources. IEEE Geoscience and Remote Sensing Magazine, 5(4), 8–36. https://doi.org/10.1109/MGRS.2017.2762307

Žížala, D., Minařík, R., & Zádorová, T. (2019). Soil Organic Carbon Mapping Using Multispectral Remote Sensing Data: Prediction Ability of Data with Different Spatial and Spectral Resolutions. Remote Sensing, 11(24), 2947. https://doi.org/10.3390/rs11242947